UNIVERSITY
OF
JOHANNESBURG

How to cite this thesis

CO₂ hydrogenation to synthetic fuel via modified Fischer-Tropsch process using cobalt-based catalysts

Report submitted in fulfillment of

Doctor of Philosophy

In

Chemical Engineering

In the

FACULTY OF EGINEERING AND THE BUILT ENVIRONMENT

Of the

University of Johannesburg

Compiled by   : Phathutshedzo Rodney Khangale
Student Number   : 201011724
Supervised by   : Prof Kalala Jalama and Prof Reinout Meijboom

Submitted: November 2019

DECLARATION

I hereby declare that this thesis which, I hereby submit in fulfilment of the qualification of: Doctor of Philosophy in CHEMICAL ENGINEERING to the University of Johannesburg, Department of Chemical Engineering is, apart from the recognized assistance from my supervisor, my own work which has not previously been submitted by me or any other person to any institution to obtain a diploma or degree.

_____

Signature of candidate

11th day of November 2019

ABSTRACT

The effect of promoting Co/Al_2O_3 catalyst with potassium on CO_2 hydrogenation to longer-chain hydrocarbons was investigated. The catalysts used in this study were synthesized using an incipient wetness impregnation of the support with cobalt nitrate solutions. All catalysts were supported on γ-alumina and promoted with potassium (0 – 8 wt.%) and/or 0 – 3 wt.% of either copper, ruthenium or palladium. The synthesized catalysts were characterized by X-ray diffraction (XRD), Brunauer-Emmett-Teller (BET), X-ray photoelectron spectroscopy (XPS), tempetature programmed reduction (TPR) and CO_2 temperature programmed desorption (CO_2–TPD) analyses. The catalysts were evaluated for CO_2 hydrogenation using a fixed-bed tube reactor. The effect of reaction temperature (190 – 345 ^{o}C) during CO_2 hydrogenation was evaluated at atmospheric pressure to determine the optimum reaction temperature that would favor the formation of longer chain hydrocarbons. Once the optimum temperature was selected, the effect of pressure (1 – 20 bar) was evaluated to determine the optimum operating pressure under the selected optimum temperature. The optimum temperature and pressure were then used to study the effect of potassium loading and the optimum potassium loading was determined. The optimum potassium-promoted catalyst was then promoted with either Ru, Pd or Cu at optimum operating conditions with the hope to improve catalyst reducibility. The optimum catalyst was then selected and used to study the catalyst stability at optimum operating temperature and pressure. The CO_2 conversion was found to increase with the reaction temperature. At higher temperatures, this influence was significant. The reaction tends to favor the CH_4 formation at higher temperature and it was concluded that higher reaction temperature does not favor the formation of longer chain hydrocarbons but rather tends to promote the methanation process. The C_{2+} yield was found to increase with the temperature, reaching its maximum of 2.19% at 330 ^{o}C and this was explained by a concomitant increase in CO_2 conversion and C_{2+} selectivity from 190 to 315 ^{o}C. Beyond this temperature, the selectivity to C_{2+} products started to decrease, while CO_2 conversion kept increasing. This resulted in a decrease in C_{2+} yield beyond 330 ^{o}C. Since the increase in C_{2+} yield with temperature was very low in the range from 190 to 290 ^{o}C and that the largest change was recorded when the temperature was increased from 290 to 300 ^{o}C, the latter was selected for the rest of the experiments in this study. The CO_2 conversion was found to increase with reaction pressure. This was expected and can be explained by an increase in reactants partial pressures in the reactor. The CH_4, C_2–C_4 and C_{5+} selectivities also increased significantly with pressure. At the same time, the selectivity of CO significantly decreased from 67.7 to 4.0%. As the operating

pressure was further increased beyond 5 bar, the CO_2 conversion did not significantly change and was limited at 41.0% at 20 bar while the CH_4 selectivity continued to increase, reaching its highest value of 88.9% at 20 bar, the CO, C_2–C_4 and C_{5+} selectivities respectively decreased to reach 1.3, 8.8 and 0.93% at 20 bar. The data suggests that higher pressures enhances the methanation ability of the catalyst. C_{2+} yield first increased from 1.83% to 7.9% when the pressure was increased from 1 to 5 bar, before decreasing at operating pressures beyond 5 bar. For this reason, 5 bar was selected as the operating pressure for the rest of the experiments in this study. TPR data revealed that introduction of potassium into the catalyst increased the catalyst reduction temperature. Potassium addition resulted in the methanation activation of $15\%Co/Al_2O_3$ catalyst to decrease while C_{2+} selectivity increased. The maximum C_{2+} yield of 10.2% with CO_2 conversion of 42.3% was obtained over the $15\%Co/Al_2O_3$ catalyst with 6 wt.% of potassium promoter content. For CO_2 hydrogenation over $15\%Co/Al_2O_3$ catalysts promoted with different potassium loading, CO_2 is first converted to CO via reverse – water – gas – shift reaction, followed by a subsequent hydrogenation of CO to hydrocarbons via modified FT synthesis. Nonetheless, the potassium–free catalyst performed as a methanation catalyst rather than FT catalyst since the selectivity of methane was 97%. The promotion effect of Ru, Pd and Cu as second catalyst promoter for 6 wt.% potassium promoted $15\%Co/Al_2O_3$ catalyst was also evaluated. TPR data showed that the addition of Ru, Pd and Cu as second catalyst promoters improved the catalyst reducibility and shifted the reduction towards lower temperatures. It was found that the CO_2 conversion decreased with a second metal promoter addition and the product produced were predominantly methane. The selectivity of CO increased with the addition of these second metal promoters. The addition of these second metals improved the catalysts reducibility and product distribution. The effect of CO_2 on the deactivation rate of $15\%Co-6\%K/Al_2O_3$ Fischer–Tropsch catalyst during CO_2 hydrogenation to longer chain hydrocarbons was also investigated. The presence of CO_2 displayed a negative influence on the catalyst stability and in the production of longer chain hydrocarbons. The main product generated was methathane; this was due to the presence of the cobalt carbide which led to the C_{5+} selectivity decrease with a concomitant increase of CH_4 formation. As the TOS was increasing, carbonaceous deposit formed an overlayer on parts of the catalyst. The latter is associated to cobalt rather than potassium as revealed by XRD results of the used catalyst. These deposits tend to lean towards the formation of methane, decrease CO_2 conversion and C_{5+} selectivity as observed in this study. Cobalt carbide formation in the spent catalyst in this study can account, at least in part, for the observed catalyst deactivation with the time-on-stream.

iii

ACKNOWLEDGEMENTS

TABLE OF CONTENTS

LIST OF FIGURES

CHAPTER 4

APPENDICES

LIST OF TABLES

CHAPTER 3

CHAPTER 4

APPENDICES

LIST OF ABBREVIATIONS AND SYMBOLS

CCS: Carbon capture and storage

CCU: Carbon capture and utilization

CNTs: Carbon nanotubes

FID: Flame ionization detector

FT: Fischer – Tropsch

FTS: Fischer – Tropsch synthesis

GC: Gas chromatograph

GHG: Greenhouse gas

HC: Hydrocarbons

MTG: Methanol – to – gasoline

RWGS: Reverse – water – gas – shift

TCD: Thermal conductivity detector

TOS: Time on stream

TPD: Temperature programmed desorption

TPR: Temperature programmed reduction

SBCR: Slurry bubble column reactor

WGS: Water – gas – shift
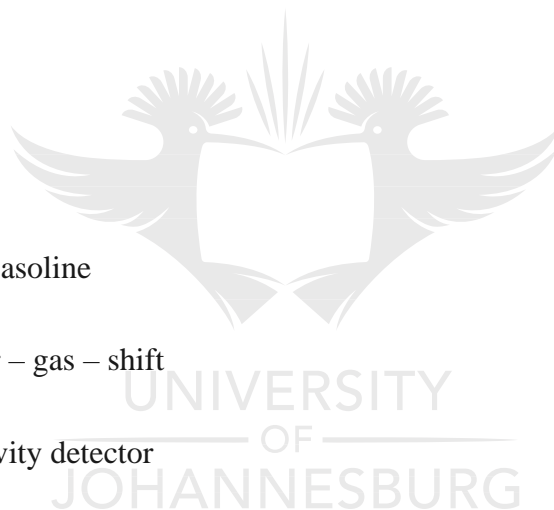
CHAPTER 1: INTRODUCTION

1.1 Theoretical background

Fischer-Tropsch (FT) synthesis is a chemical process in which a mixture of carbon monoxide and hydrogen is converted to liquid hydrocarbons [1]. It was originally established in 1925, by Franz Fischer and Hans Tropsch. The process has been considered as an alternative way of producing the transportation fuel, from typically coal, biomass or natural gas with low emission of pollutants. FT process is considered as the source of diesel fuel with low sulphur content and increases the supply of petroleum-derived hydrocarbons.

The process proceeds in the presence of a metal catalyst; there are numerous types of catalysts that may be used in FT synthesis. The most regularly used catalysts are transition metals such as iron, ruthenium and cobalt. Nickel may, under certain conditions, also be used but leans towards a selective formation of methane which, in this case, is an undesired product. Cobalt-based catalysts are highly active, particularly when the feedstock used is a natural gas. On the other hand, Fe-based catalysts are more appropriate for poor hydrogen syngas derived from low quality feedstock such as coal or biomass [2]. At large, FT catalysts are supported with materials with high surface area such as SiO_2, Al_2O_3 or zeolites. Because of good mechanical properties linked to Al_2O_3 as a catalyst support, Al_2O_3-supported catalysts are regularly used for the FT reaction. Equally, the main problem with the Co/Al_2O_3 catalyst is a deficient reducibility of cobalt species because of strong interaction between the metal and the support [3-7]. Water vapor has been reported to favor the formation of cobalt-support composites as it increases the interaction between metal with the support and by supporting the movement of cobalt ions into the tetrahedral sites of Al_2O_3 to produce non-reducible cobalt aluminate [8-9].

In general, a mixture of carbon monoxide and hydrogen, which is commonly known as the syngas, is used as the feed for traditional FT synthesis. In the modified FT synthesis, carbon dioxide and hydrogen or synthesis gas containing significant amount of carbon dioxide can be used as feedstock.

Since the Industrial Revolution, energy-driven consumption of fossil fuels resulted in a rapid increase in CO_2 emissions, disrupting the global carbon cycle and leading to a global warming impact. Global warming and a changing climate have a range of potential environmental, physical and health impacts, including extreme weather events (such as floods, droughts, storms, and

heatwaves), sea-level rise, altered crop growth, and disrupted water systems. Carbon dioxide can be chemically converted to fuels or chemical feedstock. However, in order to make a significant contribution to reducing CO_2 emissions, its utilization should focus primarily on the conversion to fuels since the market for chemicals is lower than that for fuels [10 – 11]. There are many routes possible for producing synthetic fuels from CO_2. The latter may be hydrogenated to liquid fuels either by direct or indirect routes. In the indirect route, it is converted to methanol, which can be subsequently transformed into hydrocarbons through a commercially existing methanol-to-gasoline (MTG) process based on zeolite catalysts [12]. On the other hand, in the direct route, CO_2 is converted to fuels through a modified Fischer-Tropsch (FT) process, eventually followed by a product upgrading (hydrotreating) step [13 – 37].

1.2 Research rationale and motivation

International annual CO_2 emissions reached ca. 34 gigatons in 2011 with China being the top emitter (29%), followed by the United States (16%), the European Union (11%), India (6%), the Russian Federation (5%), Japan (4%), etc. [38]. The involvement of Africa is a small percentage of global CO_2 emissions (ca. 3.6% in 2003) [39]. This contribution is likely to increase in the next few years as the population of the continent rises, resulting in the energy demand going up. In general, three main possibilities are considered to address the problems allied with CO_2 emissions: i) reduction or stabilization of CO_2 emissions by, for instance, improving process efficiencies [40]; ii) carbon capture and storage [40] and iii) CO_2 conversion to valuable products. All these three choices are among the significant issues that have captured the attention of researchers all over the world. An example of the third option is CO_2 conversion to methanol [41 – 43]. Yong *et al.* [41] have reported a highly efficient conversion of CO_2-rich bio-syngas to methanol using biomass char. Nieskens *et al.* [42] measured CO_2/H_2 conversions to methanol over a CoMoS-based catalyst in a fixed-bed reactor. Conversions of $CO/CO_2/H_2$ to methanol over a series of promoted CuO-ZnO-Al_2O_3 catalysts have been reported by Gao *et al.* [43].

The conversion of carbon dioxide into hydrocarbon fuels via the modified FT process has also attracted the interest of the research community. For example, hydrogen and carbon dioxide have been reported in to react over a cobalt-based catalyst, forming methane [44]. With Fe-based catalysts, other short-chains, unsaturated hydrocarbons are also produced addition to

methane [44]. This process still suffers from high methane selectivity. The kinetics and mechanism thereof are not yet well understood and require more investigation.

1.3 Problem statement

As a result of human activities, the atmospheric concentration of carbon dioxide has been intensifying comprehensively since the Industrial Revolution and has now reached dangerous levels not seen in the last three million years [45]. Human activities such as the burning of oil, coal and gas, as well as deforestation are the main causes of the increased carbon dioxide concentrations in the atmosphere. Burning these fuels discharges energy, which is most commonly converted into heat, electricity or power for transportation. Some examples of where they are used are in power plants, cars, planes and industrial facilities. In 2011, the use of fossil fuel generated 33.2 billion tonnes of carbon dioxide emissions globally [38]. The production of carbon dioxide leads to the increase in global temperatures and climate changes. More heat is trapped by the atmosphere, causing the planet to become warmer than it would be naturally. This situation has encouraged research studies towards developing CO_2 diminution processes such as reverse water gas shift, methanol synthesis, dimethyl ether synthesis and hydrocarbon synthesis to name a few [46 – 47]. Regarding the conversion of CO_2 into hydrocarbons through modified FT reaction over cobalt-based catalysts, the process still suffers from excessive methane production and poor yield of liquid fuel. Fundamental differences in the mechanism of CO hydrogenation (during normal FT reaction) and CO_2 hydrogenation (in modified FT reaction) are still not understood. This has made it difficult to design catalysts that can efficiently convert CO_2 into liquid fuels. The limited data reported in literature [48 – 52] suggest that promotion of cobalt-based catalysts with alkali metals offers the potential for improving the selectivity of CO_2 hydrogenation toward long-chain hydrocarbons. However, no systematic study has been conducted to determine the optimum loading of promoters and the operating conditions most favorable to the process. Furthermore, it is not clearly understood whether the promoting effect of alkali metals is due to geometric or electronic effects. On the other hand, the combination of alkali metals with other promoters such as copper, ruthenium, etc. has not been significantly explored. Lastly, because of the potential application of this process at industrial scales, catalyst stability becomes an important factor as it affects the economics of the process. To date, studies on cobalt-based catalyst stability during CO_2 hydrogenation are scarce, or inexistent.

3

1.4 Research aim and objectives

The aim of this project was to design a cobalt-based catalytic system that hydrogenates CO_2 into liquid fuel with improved selectivity, via a modified FT process. In particular, alumina-supported cobalt catalyst synthesis and modified FT process operating parameters favoring CO_2 conversion into synthetic fuel were investigated. The effect of the following on the process performance were evaluated:

   i.   Reaction temperature
  ii.   Reaction pressure
 iii.   Catalyst activation temperature
 iv.   Catalyst promotion with potassium (K) at different loading
  v.   Catalyst promotion with second metals such as ruthenium (Ru), copper (Cu) and palladium (Pd)
 vi.   Catalyst stability

1.5 Research description and methodology approach

The project consists of the preparation of several alumina-supported catalysts that were characterized and tested for modified Fischer-Tropsch reactions that facilitate CO_2 conversion into synthetic fuel. Research activities included the following:

1.5.1 Literature review

Literature review was done for the following reasons:

- To see what has and has not been investigated;
- To identify data sources that other researchers have used;
- To study how others have defined and measured key ideas;
- To develop alternative research projects and
- To provide evidence that may be used to support my own findings.

1.5.2 Catalyst synthesis

Various catalysts were prepared by incipient wetness impregnation method to have a range of cobalt dispersion on the alumina support. Some samples were promoted with a second metal such ruthenium, palladium and copper.

4

1.5.3 Catalyst characterization

The following techniques were used to characterize the prepared catalysts in order to understand their catalytic performance:

- X-Ray diffraction analysis (XRD)
- Brunauer, Emmett and Teller (BET) measurements
- Temperature programmed reduction (TPR)
- X-ray photoelectron spectroscopy (XPS)
- CO_2-Temperature programmed desorption.

1.5.4 Catalyst testing for modified Fischer-Tropsch reaction

Fischer-Tropsch catalyst testing was conducted in a fixed-bed tubular reactor available in our laboratory. The reaction product analysis was performed using a gas chromatograph (GC) equipped with a thermal conductivity detector (TCD) and a flame ionization detector (FID) available in our laboratory. Experimental data were processed using an excel spreadsheet.

REFERENCES

[1]. K. Jalama, J. Kabuba, H. Xiong, L.L. Jewell, "Co/TiO$_2$ Fischer–Tropsch catalyst activation by synthesis gas", Catalysis Communications, 17, (2012) 154–159.

[2]. L. Braconnier, E. Landrivon, I. Clemencon, C. Legens, F. Diehl, Y. Schuurman, "How does activation affect the cobalt crystallographic structure? An in situ XRD and magnetic study", Catalysis Today, 215, (2013) 18-23.

[3]. K. Jalama, N.J. Coville, H. Xiong, D. Hildebrandt, D. Glasser, S. Taylor, A. Carley, J.A. Anderson, G.J. Hutchings, "A comparison of Au/Co/Al$_2$O$_3$ and Au/Co/SiO$_2$ catalysts in the Fischer–Tropsch reaction", Applied Catalysis A: General, 395, (2011) 1–9.

[4]. S-J. Park, J.W. Bae, G-I. Jung, K-S. Ha, K-W. Jun, Y-J. Lee, H-G. Park, "Crucial factors for catalyst aggregation and deactivation on Co/Al$_2$O$_3$ in a slurry-phase Fischer–Tropsch synthesis", Applied Catalysis A: General, 413– 414, (2012) 310– 321.

[5]. L. Shi, Y. Jin, C. Xing, C. Zeng, T. Kawabata, K. Imai, K. Matsuda, Y. Tan, N. Tsubaki, "Studies on surface impregnation combustion method to prepare supported Co/SiO$_2$ catalysts and its application for Fischer–Tropsch synthesis", Applied Catalysis A: General, 435– 436, (2012) 217– 224.

[6]. A.M. Venezia, V.L. Parola, L.F. Liotta, G. Pantaleo, M. Lualdi, M. Boutonnet, S. Järås, "Co/SiO$_2$ catalysts for Fischer–Tropsch synthesis; effect of Co loading and support modification by TiO$_2$", Catalysis Today, 197, (2012) 18– 23.

[7]. U. Cornaro, S. Rossini, T. Montanari, E. Finocchio, G. Busca, "K-doping of Co/Al$_2$O$_3$ low temperature Fischer–Tropsch catalysts", Catalysis Today, 197, (2012) 101– 108.

[8]. A. Kogelbauer, J.G. Goodwin, R.J. Oukaci, "Ruthenium Promotion of Co/Al$_2$O$_3$ Fischer–Tropsch Catalysts", Journal of Catalysis, 160, (1996) 125-133.

[9]. A.M. Hilmen, D. Schanke, K.F. Hanssen, A. Holmen, "Study of the effect of water on alumina supported cobalt Fischer–Tropsch catalysts", Applied Catalysis A: General, 186, (1999) 169-188.

[10]. T. Herranz, S. Rojas, F.J. Pérez-Alonso, M. Ojeda, P. Terreros, J.L.G. Fierro, "Hydrogenation of carbon oxides over promoted Fe-Mn catalysts prepared by the microemulsion methodology", Applied Catalysis A: General, 311, (2006) 66–75 .

[11]. C. Hao, S. Wang, M. Li, L. Kang, X. Ma, "Hydrogenation of CO$_2$ to formic acid on supported ruthenium catalysts", Catalysis Today, 160, (2011) 184–190.

[12]. P. Kaiser, R.B. Unde, C. Kern, A. Jess, "Production of liquid hydrocarbons with CO_2 as carbon source based on reverse water-gas shift and Fischer-Tropsch synthesis", Chemie Ingenieur Technik, 85, (2013) 489–499.

[13]. W. Wang, S. Wang, X. Ma, "Recent advances in catalytic hydrogenation of carbon dioxide", Chemical Society Reviews, 40, (2011) 3703–3727.

[14]. M.K. Gnanamani, G. Jacobs, W.D. Shafer, D. Sparks, B.H. Davis, "Fischer–Tropsch synthesis: deuterium kinetic isotope study for hydrogenation of carbon oxides over cobalt and iron catalysts", Catalysis Letters, 141, (2011) 1420–1428.

[15]. T. Riedel, M. Claeys, H. Schulz, G. Schaub, S.S. Nam, K.W. Jun, M.J. Choi, G.Kishan, K.W. Lee, "Comparative study of Fischer–Tropsch synthesis with H_2/CO and H_2/CO_2 syngas using Fe- and Co-based catalysts", Applied Catalysis A: General, 186, (1999) 201–213.

[16]. C.G. Visconti, L. Lietti, E. Tronconi, P. Forzatti, R. Zennaro, E. Finocchio, "Fischer–Tropsch synthesis on a Co/Al_2O_3 catalyst with CO_2 containing syngas", Applied Catalysis A: General, 355, (2009) 61–68.

[17]. M.K. Gnanamani, W.D. Shafer, D.E. Sparks, B.H. Davis, "Fischer–Tropsch synthesis: Effect of CO_2 containing syngas over Pt promoted Co/γ-Al_2O_3 and K-promoted Fe catalysts", Catalysis Communications, 12, (2011) 936–939.

[18]. Y. Zhang, G. Jacobs, D.E. Sparks, M.E. Dry, B.H. Davis, "CO and CO_2 hydrogenation study on supported cobalt Fischer–Tropsch synthesis catalysts", Catalysis Today, 71, (2002) 411–418.

[19]. G.D. Weatherbee, C.H. Bartholomew, "Hydrogenation of CO_2 on group VIII metals: IV. Specific activities and selectivities of silica-supported Co, Fe, and Ru", Journal of Catalysis, 87, (1984) 352–362.

[20]. T. Riedel, H. Schulz, G. Schaub, K.W. Jun, J. Hwang, K.W. Lee, "Fischer–Tropsch on Iron with H_2/CO and H_2/CO_2 as Synthesis Gases: The Episodes of Formation of the Fischer–Tropsch Regime and Construction of the Catalyst", Topics in Catalysis, 26, (2003) 41–54.

[21]. H. Ando, Y. Matsumura, Y. Souma, "A comparative study on hydrogenation of carbon dioxide and carbon monoxide over iron catalyst", Journal of Molecular Catalysis A: Chemical, 154, (2000) 23–29.

[22]. Y. Yao, X. Liu, D. Hildebrandt, D. Glasser, "Fischer–Tropsch Synthesis Using H_2/CO/CO_2 Syngas Mixtures over an Iron Catalyst", Industrial & Engineering Chemistry Research, 50, (2011)11002–11012.

[23]. Y. Liu, C.H. Zhang, Y. Wang, Y. Li, X. Hao, L. Bai, H.W. Xiang, Y.Y. Xu, B. Zhong,Y.W. Li, "Effect of co-feeding carbon dioxide on Fischer–Tropsch synthesis over an iron–manganese catalyst in a spinning basket reactor", Fuel Processing Technology, 89, (2008) 234–241.

[24]. T. Riedel, G. Schaub, K.W. Jun, K.W. Lee, "Kinetics of CO_2 Hydrogenation on a K-Promoted Fe Catalyst", Industrial & Engineering Chemistry Research, 40, (2001)1355–1363.

[25]. R.W. Dorner, D.R. Hardy, F.W. Williams, H.D. Willauer, "K and Mn doped iron-based CO_2 hydrogenation catalysts: Detection of $KAlH_4$ as part of the catalyst's active phase", Applied Catalysis A: General, 373, (2010) 112–121.

[26]. R.A. Fiato, E. Iglesia, G.W. Rice, "Iron catalyzed CO_2 hydrogenation to liquid hydrocarbons", Studies in Surface Science & Catalysis, 114, (1998) 339–344.

[27]. T. Herranz, S. Rojas, F.J. Pérez-Alonso, M. Ojeda, P. Terreros, J.L.G. Fierro, "Hydrogenation of carbon oxides over promoted Fe-Mn catalysts prepared by the microemulsion methodology", Applied Catalysis A: General, 311, (2006) 66–75.

[28]. M. Martinelli, C.G. Visconti, L. Lietti, P. Forzatti, C. Bassano, P. Deiana, "CO_2 reactivity on Fe–Zn–Cu–K Fischer–Tropsch synthesis catalysts with different K-loadings", Catalysis Today, 228, (2014) 77–88.

[29]. M.K. Gnanamani, G. Jacobs, H.H. Hamdeh, W.D. Shafer, B.H. Davis, "Fischer–Tropsch synthesis: Mössbauer investigation of iron containing catalysts for hydrogenation of carbon dioxide", Catalysis Today, 207, (2013) 50–56.

[30]. N. Fischer, R. Henkel, B. Hettel, M. Iglesias, G. Schaub, M. Claeys, "Hydrocarbons via CO_2 Hydrogenation Over Iron Catalysts: The Effect of Potassium on Structure and Performance", Catalysis Letters, 146, (2016) 509–517.

[31]. M.L. Cubeiro, H. Morales, M.R. Goldwasser, M.J. Perez-Zurita, F.Gonzàlez-Jimènez, C.U. de N, "Hydrogenation of carbon oxides over Fe/Al_2O_3 catalysts", Applied Catalysis A: General, 189, (1999) 87–97.

[32]. P.S.S. Prasad, J.W. Bae, K.-W. Jun, K.-W. Lee, "Fischer–Tropsch synthesis by carbon dioxide hydrogenation on Fe-based catalysts", Catalysis Surveys from Asia, 12, (2008) 170–183.

[33]. Y. Yao, X. Liu, D. Hildebrandt, D. Glasser, "Fischer–Tropsch synthesis using $H_2/CO/CO_2$ syngas mixtures: A comparison of paraffin to olefin ratios for iron and cobalt based catalysts", Applied Catalysis A: General, 433–434, (2012) 58–68.

[34]. Y. Yao, X. Liu, D. Hildebrandt, D. Glasser, "The effect of CO_2 on a cobalt-based catalyst for low temperature Fischer–Tropsch synthesis", Chemical Engineering Journal, 193–194, (2012)318–327.

[35]. A.N. Akin, M. Ataman, A.E. Aksoylu, Z.I. Onsana, "CO_2 fixation by hydrogenation over coprecipitated Co/Al_2O_3", Reaction Kinetics and Catalysis Letters, 76, (2002) 265–270.

[36]. J.A. Dìaz, A.R. de la Osa, P. Sànchez, A. Romero, J.L. Valverde, "Influence of CO_2 co-feeding on Fischer–Tropsch fuels production over carbon nanofibers supported cobalt catalyst", Catalysis Communications, 44, (2014) 57–61.

[37]. G. Melaet, A.E. Lindeman, G. Somorjai, "Cobalt Particle Size Effects in the Fischer–Tropsch Synthesis and in the Hydrogenation of CO_2 Studied with Nanoparticle Model Catalysts on Silica", Topics in Catalysis, 57, (2014) 500–507.

[38]. J.G.J. Olivier, G. Janssens-Maenhout, J.A.H.W. Peters, Trends in global CO_2 emissions, 2012 Report, PBL Netherlands Environmental Assessment Agency, The Hague/Bilthoven, 2012, PBL publication number: 500114022, DOI: 10.2788/33777.

[39]. M. Sengul, A.E. Pillay, C.G. Francis, M. Elkadi, "Climate change and carbon dioxide (CO_2) sequestration: an African perspective", International Journal of Environmental Studies, 64, (2007) 543-554.

[40]. S. Pacala, R. Socolow, "Stabilization wedges: solving the climate problem for the next 50 years with current technologies", Science, 305, (2004) 968–972.

[41]. X. Yong, Y. Tong-qi, Q. Song-bai, N. Shen, G. Fei-yan, L. Yong, L. Quan-xin, "High efficient conversion of CO_2-rich bio-syngas to CO-rich bio-syngas using biomass char: a useful approach for production of bio-methanol from bio-oil", Bioresource Technology, 102, (2011) 6239-6245.

[42]. D.L.S. Nieskens, D. Ferrari, Y. Liu, R. Kolonko, "The conversion of carbon dioxide and hydrogen into methanol and higher alcohols", Catalysis Communications, 14, (2011) 111-113.

[43]. W.G. Gao, H. Wang, W.Y. Liu, F.J. Zhang, "Modified $Cuo/ZnO/Al_2O_3$ Catalysts for Methanol Synthesis from Co and CO_2 Co-Hydrogenation", Advanced Materials Research, 690-693, (2013)1529-1534.

[44]. R.W. Dorner, D.R. Hardy, F.W. Williams, H.D. Willauer, "Heterogeneous catalytic CO_2 conversion to value-added hydrocarbons", Energy & Environmental Sciences, 3 (2010) 884–890.

[45]. J. Fenger, "Urban air quality", Atmospheric Environment, 33, (1999) 4877-4900.

[46]. W. Wang, S. Wang, X. Ma, J. Gong, "Recent advances in catalytic hydrogenation of carbon dioxide", Chemical Society Reviews, 40, (2011) 3703-3727.

[47]. S. Saeidi, N.A.S. Amin, M.R. Rahimpour, "Hydrogenation of CO_2 to value-added products—A review and potential future developments", Journal of CO_2 utilization, 5, (2014) 66-81.

[48]. Z. Shi, H. Yang, P. Gao, X. Li, L. Zhong, H. Wang, H. Liu, W. Wei, Y. Sun, "Direct conversion of CO_2 to long-chain hydrocarbon fuels over K–promoted $CoCu/TiO_2$ catalysts", Catalysis Today, 311, (2018) 65-73.

[49]. J. Wei, J. Sun, Z.Y. Wen, C.Y. Fang, Q.J. Ge, H.Y. Xu, "New insights into the effect of sodium on Fe_3O_4-based nanocatalysts for CO_2 hydrogenation to light olefins", Catalysis Science & Technology, 6, (2016) 4786–4793.

[50]. J. Zhang, S. Lu, X. Su, S. Fan, Q. Ma, T. Zhao, "Selective formation of light olefins from CO_2 hydrogenation over Fe–Zn–K catalysts", Journal of CO_2 Utilization, 12, (2015) 95–100.

[51]. C.G. Visconti, M. Martinelli, L. Falbo, A. Infantes-Molina, L. Lietti, P. Forzatti, G. Iaquaniello, E. Palo, B. Picutti, F. Brignoli, "CO_2 hydrogenation to lower olefins on a high surface area K-promoted bulk Fe-catalyst", Applied Catalysis B: Environmental, 200, (2017) 530–542.

[52]. M. Rafati, L. Wang, A. Shahbazi, "Effect of silica and alumina promoters on co-precipitated Fe–Cu–K based catalysts for the enhancement of CO_2 utilization during Fischer–Tropsch synthesis", Journal of CO_2 Utilization, 12, (2015) 34–42.
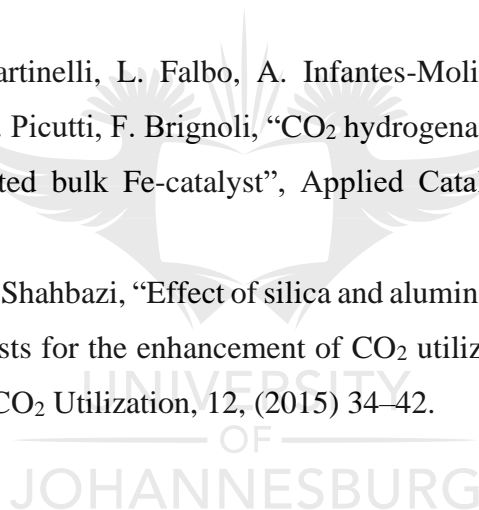
CHAPTER 2: LITERATURE REVIEW

2.1 Introduction

This chapter introduces the CO_2 hydrogenation process in the following aspects: the history of CO_2 hydrogenation, CO_2 hydrogenation to synthetic fuel, catalyst activity and product selectivity during CO_2 hydrogenation, product distribution during CO_2 hydrogenation to liquid hydrocarbons, effect of CO_2 hydrogenation on the catalyst deactivation, effect of catalyst promoters during CO_2 hydrogenation to liquid hydrocarbons, effect of catalyst support and metal loading during CO_2 hydrogenation to liquid hydrocarbons, effect of reaction conditions during CO_2 hydrogenation to liquid hydrocarbons, reverse-water-gas-shift reaction, CO_2 methanation, CO_2 hydrogenation to methanol, direct and indirect CO_2 hydrogenation to liquid fuel, CO_2 hydrogenation mechanism, and kinetic models for CO_2 hydrogenation over traditional FT catalysts.

The Literature review was performed to gain a better understanding of how CO_2 hydrogenates over cobalt-based catalysts. Compared to their iron-based counterparts, cobalt catalysts do not promote water-gas-shift reaction, which is believed to be essential during the conversion of CO_2 to hydrocarbons. In addition, the product distribution is reported in many occasions to be different from typical FT when CO_2 is used as carbon source. Many reports have indicated that cobalt-based catalysts tend to behave as methanation catalysts rather than FT catalysts. Alkali promoters such as potassium are also reported to enhance chain growth over iron-based catalyst and it is essential to determine if they possess similar behavior when cobalt-based catalysts are used. For this reason, it was vital to understand how CO_2 hydrogenates over cobalt-based catalysts.

2.2 Historical background

The reduction of CO_2 to release into the atmosphere has turned out to be a central research focus nowadays since carbon dioxide is one of the main contributors to the green-house effect, and its global production is on the rise [1]. The first approach to decrease CO_2 emissions, which has been intensely probed in the most recent years and which has been recently applied for the first time to a large-scale power station in Canada [2], is Carbon Capture and Storage (CCS) [3]. It involves permanent storage of CO_2 in explicit geological locations deep underground. An alternative to this technology is signified by Carbon Capture and Utilization (CCU)

11

processes, which involves chemical transformation of CO_2 to valuable carbon-bearing products. Among them, the transformation of CO_2 into liquid gasolines is of significant importance because the extensive market of these products would potentially reduce the global CO_2 production, at the same time minimizing the consumption of fossil fuels. Understandably, this is only possible if the source of hydrogen required for the process does not emit CO_2. Carbon dioxide could be hydrogenated to liquid fuels both by direct or indirect methods. In the indirect method, CO_2 is converted to methanol, which can be then converted into hydrocarbons through the commercially existing methanol-to-gasoline (MTG) method [4]. Contrary, in the direct method, CO_2 is converted to fuels by means of a modified Fischer-Tropsch (FT) process, ultimately accompanied by a product upgrading step [5].

Fischer –Tropsch synthesis is a chemical reaction which transforms a combination of carbon monoxide and hydrogen ($CO + H_2$ generally referred to as syngas) into liquid hydrocarbons. The process was originally established by two German scientists Franz Fischer and Hans Tropsch in 1925. The process has ever since been considered as another way of generating transportation fuel. The FT process is considered as the basis of low-sulphur diesel fuel and increases the supply of petroleum-derived hydrocarbons. The most desirable FT reaction must produce high molecular weight alkanes. The formation of methane is objectionable in this process.

FT takes place in the presence of a metal catalyst; there are numerous kinds of catalysts which can be used to facilitate the process. Transition metals such as cobalt-, iron- and ruthenium-based catalysts are normally used. Nickel might correspondingly be employed but tends to stimulate the formation of methane, which in this occasion, is an undesirable product. Ruthenium is considered the most active catalyst but is expensive and its availability is limited [6 – 7]. Iron- and cobalt-based catalysts are the mere two catalysts used for industrial applications. Cobalt-based catalysts are highly active and are essentially preferred when the feedstock is natural gas. Equally, Fe-based catalysts are recommended for poor hydrogen-containing syngas resulting from poor quality feedstock such as coal and biomass [8].

Literature data displayed that both CO and CO_2 can be hydrogenated using both cobalt [9] and iron [10] FT catalysts. On the other hand, most of the researchers established that the product distribution during CO and CO_2 hydrogenation are not the same [11 – 12]. Without a doubt, CO_2 hydrogenation leads essentially to smaller chain saturated hydrocarbons with poorer chain growth probability (α) values as compared to CO hydrogenation. On cobalt-based catalysts,

12

which are acknowledged to be significantly inactive in the water-gas-shift (WGS) and in the reverse-water-gas-shift (RWGS) processes, the reason of the different reactivity of CO and CO_2 is still interrogated. Furthermore, the catalyst stability in the presence of CO_2 is still vague and limited experimental data are presented to date.

2.3 CO_2 hydrogenation to synthetic fuel

Generally, the Fischer-Tropsch synthesis (FTS) reaction converts syngas (H_2 + CO) derived from coal, biomass or natural gas into liquid fuels and chemicals [13]. On the other hand, production of syngas from these carbon reservoirs also generate significant amounts of CO_2. As a result, current hydrocarbon synthesis processes adopt separation of CO_2 from gas reformers using solvents such as Rectisol [14]. The reduction of CO_2 discharges into the atmosphere has turned out to be a vital research subject matter in recent years for the reason that carbon dioxide is one of the main contributors to the green-house effect, and its global production is on the rise [15 – 16]. In recent years, the growing awareness of the dramatic impact of its atmospheric concentration on the climate has brought to deduction that the reduction of CO_2 emissions from all anthropogenic processes is required. In addition to the improvement of the efficiency of energy conversion and utilization processes, greenhouse gas (GHG) reduction policies recommended in the last decades also take account of secondary methods such as carbon dioxide capture and the storage (CCS) [17]. Nonetheless, several recent studies have shown that carbon dioxide can be hydrogenated into fuels and chemicals [18 – 19]. Most explored paths for CO_2 hydrogenation to hydrocarbons can be categorized into two groups: (i) CO_2 hydrogenation to hydrocarbons passing through methanol synthesis [20 – 21]; and (ii) CO_2 hydrogenation to hydrocarbons via modified FTS using iron-based catalysts [22 – 25]. Different from iron, cobalt-based catalysts do not display substantial water-gas-shift (WGS) activity; hence, several researchers have suggested that cobalt is not as active as iron for the hydrogenation of CO_2. Reverse water-gas-shift (WGS) reaction is believed to be vital for transforming CO_2. By the principle of microscopic reversibility, it is assumed that a catalyst that enables a forward reaction must also catalyze the reverse reaction. Actually, the principle applies to equilibrium, and away from equilibrium, other aspects must also be considered [26].

Based on product distributions, Zhang *et al.* [27] reported that CO_2 and CO hydrogenation seems to follow different reaction pathways. According to Yao *et al.* [28], at high content of CO_2, CO_2 does not behave like an inert gas, however is converted to hydrocarbon products when the CO conversion is about 70%, using cobalt–TiO_2 catalyst in a fixed-bed micro reactor.

13

These authors utilized a fixed bed reactor so that the conversion and the partial pressures are different down the catalyst bed. They concluded, however, that CO_2 and CO can be used as a feed for cobalt FT reaction, regardless of the feed gas being CO_2 rich. In contrast, Riedel and Schaub [26] concluded that CO_2 behaves as an inert gas and no quantifiable hydrocarbon production was obtained from CO_2. Using Co/Al_2O_3, Visconti *et al.* [29] similarly disclosed that CO_2 is barely hydrogenated in the presence of CO and acts like an inert species. It was reported that CO_2 only starts reacting when the conversion of CO is almost 100% [30]. These authors further indicated that CO_2 acts as a diluting gas and favors the formation of methane as a main product when the CO conversion is nearly 100%. Therefore, substituting CO_2 with N_2 in the syngas for the cobalt catalyst does not have a significant impact on the product distribution. CO_2 conversion changes the product composition for the cobalt from an FT type to mostly methanation [30].

2.4 Catalyst activity and product selectivity during CO_2 hydrogenation

Because of their good activity and selectivity, and their high resistance towards deactivation and low activity for water-gas-shift reaction, supported cobalt catalysts are repeatedly the choice for CO hydrogenation to hydrocarbons in the low temperature FT synthesis. This mode of the process operates in a temperature range of 190 – 230 °C [31 – 32], compared to 300 – 350 °C for the high temperature FT, which exclusively uses Fe-based catalysts [33]. In some circumstances, CO_2 may be an important constituent in the synthesis gas fed to FT plants [26]. It is acknowledged for FT synthesis with Co catalysts that CO_2 is not being produced [34 – 35]. However, in other processes such as the production of methanol from synthesis gas, it appears that methanol forms through CO_2 as an intermediate; carbon monoxide is initially transformed to carbon dioxide, which is subsequently converted to methanol [36 – 49]. It is therefore important to investigate whether a comparable situation applies to FT synthesis. It is well recognized that for high-temperature FTS with an iron catalyst the water-gas-shift reaction is basically at equilibrium so that both CO and CO_2 are converted [40]. Several studies [41 – 44] have been carried out on CO_2 hydrogenation using Fe-based catalysts and merely very limited studies have focused on hydrogenation of CO_2 over cobalt FT catalysts [26, 45 – 47]. Nevertheless, inconsistent results are repeatedly reported for hydrogenation of CO_2 using low temperature Co-based catalysts [26, 47 – 48].

Comparing the catalytic activity for a 36 wt.% Co/Al_2O_3 catalyst during respective hydrogenation of CO and CO_2 under similar process conditions, Akin *et al.* [11] measured three

14

times more conversion of CO_2 compared to CO. They also revealed that the hydrogenation of carbon dioxide resulted in the production of CH_4 and C_2H_6 only. Their conclusion was that the kinetics and the reaction mechanism in the two processes are alike: CO_2 hydrogenation occurs through the reverse water-gas-shift (RWGS) reaction accompanied by the FTS. Riedel *et al.* [49] working on a 100 Co/60 MnO/147 Aerosil (SiO_2)/0.15 Pt catalyst, perceived that when increasing the CO_2 content in the syngas (even though at the same time reducing the CO content in order to retain both the total pressure and the inlet flow constant), the products composition shifted from typical FTS (paraffins and olefins from C_1 up to C_{100}) to unusual presence of methane. They concluded that this behavior was allied with the shift from the Fischer-Tropsch regime, usual of the mixture of CO and H_2, to the methanation regime, usually associated with the mixture CO_2 and H_2. Another conclusion was that the formation path to methane was independent to that of long-chain hydrocarbons: CO_2 acts purely as diluent in FT process, despite the fact that it is a reactant in the methanation reaction.

Riedel and Schaub [26] also reported that CO_2 can either be inert or can lead to catalyst deactivation, subject to the Co-based catalyst type employed. Working with various supported cobalt catalysts; Zhang *et al.* [27] reported that CO_2 hydrogenation takes place very slowly in the presence of CO, although in the case of CO or CO_2 hydrogenation, comparable catalytic activities were achieved, with different selectivity. Visconti *et al.* [50] studied the influence of CO_2 over Co/Al_2O_3 catalyst and established that carbon dioxide is easily hydrogenated on the adopted Co-based FT catalyst, this process occurring quicker relative to the carbon monoxide hydrogenation. Moreover, the hydrogenation of carbon dioxide requires a quantity of hydrogen which is more or less three times greater compared to that used in the hydrogenation of CO. This was explained by a significant improvement of the methanation reaction during CO_2 hydrogenation.

Gnanamani *et al.* [51] probed the influence of CO_2 on a Pt promoted Co/γ-Al_2O_3 catalyst and reported that, CO_2 acts as an inert gas and yields methane as a main product. They concluded that CO_2 conversion alters the product structure for the cobalt-based catalyst from typically FT to typically methanation. Riedel *et al.* [52] observed that at a constant total synthesis pressure of 1 MPa, CO in the feed gas was substituted stepwise by CO_2; the production of organic products diminished gradually with up to 50 carbon percent (C%) of the CO being substituted by CO_2. Yet, towards a further substitution of CO by CO_2, a decrease in the production of organic compounds was observed, resulting in a production value of 20 C% without CO in the

synthesis gas. Methane selectivity increased from 10 C% for pure CO up to 95 C% in case of pure CO_2. The reason for this behavior was that with decreasing CO content of the syngas, the selective inhibitions are unrestricted, and the system shifts from an FT regime to a methanation regime. Even if the reverse CO shift reaction was fast, the possible CO partial pressure would stay small due to thermodynamic boundaries and would not be enough to establish the FT regime. Their conclusion was that FT synthesis with a CO_2/H_2 syngas on cobalt catalysts is not viable, even on hybrid catalysts which also comprise a CO shift catalyst.

Yao *et al.* [53] investigated the effect of CO_2 on cobalt-based FT catalyst and established that the CO conversion, CH_4 selectivity and C_{2+} selectivity did not change with a huge margin when moving between the CO and CO_2 feeds at each operating temperature. The conversions improved when the temperature increased from 180 to 220 °C. Meanwhile, the CH_4 selectivity marginally increased from 8% to 12%. In contrast, the C_{2+} selectivity dropped with increasing reaction temperature. On the other hand, the CO_2 followed a different route: similar to CO hydrogenation, CO_2 conversion upgraded with an increase in temperature. At a lower temperature of 180 °C, the catalyst activity for CO_2 was adjacent to that of CO. Though, when the reaction temperature was increased from 200 to 220 °C, CO_2 displayed a lower activity as compared to CO. The selectivity ranged between 87 and 95% when the temperature was increased from 180 to 220 °C. The maximum CH_4 selectivity was observed at 180 °C. It declined when the temperature was increased from 200 to 220 °C. The C_{2+} selectivity was between 5–13%, even though it increased with incremental increases in temperature (200–220 °C).

When investigating the impact of CO_2 co-feeding on Fischer-Tropsch fuels production using carbon nanofibers (CNFs)-supported cobalt catalysts, Diaz *et al.*[54] established that, as the reaction temperature increases, the catalytic activity and the rate of undesired reactions (water – gas - shift and methanation) also increases. Also, once the reaction temperature was fixed at 523 K, the existence of CO_2 in the feed was reported to have an impact on both the rate of catalytic hydrogenation of CO and product distribution. H_2/CO_2 acts as a slight oxidizing agent on Co/CNFs under certain circumstances. In the absence of CO, secondary catalytic activity decayed and methanation process reached its maximum. The explanation for the decrease of CO conversion and C_{5+} selectivity with CO_2 addition was attributed to the lower activity of this constituent. Likewise, the presence of CO_2 in the feed stream appears to cause that CO and CO_2 competed in adsorption on active sites in the catalyst. The selectivity to CH_4 declined on

increasing CO_2 content in the presence of a certain quantity of CO as a result of the lower concentration of hydrogen in the feed stream. Similarly, the existence of CO_2 in the feed stream may possibly prevent the water–gas–shift process. They concluded that C_7-C_{20} hydrocarbon product distribution shifted in the direction of light (smaller chain) hydrocarbons by feeding higher quantities of CO_2, essentially produced by the simple desorption of the chains.

Working on cobalt-based catalysts, Visconti *et al.* [55] suggested that CO_2 is more reactive than CO but leads to absolutely dissimilar products; the methanation regime dominates in the presence of CO_2/H_2 mixtures, despite the fact that the FT regime dominates in the presence of syngas (CO/H_2 mixtures). In addition, their data propose that, on cobalt-based catalysts, CO and CO_2 hydrogenation processes follow the same reaction path, with CO acting as intermediate (rapidly transformed on Co-based catalysts) in the case of CO_2 hydrogenation. The different selectivity of the two processes, on the other hand, is due to several reasons. On cobalt-based catalyst, it can be attributed to a different H/C ratio that is achieved on the catalyst surface as a result of the different adsorption strengths of CO and CO_2.

2.5 Product distribution during CO_2 hydrogenation to liquid hydrocarbons

The formation of products during FT synthesis can be described by a chain growth mechanism (fig. 2.1), where a C_1 unit is added to a growing chain. α-olefins and paraffins are the major products of the synthesis. α-olefins can also participate in the secondary reactions adding complication to the reaction network. For cobalt catalysts, oxygen is released as water which has a great influence on the catalytic activity and product selectivity [56]. Various types of oxygenates are formed as well during this process. N_2, CH_4 and CO_2 that may exist in the feed are generally considered as inert [57].
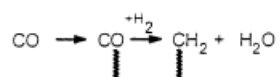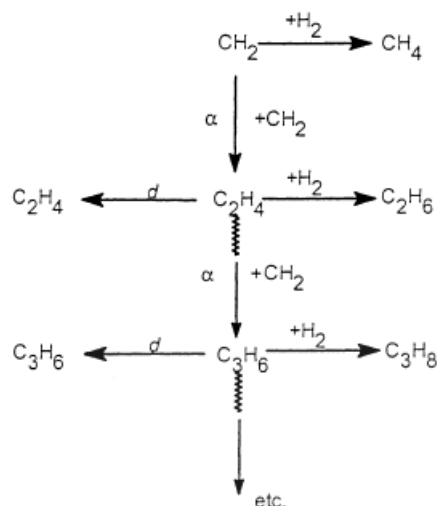
Figure 2. 1: FT stepwise growth process [33].

In general, longer chain hydrocarbons are expected during FT reaction. During CO_2 hydrogenation, it has been reported in most circumstances that methane is the main product. According to Visconti *et al.* [50], olefins product distribution obtained during CO_2 hydrogenation was not the same as compared to that of CO hydrogenation. Only ethylene and propylene were generated during CO_2 hydrogenation, however, the formation of other olefins was approximately zero. In addition, their relative ratio was not the same relative to that achieved during FT synthesis. Ethylene was the major olefin obtained during carbon dioxide hydrogenation, whereas propylene was dominant in the case of CO hydrogenation. Likewise, during CO hydrogenation, the ratio of olefins to paraffins was considerably greater than that achieved in the hydrogenation of CO_2. Similar findings were reported by Riedel *et al.* [52]. In addition, alcohol products were obtained during CO_2 hydrogenation, to be specific, only C_1 and C_2 alcohols were obtained in the reaction products during CO_2 hydrogenation, while no alcohol products were observed during CO hydrogenation. The authors similarly indicated that the replacement of CO with CO_2 induces a speedy alteration of the product distribution, characterized primarily by a strong improvement of the yield of smaller chain hydrocarbons and alcohols and by the fading of longer chain hydrocarbons. The product distribution obtained during CO or CO_2 hydrogenation was found to be dissimilar. For CO hydrogenation, a usual FTS product distribution was noticed, with a chain growth probability for the C_{8+} products

close to 0.9. In contrast, CO_2 hydrogenation resulted in C_1–C_6 hydrocarbons, together with C_1–C_2 alcohols; specifically, methane accounted for more than 90% of the products during CO_2 hydrogenation compared to less than 10% when CO was used.

Based on TPR studies during CO and CO_2 hydrogenation at atmospheric pressure, Falconer *et al.* [59] indicated that both reactions follow the same reaction route. In the case of a Ru/SiO$_2$ catalyst [59], it was suggested that CO_2 dissociates to adsorbed CO and O atoms, followed by dissociation of CO to C and O. Adsorbed C is then hydrogenated to methane and other heavy molecular weight hydrocarbons, while O is freely hydrogenated to water. In agreement with Visconti *et al.* [50] findings, they too observed different product selectivity during CO and CO_2 hydrogenation. Meanwhile, during CO_2 hydrogenation methane was predominant over higher molecular weight hydrocarbons. The difference in product selectivity has been clarified by the authors by invoking a lower CO_2 adsorption strength with respect to CO. This would lead to higher H_2/CO surface ratio than that existing in case of CO adsorption, thus giving preference to methane formation over longer chain hydrocarbons. Similar results have been reported in literature [61 – 62], where it was concluded that CO_2 hydrogenation proceeds via an intermediate CO formation. Different selectivity during CO or CO_2 hydrogenation were observed, with CO_2 producing predominantly methane and CO. This was explained by considering a higher concentration of adsorbed oxygen as a result of CO_2 dissociation.

It has been speculated by many researchers that CO and CO_2 hydrogenation follow reaction paths which are dissimilar [63], with CO hydrogenation proceeding via the intermediacy of HC and OH adsorbed species, and CO_2 hydrogenation proceeding via a HC-O intermediate. The HC-O species would be hydrogenated to yield adsorbed methanol, which is subsequently hydrogenated to methane. Other authors reported that methanol is not considerably hydrogenated to methane but is a final product [51]. Gnanamani *et al.* [30] reported that CO_2 conversion alters the product composition for cobalt catalyst from typical FT to methanation regime. Riedel *et al.* [52] reported that methane formation and the formation of longer chain hydrocarbons take place individually; further, with decreasing CO partial pressure, more active sites of the cobalt catalyst attain the character of methane formation sites, correspondingly lose the character of FT sites.

Kim *et al.* [63] observed that the selectivity of CH_4 improved with increasing time on stream under both reaction conditions, with and without CO_2 addition, with decreased selectivity to C_{5+} until 30 h on stream. In addition, the selectivities of CH_4 and C_{5+} were found to be

comparable for both reaction conditions. On the other hand, from 45 h on stream, the selectivities of CH_4 and C_{5+} sharply declined, while $C_2 - C_4$ selectivity improved, with a simultaneous reduction in CO conversion. The deviation of both activity and product distribution was considerably higher in the CO_2-added reaction conditions. Similar trend was observed by de la Pena O'Shea *et al.* [64] who indicated that with CO_2 addition on Co/γ-Al_2O_3 catalyst, the cobalt metal becomes reoxidized by the CO_2 dissociation to CO and O on Co metal surface with the co-existence of produced water during the FTS reaction, leading to the decline in CO conversion and C_{5+} selectivity with a simultaneous increase of CH_4 production.

According to Zhang *et al.* [65], the difference in the product distributions between the hydrogenation of CO and CO_2 prevents a common reaction pathway for FTS unless there is a second reaction pathway for the conversion of CO_2, but not CO to methane. Similarly, if there is another path, then the FTS with CO_2 takes place at a lower rate compared to CO. It was suggested that the conversion of CO and CO_2 follows different reaction paths. The authors assumed that the hydrogenation and breaking of the two C–O bonds of the CO_2 offer the source of the different paths. In this suggestion, the breaking of the C–O bond, most probably by the adding adsorbed H to form C–O–H, competes with, and most likely leads, the addition of adsorbed H to form the C–H bond. Accordingly, for CO the following reaction path could apply [65]:

$$C–O_a + 2\ H_a \rightarrow [H–C \cdot \cdot \cdot O–H]_a \rightarrow H–C_a + O–H_a \ldots\ldots\ldots\ldots\ldots\ldots\ldots\ldots\ldots\ldots(2.1)$$
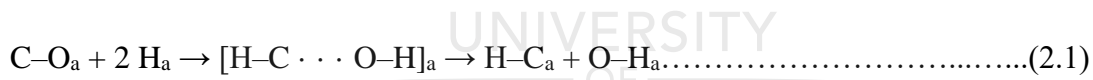
When CO_2 is used, the reaction becomes more complex as there are two C–O bonds that need to be broken before or concurrently with the formation of the C–H bond. If it is assumed that comparable rates apply for the formation of the first O–H and C–H bonds as in the case of CO, the situation would be different, as idealized in the reaction below:

$$O–C–O_a + 2\ H_a \rightarrow [H–CO\text{-}\text{-}\text{-}O–H]_a \rightarrow [H–C]_a + O–H_a \ldots\ldots\ldots\ldots\ldots\ldots\ldots(2.2)$$
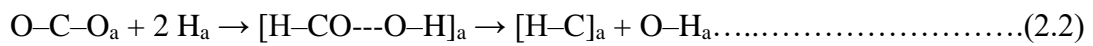
Assuming that the above reaction is valid, the absorbed oxygen species will be hydrogenated to produce water, while the adsorbed H-CO species is subsequently hydrogenated as shown in the reaction below to produce methane.

$$[H–C–O]_a + 3H_a \rightarrow [H_3C–O–H]_a + 2H_a \rightarrow CH_4 + H_2O \ldots\ldots\ldots\ldots\ldots\ldots\ldots(2.3)$$
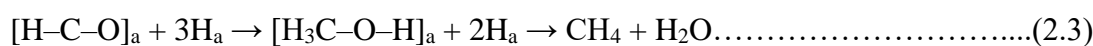
Based on the carbon mass balance, approximately 75% of the hydrogenation of CO_2 would follow reaction (2.3) and the rest would consist of the breaking of the second C–O bond to continue along the usual FTS reaction route like in CO hydrogenation. Meanwhile, the latter mechanism would be responsible for the products that are generated from the hydrogenation of CO_2; this is hypothetical [66]. Alternative probability is that the conversion of CO_2 follows the same mechanism as has been reported by Fischer and Bell [67] that used a Rh/SiO_2 catalyst.

2.6 Effect of CO_2 hydrogenation on the catalyst deactivation

Supported cobalt catalysts exhibit high activity and selectivity towards linear paraffins and demonstrate high resistance towards deactivation; they display low activity for water - gas - shift reaction. Catalyst deactivation in the Fischer – Tropsch reaction has been a theme of industrial as well as academic interest for numerous years. The main causes of catalyst deactivation in cobalt-based FTS are poisoning, reoxidation of cobalt active sites, formation of surface carbon species, carbidization, surface reconstruction, sintering of cobalt crystallites, metal – support solid state reactions and attrition [68]. Fischer – Tropsch catalysts are generally very sensitive to poisoning and cleansing of the synthesis gas is for that reason a significant part of the process, specifically for the processes using coal and biomass as feedstock [69]. The loss of activity is also related to reaction conditions such as temperature, pressure, conversion, partial pressures of synthesis gas and steam and the type of reactor used. The major challenge for studying catalyst deactivation in FTS is the fact that the catalyst is inserted in wax after use. The wax limits the variety of techniques that can be used for characterization of the used-up catalysts. Furthermore, the sensitivity of the active phase against air hinders the treatment of the dewaxed catalysts.

The difference in the catalytic activity during CO and CO_2 hydrogenations for producing heavy molecular weight hydrocarbons has also been studied [23, 70-71]. Riedel and Schaub [26] indicated that CO_2 contained in syngas is favorably eliminated to decrease the reactor size, particularly for the operation of slurry bubble column reactor (SBCR). Furthermore, the authors reported that CO_2 acts as an inert gas on cobalt-based catalysts, and has an undesirable influence on reaction rate, resulting in the deactivation of a Co–La–Ru–SiO_2 catalyst. The reason for this deactivation could not be clarified, and therefore, they recommended that further studies be conducted before a sound generalization can be made.

Kim *et al.* [63] reported that the conversion of CO, with CO_2 addition, was marginally lower than that without CO_2 addition, particularly after 30 h of reaction. In addition, after 60 h on stream, the conversion of CO was 41.3% for the reaction without addition of CO_2 with little deactivation rate, whereas it was 34.6% for the reaction with CO_2 addition. This behavior was ascribed to the partial oxidation of active cobalt metal by CO_2, causing gradual catalyst deactivation. Comparing the effect of CO and CO_2 hydrogenation on supported cobalt catalyst, Zhang *et al.* [65] reported that during CO_2 hydrogenation over Co/SiO_2 catalyst, deactivation is slower as compared to CO hydrogenation, even at high conversion. The authors also indicated that one of the explanations for the deactivation mechanism of cobalt FTS catalyst was the oxidation of surface cobalt to oxide or the formation of cobalt aluminate, promoted by water vapour.

2.7 Effect of catalyst promoters during CO_2 hydrogenation to liquid hydrocarbons

Catalyst promotors have been reported to exhibit an essential influence on the activity and product selectivity during traditional Fischer–Tropsch synthesis. Promoters usually added to cobalt Fischer-Tropsch catalysts, such as platinum and palladium have a little effect on the product distribution when CO_2 is used as the source of carbon [65]. Russell and Miller [72] examined several copper-promoted cobalt catalysts for the synthesis of heavy molecular weight hydrocarbons using carbon dioxide and hydrogen at atmospheric pressure and in a temperature range of 175 to 300 °C. They established that the catalysts which do not contain alkali promoters did not yield liquid hydrocarbons or only produced traces of them. However, the catalysts yielded a small amount of liquid hydrocarbons after a suitable poisoning. Cobalt catalysts have been reported to demonstrate good catalyst performance for CO_2 hydrogenation to light hydrocarbons and C_{2+} alcohols recently [73 – 75]. Besides, other metals such as Cu, Ru, Pd and Pt may be introduced to improve CO production since Co is not active for water – gas – shift and reverse – water – gas – shift reactions. Alkali metals such as Na and K have also been investigated as promoter of Fe – based catalyst for CO_2 hydrogenation [76 – 79]. It has been shown that they suppressed the formation of CH_4, increased the chain growth probability and enhanced the production of olefins. Furthermore, their effects on the product selectivity have been found to be strongly dependent on their concentration. In the case of traditional cobalt FT catalysts supported on metal oxides, these alkali promoters have been reported to enhance the catalyst selectivity [80]. The explanations for this phenomenon may be that the incorporation of alkali metals can cause a charge transfer from the alkali metals to the surface

of the catalysts, thereby inhibiting H_2 adsorption but enhancing CO_2 chemisorption and dissociation [81]. For FTS catalysts, the support can significantly influence the morphology, structure and adsorption properties of the active phase. Some researchers found that TiO_2-supported cobalt catalysts possess higher reducibility and catalytic activity for CO hydrogenation compared with other typical oxide support, for instance Al_2O_3, SiO_2 and MgO [82 – 83]. On the other hand, during traditional FT synthesis with cobalt – based catalysts, noble metals like Ru, are frequently used to improve the reduction of cobalt oxides and improve the dispersion of cobalt clusters [84]. Nonetheless, synergistic bimetallic interactions between cobalt and ruthenium enhances the rate and C_{5+} selectivity for FTS. The question remains whether the same behavior could be observed for CO_2 hydrogenation to hydrocarbons over cobalt-based catalysts.

Shi *et al.* [81] investigated the effect of potassium promoter over $CoCu/TiO_2$ catalyst and found that potassium promoter had no obvious effect on the textural properties and crystal structures, while decreased the reducibility of $CoCu/TiO_2$ catalysts. In addition, the introduction of K increased the chemisorption of CO_2, as seen by the increased desorption amount of CO_2 with increasing K content. However, the amount of H_2 adsorption decreased with the increase of K loading. The CO_2/H_2 adsorption behaviors changed slightly with further increase of K content, which was related to the slight change of surface K content. For the K-free $CoCu/TiO_2$ catalyst, the main product was CH_4, and its selectivity was up to 89.5 C-mol%. With the introduction of K, methane formation was suppressed and C_{5+} selectivity increased significantly with increasing potassium content. At the same time, CO_2 conversion decreased, and CO selectivity increased gradually. Therefore, a maximum C_{5+} yield with CO_2 conversion of 13% and C_{5+} selectivity of 35.1 C-mol% was obtained over the $CoCu/TiO_2$ catalyst with 2.5 wt.% of potassium promoter loading, which also afforded a considerable stable catalytic performance, indicating promising potential for industrial application. In a separate study, Shi *et al.* [85] reported that alkali metals addition could increase the CO_2 adsorption and reduce the H_2 chemisorption, which in turn reduces CH_4 formation, improves C_{5+} production, and decreases the hydrogenation activity. They also reported that Na-modified $CoCu/TiO_2$ catalyst showed highest C_{5+} yield of 5.4%, with a CO_2 conversion of 18.4% and C_{5+} selectivity of 42.1%, because it showed the strongest basicity and a slight decrease in the amount of H_2 desorption; it also exhibited excellent catalytic stability of more than 200 h.

2.8 Effect of catalyst support and metal loading during CO_2 hydrogenation to liquid hydrocarbons

Supported cobalt catalysts are employed for numerous chemical reactions for instance Fischer–Tropsch synthesis (FTS), CO preferential oxidation, CO_2 hydrogenation, soot conversion, steam reforming of ethanol and methane, hydrogen production, and hydrodesulphurization [86–94]. Several supports have been used to prepare cobalt-based catalysts, including SiO_2, Al_2O_3, MgO, TiO_2, Nb_2O_5, CeO_2, and ZrO_2 [90, 95–99]. Earlier reports indicated that during the preparation of some of these supported cobalt catalysts, cobalt-aluminate, cobalt-silicate, cobalt-niobate, cobalt-titanate, and cobalt-magnesia solid solutions are formed. The formation of these cobalt-support compounds may be disadvantageous to the catalytic activity of the cobalt metal as they are difficult to reduce [86, 91, 93, 96–101]. As a result, the formation of cobalt metal during reduction is subject to the type and degree of interaction of specific support with the cobalt metal. In addition, interactions of the cobalt with the support might as well be determined by the metal loading.

Das and Deo [102] investigated the effect of metal loading and support over several supported cobalt catalysts and reported that the hydrogenation of CO_2 depends on the type of metal oxide used as support and cobalt loading. Adsorbed CO and/or formate species were detected using FTIR on supported cobalt catalysts under reaction conditions. The existence and amount of the adsorbed species depended on cobalt particle size in the supported catalysts. The amount of the adsorbed CO was observed to rise with metal loading for silica supported cobalt catalysts, while it declined for alumina and zirconia supported cobalt catalysts. The difference in the amount of the adsorbed CO was difficult to determine for magnesia, titania and ceria supported cobalt catalysts. Adsorbed formate species were not detected for the series of silica- and niobia-supported catalysts, which seems to be linked to the ability of CO_2 to adsorb on the oxide support. It was previously proposed that the formate species is formed on the metal–support interface [91]. In addition, the location of the formate species in the supported cobalt catalysts is influenced by the specific support, which reiterates the significance of the metal–support interface towards the formation of the formate species. The deviation of the formate FTIR band seems to vary with metal-loading for the xCoAl, xCoMg, xCoTi, xCoCe and xCoZr catalysts (where x represents cobalt loading in %). In all these catalysts the formate amounts seem to decline with an increase in cobalt loading. The authors also concluded that the CO_2 conversion and the formate amounts are not connected. The CO_2 conversions and methane yields continuously increased with cobalt loading for the silica, alumina, zirconia and ceria supported

catalysts, whereas the conversion reached a maximum for the magnesia and titania supported cobalt catalysts. For the high cobalt loading catalysts, the CO_2 conversion and methane yield followed this trend: xCoCe > xCoMg>CoAl > xCoZr> xCoTi > xCoSi > xCoNb. This trend was inversely proportional to the cobalt metal crystallite size, with the exception of the xCoCe and xCoMg catalysts, where the cobalt metal crystallite size could not be determined, and the xCoTi catalysts where the crystallite size was relatively large. For lower loadings, on the other hand, the CO_2 conversion and methane productions were diverse and followed the following trend: 10CoMg > 10CoAl > 10CoZr >10CoSi > 10CoTi > 10CoCe > 10CoNb. The reasons for the strange behavior of the ceria supported cobalt catalysts, which displayed high conversions and CH_4 yields at high ceria loadings and very low conversions and yields at low loadings, is unknown.

Suslova *et al.* [103] studied the impact of CO_2 hydrogenation using cobalt-based FT catalysts and found that CO_2 conversion increases with an increasing metal loading of the catalyst for all support types used in their study. They also found that the methane selectivity was 100% over catalysts supported on Al_2O_3 and CNTs–Al_2O_3 composite and over all catalysts containing 45 wt % Co. The study of the catalysts containing 0.56 to 5 wt.% Co, that were prepared by impregnation and non-forced adsorption, revealed that 5Co/CNTs and 0.56Co/FLG were inactive in a wide temperature range. The authors concluded that Co/CNTs catalysts containing 0.56–5 wt.% Co are inactive in carbon dioxide hydrogenation. It was also evidenced that these catalysts can be activated by thermally prompted cobalt crystallization. It was suggested that carboxylated CNTs and nitrogen-hetero-substituted FLG fragments should be used to reduce the degree of deactivation of the Co nanoparticles on the support surface.

Investigating the effect of support for Co-Na-Mo catalysts on the direct conversion of CO_2 to hydrocarbons, Owen *et al.* [104] reported that the Co-Na-Mo catalysts supported on SiO_2 and ZSM-5 exhibited maximum CO_2 conversion values, with similar CO and hydrocarbon selectivity. In addition, catalysts supported on CeO_2, TiO_2, Al_2O_3 and ZrO_2 displayed comparable CO_2 conversions. On the other hand, the hydrocarbon selectivity, as opposed to, decreases in the order of ZrO_2< Al_2O_3< TiO_2< CeO_2. The catalyst displaying the lowest conversion, without any hydrocarbons formed, was supported on MgO, with only CO in the exit stream. The variation in CO_2 conversion was explained based on the difference in cobalt crystallite size. The metal–support interaction has also been revealed to be critical in determining not only the metals particle size but also their stabilization against sintering [105].

Owen *et al.* [104] observed a direct relationship between cobalt particle size and CO_2 conversion. Cobalt with particle sizes of 15 nm, existing in SiO_2 and ZSM-5, displayed just about double the CO_2 conversion compared to particles with sizes > 20 nm. In addition, the CO_2 conversion appears to be independent from the cobalt size, within the 20–35 nm range. The cobalt particle size similarly seems to influence the yield for CO and hydrocarbons. Co-Na-Mo supported on SiO_2 and ZSM-5 displayed higher hydrocarbon selectivities. Larger cobalt particles size (supported on CeO_2, TiO_2, Al_2O_3 and ZrO_2) showed a negative effect on the hydrocarbon yield, the HC/CO yield ratios were below 1. Instead, very small cobalt crystallites (< 2 nm) supported on MgO produced CO. The hydrocarbon distribution obtained from all catalysts fits the Anderson-Schulz-Flory (ASF) FT product distribution model [106], which backs the RWGS-FT tandem mechanism for the reduction of CO_2 to hydrocarbons. Co-Na-Mo supported on TiO_2 had the highest chain growth probability explaining the formation of heavy molecular weight hydrocarbon products. The other inorganic oxide supports showed marginally lower chain growth probability values with the following trend: TiO_2 > CeO_2 > Al_2O_3 > ZrO_2, where the methane selectivities varied in the range of 20–30%. These low methane selectivities are comparable to values published for iron-based catalysts [107] and are considerably lower than earlier data reported for cobalt based catalysts [65, 108 – 110]. It has been reported [100] that methane selectivity rises as the cobalt particle size decreases, with larger particles (> 20 nm) favouring the formation of heavy molecular weight hydrocarbons.

2.9 Effect of reaction conditions during CO_2 hydrogenation to liquid hydrocarbons

Fischer-Tropsch process conditions, including the operating pressure and temperature, have a complex relationship with the liquid product distribution. Normally, the process is run in the temperature range of 150–350 °C. If the catalyst selected is cobalt-based, the temperature range required is 200–240 °C, which represents the low-temperature Fischer-Tropsch (LTFT) process. On the other hand, if the catalyst used is iron-based, a temperature range of 300–350 °C is used and constitutes the high-temperature process Fischer-Tropsch (HTFT) but can, however, operate successfully using either cobalt-based or iron-based catalysts. Higher temperatures cause more rapid reactions but correspondingly lean towards formation of methane. Therefore, the temperature is generally kept at the low to mid portion of the range (200–300 °C). On the other hand, increasing the pressure generally results in higher rate of conversion and also promotes the production of heavy molecular weight alkanes. Higher

pressures would be favorable, but then the benefits might not justify the extra expenses of high-pressure equipment, and higher pressures may possibly result in catalyst deactivation through coke formation.

Dorner *et al.* [108] investigated the effect of pressure on the hydrogenation of CO_2 and found that the rate of both CO_2 and H_2 consumption continued to drop during a time period of 1000 h on stream by roughly 86 and 37% respectively. The decline in conversion rate was related to the deactivation of the catalyst with time-on-stream (TOS) instead of a change in gas feed composition. This was confirmed by the fact that, when changing from CO_2 back to CO in the feed gas after 1000 h, a noticeable decrease in syngas conversion rates (around 24%) was observed relative to the initial rates attained over a fresh catalyst. When CO_2 was added to the feed gas (with a ratio of $H_2/CO_2= 3:1$), the major product that formed was methane (97.6%). As the authors were trying to move product distribution away from methane in the direction of longer chain hydrocarbons, they changed the ratio of H_2/CO_2 from 3:1 to 2:1 (using N_2 as an inert gas equaling the volume of replaced CO_2) and successively to 1:1. Besides the feed gas ratio (or the partial pressure of reactants), other reaction conditions were kept constant. Remarkably, the portion of longer chain hydrocarbons (i.e., hydrocarbons other than methane) increased with increasing TOS, regardless of the H_2/CO_2 ratio (i.e., between 753 and 1000 h TOS at a constant H_2/ CO_2 ratio equals to 1:1). The product distribution throughout the run, on the other hand, vastly favored methane as the leading product. It was possible to obtain a larger fraction of C_2-C_4 products though (up to 6.9% at H_2/CO_2 equals to 1:1) upon decreasing the H_2 partial pressure in the feed gas. The production of olefins was negligible, but, when decreasing the H_2/CO_2 ratio to 1:1, it was possible to marginally increase the amount of olefins formed. This was presumably caused by the deficiency of H_2 in the gas feed.

They also observed that, as the H_2 consumption in the feed gas declined from 45.19 to 28.58%, the CO_2 conversion was reduced from 40.03 to 5.56%. Overall, the best C_2-C_4/methane ratio was obtained when switching to a 1:1 H_2/CO_2 feed gas ratio. Parallel to the decline in methane selectivity when reducing the H_2 content in the feed gas, the overall conversion of the catalyst decreased, and this was explained by deactivation of the catalyst with increasing TOS. The influence that pressure had on the reaction products at a fixed H_2/CO_2 ratio of 3:1 was also considered. As the pressure was decreased from 450 to 150 psi, the rate of CO_2 and H_2 conversion was reduced from 41.18 to 4.67% and 50.55 to 10.55% respectively. They also observed that, with a drop in pressure, the selectivity of longer chain hydrocarbons increased

and methane formation was suppressed, but the olefin selectivity became negligible as the pressure was reduced to 150 psig.

Methane was the predominant reaction product when the feed contained CO_2. But, with increasing TOS, a small increase in CO_2 conversion to C_2-C_4 products was noticed. This behavior was explained by a change in catalyst morphology; as the H_2/CO_2 consumption ratio adjusted to changes in the ratio in the feed, an overall constant consumption of the different feed components was detected. The supported cobalt-based catalyst used was promoted with Pt. Since it was previously reported that the addition of Pt enhances the CO hydrogenation rate without disturbing the active sites of cobalt [111], it was therefore suggested that Pt increases the hydrogenation rate on cobalt by increasing the amount of cobalt being reduced [111-113]. As the TOS was increasing, the possibility for carbonaceous deposits to coat portions of the catalyst arose [114], these deposits were assumed to be most likely located on cobalt particles instead of the Pt promoter, due to the role that cobalt plays in the CO_2 hydrogenation mechanism. These deposits seem to favor certain active sites of the catalyst, that is, stepped versus flat surfaces, resulting in a reduction in the overall methanation capability of the catalyst and, accordingly, an increase in heavy molecular weight hydrocarbons being produced instead of methane. The step sites have shown to be the actively more favorable for chain growth over other sites in the FT process [115]. Dorner *et al.* [108] also indicated that the same type of sites are responsible for chain growth in the hydrogenation of CO_2 to higher chain hydrocarbons. The nature of the reaction products and the change in their distribution with increasing TOS shows the existence of at least two different sites for CO_2 hydrogenation. They concluded that methane production occurs on one specific surface, probably a flat surface because it might display a preference for tripodal CO_2 adsorption [116]. As carbonaceous deposits display a preference for this site and, methane formation declines with increasing TOS. The C-C combination reaction site was perhaps not as much affected by coking, which led to the increased fraction of C_2-C_4 products being produced. The deactivation of certain active sites which contributed to the formation of methane appears to play part in the small change in products leaning towards heavy molecular weight hydrocarbons with increasing TOS, as can be inferred by the decreased amount of methane being formed.

2.10 Reverse – water – gas – shift reaction

For many years, emission of CO_2, which is the core greenhouse gas has increased. Catalytic reduction by the reverse water gas shift (RWGS) reaction is an effective technique to make use

of carbon dioxide and shrink its environmental influence as a greenhouse gas. The water gas shift reaction was discovered by an Italian physicist Felice Fontana in 1780 [117]. It consists of reacting carbon monoxide with water to produce hydrogen and carbon dioxide. The reverse of this reaction is shown by equation 2.4, where CO_2 is hydrogenated to CO. Direct conversion of CO_2 into valuable products is characterized by very low conversion rates, even though CO is extremely reactive and the RWGS reaction (2.4) has comparatively high equilibrium conversion rate [118]. By eliminating water from the product stream, the formed CO together with suitable quantity of H_2 can form synthesis gas and be used as feedstock for methanol and Fischer-Tropsch synthesis.

$$CO_2 + H_2 \rightarrow CO + H_2O \quad \Delta H_{298K} = 41.2 \text{ kJmol}^{-1}$$ …………………………….. (2.4)
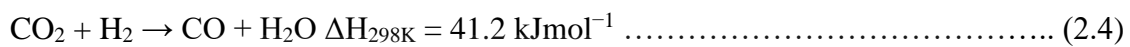
An application of this reaction can be summarized by Figure 2.2.
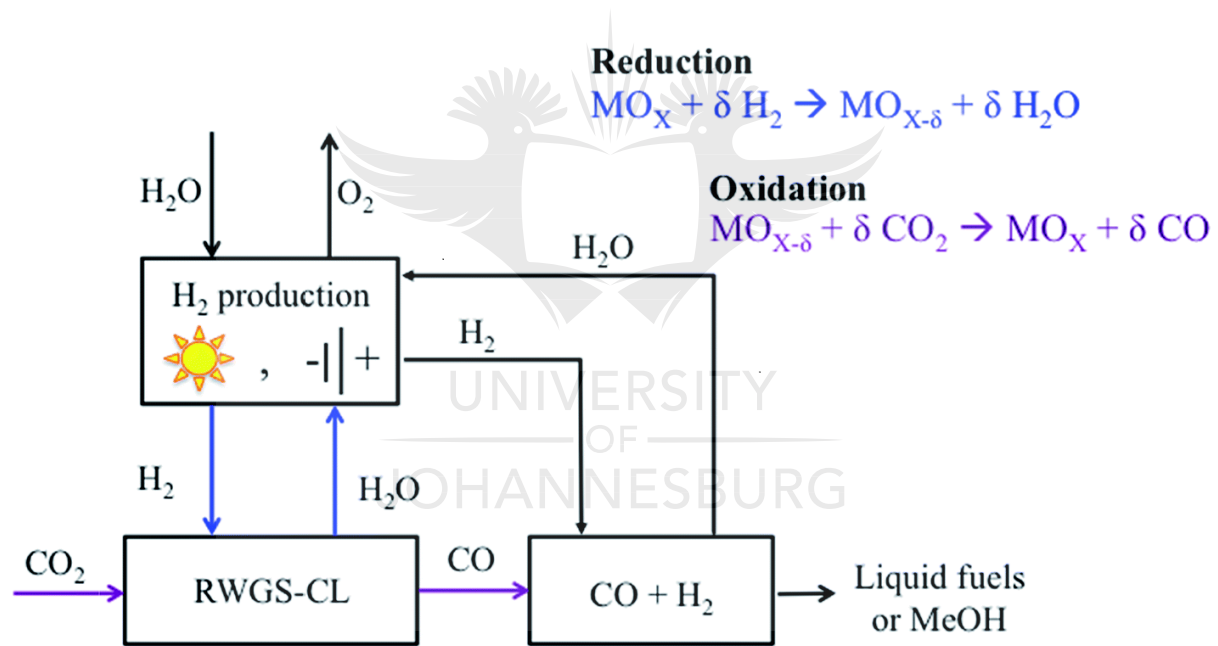
Figure 2. 2: Reverse water gas shift reaction [119].

An important aspect of this figure is the fact that CO_2 enters the system, which in turn produces liquid fuels or methanol and only reject O_2 to the environment. This is only possible if the hydrogen used comes from a source that does not emit CO_2, such as solar.

Carbon dioxide has been considered a promising contestant for RWGS reaction, as it can be converted to CO via the reverse water–gas shift reaction. The RWGS reaction has been broadly studied by using supported metal catalysts like Pt [120–123], Ni [124–127], Cu/Zn [128–132], Au [133–135], Fe [136–139] and so on. In addition to these catalyst systems, RWGS reaction

using solid oxide fuel cell system has also been probed [140]. Many of these reactions are conducted at high temperature, above 300 °C. Some researchers have performed RWGSR by using complexes of transition metals such as Rh [141] and Ru [142–144] as homogeneous catalysts. These catalysts can make the RWGSR to proceed at reasonably low temperature, below 200 °C. In hydroformylation [145–148], an alkene reacts with synthesis gas in the presence of a catalyst to give an aldehyde or an alcohol that contain an extra carbon in their chemical structure as compared to the starting alkene. Hence, this reaction has been broadly investigated for application to largescale industrial chemical processes. Lately, Tominaga tried to develop an environmentally-friendly hydroformylation reaction using non-toxic CO_2 as an alternative of CO, and found that, by using the ruthenium cluster homogeneous catalyst $Ru_3(CO)_{12}$, hydroformylation of various kinds of alkenes (1-hexene [149], cyclohexane [150], α-methylstyrene [151] and so on) can proceed under a H_2/CO_2 mixed gas atmosphere. In these cases, the reaction begins from CO evolution by the RWGSR and hydroformylation subsequently occurs [150]. An attractive feature of this one-pot reaction is that hydroformylation can proceed without any purification of the mixed gas resulting from the RWGSR; consequently, the RWGSR and subsequent hydroformylation happen in the same reactor vessel, making this process a likely substitute to conventional CO-based industrial processes.

Numerous supports have been examined in this process. CeO_2 is usually studied as catalyst support because of its high oxygen storage capability [152]. Ni, Cu, Co, Fe, Mn and Pt have been supported on CeO_2 [153–156]. Nickel catalysts supported on ceria demonstrated good catalytic activity. On the other hand, by increasing the nickel content higher than 2%, methanation as the main side reaction increased and the selectivity to CO decreased. Monometallic Ni, Cu, Fe, Pd and bimetallic combinations such as Ni-Cu, Fe-Mo, Fe-V_2O_5, Fe-K, Ni-K, Pd-La and Pd-Ce were supported on Al_2O_3 as cost effective support [157–162]. Al_2O_3-supported nickel catalysts displayed high CO_2 conversion and low selectivity towards CO. Addition of K as alkaline promoter to Ni/Al_2O_3 catalysts suppressed methanation. Potassium increased the basicity of catalyst and created new active sites that expedited formation and decomposition of formate intermediate [161]. Ni, Cu, Fe, Pt, Au and bimetallic combinations like Pt-K, Au-Mo have been supported on silica. Silica-supported nickel catalysts suffer from low CO_2 conversion rates at low metal contents, where addition of nickel loading promotes the methanation process [163–168]. Mesostructured silica supports such as SBA-15, with their modified structure and high specific surface area, could better disperse Ni particles;

they displayed higher CO_2 conversion and CO selectivity as compared to SiO_2 [169]. Transition metal carbides (TMCs) have received significant attention with their dual functionalities for H_2 dissociation and C=O bond scission. Ni, Cu and Co have been supported on Mo_2C; they all exhibited high CO_2 conversion and CO selectivity at higher pressures. The main problem of TMCs is that they cannot stand high temperatures [170 – 171]. Rodrigues *et al.* used Mg(Al)O ($MgO:Al_2O_3$=70:30) mixed oxide as support for Ni catalysts [172]. Great catalytic performance and CO selectivity on these catalyst were related to Mg(Al, Ni)O vacancies and Ni species on the surface of the catalyst. Other types of oxides like ZrO_2, ZnO, In_2O_3, Ga_2O_3 and their mixture with CeO_2 were also utilized in RWGS reaction. The presence or incorporation of CeO_2 created more oxygen vacancies and enhanced CO_2 adsorption [173–179]. Mixed oxide solid solutions like $Zn_xZr_{1-x}O_{2-y}$, Fe_2O_3-$Ce_{0.5}Zr_{0.5}O_2$, $La_{0.75}Sr_{0.25}CoO_3$ and $BaZr_{0.8}Y_{0.16}Zn_{0.04}O_3$ have also been evaluated in RWGS reaction. These solid solutions displayed high oxygen mobility and activity at high temperatures [180–183].

2.11 CO_2 methanation

Carbon dioxide methanation, known as Sabatier reaction, has been studied for over a century [184–185]. Initially, the research activity has been focused on the development of catalysts for improvement of coal gasification processes. In the next years, studies were also broadened to the environmental aspects of CO_2 reduction [186–189]. Rising consumption of fossil fuels, which results in the increase of carbon dioxide production, is regarded as one of the most significant aspects contributing to the greenhouse effect. Carbon dioxide is also discharged to the atmosphere during oxidative degradation of several products manufactured from natural gas, oil or coal. Furthermore, it is formed as a byproduct in the processing of biomass, e.g. during biogas or bioethanol production or biomass gasification. Biogas is produced in the anaerobic fermentation of organic materials. It contains in average from 40 to 75% of CH_4 and from 25 to 50% of CO_2. Conversion of CO_2 separated from biogas to methane by the application of renewable hydrogen, may increase its heating value and as a result improve the economic impact of renewable energy production.

CO_2 methanation is a very exothermic reaction (2.5); from the thermodynamic point of view, it can be conducted with high selectivity to methane at low temperatures and high pressure [184–192]:

$$CO_2 + 4H_2 \rightarrow CH_4 + 2H_2O \quad \Delta H^0_{298K} = 165 \text{ kJ mol}^{-1} \tag{2.5}$$

31
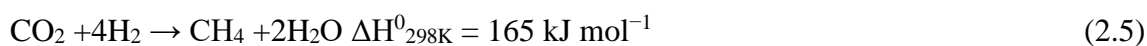
Nickel supported catalysts are most active in CO_2 methanation reaction and at the same time reasonably low-priced. High activity and selectivity were reported for nickel catalysts with various supports, including ceria, zirconia, alumina and silica [184–192]. It is generally acknowledged that catalyst support plays multiple roles in the CO_2 methanation reaction. It may slow down sintering of nickel oxide species and metallic nanoparticles on the later stages of catalyst preparation, activation and operation under reaction conditions with the time-on-stream. The support may also affect the course of surface catalytic reactions, for example. by facilitating dissociative adsorption of CO_2, transformation of surface species, as well as products desorption [190–192].

2.12 CO_2 hydrogenation to methanol

The synthesis of the base chemical methanol from the greenhouse gas CO_2 and H_2 is a promising approach to store renewable energy and produce a chemical feedstock ($CO_2 + 3H_2 \rightarrow CH_3OH + H_2O$) [193 – 194]. Contrary to H_2, methanol is liquid at room temperature and therefore it can easily be stored, transported and further processed e.g. to oxymethylenedimethylethers (a novel class of fuels that promises rich applications [195]). Moreover, conversion of CO_2 to methanol is of great environmental relevance as a strategy for decreasing the concentration of this anthropogenic greenhouse gas in the atmosphere [196 – 197].

Hydrogen as a high energy compound can react with carbon dioxide to produce hydrocarbon fuels, methanol, carboxylic acids, etc. [198 – 201]. Among these processes, methanol (MeOH) is of great interest for the conversion of CO_2 with H_2. Methanol can be used in the petrochemical and energy industries for chemical or energy uses [198, 202 – 207]. Similarly, direct methanol fuel cell, as an innovative application leads to give it more attention [208 – 210]. Hydrogen from a renewable source such as water splitting, is required to reduce the life cycle carbon dioxide emissions in the process. The eco-friendly sources of raw materials yield to an attractive green methanol synthesis process [200, 211].

Two different synthesis routes for CO_2 conversion into methanol were proposed: direct and indirect hydrogenation. In the former, CO_2 and H_2 are directly converted into methanol, while in the later, syngas is first produced by hydrogenation of CO_2 in a reverse water gas shift (RWGS) reactor and next the syngas is conveyed to a reactor as raw material to produce methanol. The second route is called the CAMERE (carbon dioxide hydrogenation to methanol

via reverse water gas shift reaction) process (fig. 2.3). This process was suggested because of low conversion of CO_2 over the traditional methanol synthesis catalyst ($Cu/ZnO/Al_2O_3$) during the direct synthesis process [4]. There are only a few publications on the topic related to methanol production by the CAMERE process, where the main focus of the research was the catalyst development. Joo *et al.* [212] studied methanol synthesis from carbon dioxide via RWGS reaction (CAMERE process). Their results showed that the low efficiency of the commercial catalyst ($Cu/ZnO/Al_2O_3$) was dominated by integrating of the RWGS reactor with the methanol synthesis reactor. Park *et al.* [213] synthesized and developed Zn/Al_2O_4 and ZnO/Al_2O_3 catalysts for RWGS reaction. Although ZnO/Al_2O_3 showed a higher activity than $ZnAl_2O_4$, it was deactivated due to the reduction of ZnO. In another related work, they investigated and compared the activity and stability of Fe_2O_3/Cr_2O_3 and ZnO/Cr_2O_3 catalysts for the RWGS reaction. Their results revealed that ZnO/Cr_2O_3 is a more suitable catalyst for this reaction [214].
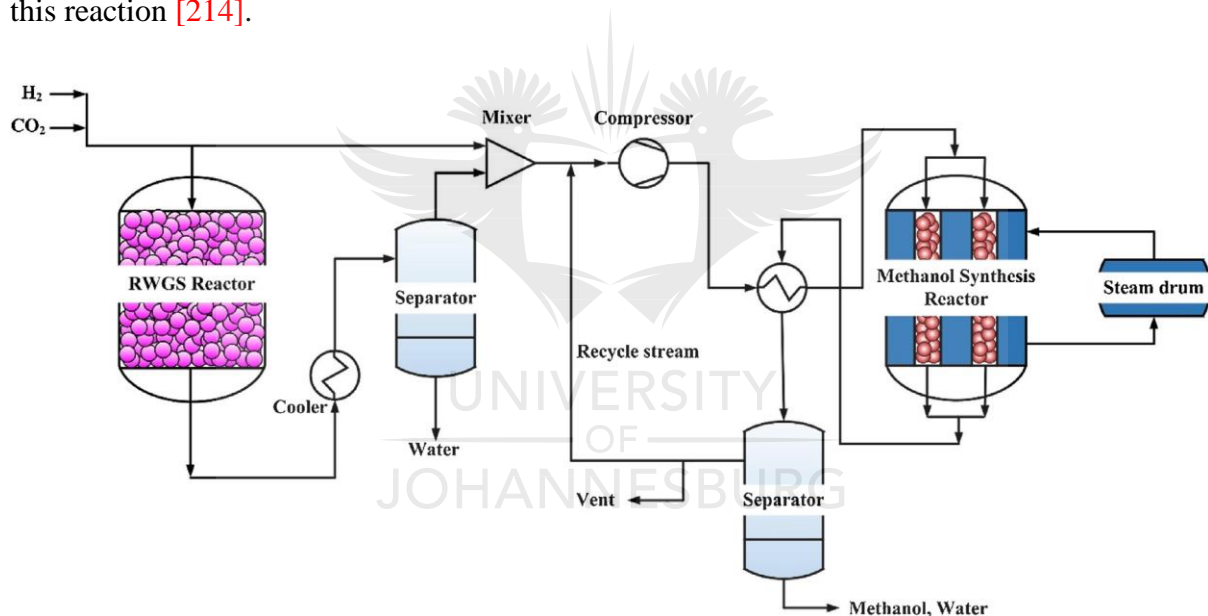
Figure 2. 3: A schematic diagram of the CAMERE process [215].

Fig 2.3 shows a schematic diagram of the CAMERE process. Methanol synthesis by the CAMERE process comprises a RWGS reactor and a methanol synthesis reactor. The feedstock containing carbon dioxide and hydrogen is divided into two streams: the main portion which is sent to the RWGS reactor, while the remaining portion is required to adjust the composition of produced syngas. CO_2 and H_2 are partially converted into CO and H_2O by the RWGS reaction in an adiabatic reactor. The reaction products, which include syngas (CO, CO_2 and H_2) and water are sent to the condenser to eliminate water from the stream, as it is a poison for the $Cu/ZnO/Al_2O_3$ catalyst in the next reactor. The produced syngas is then fed into the methanol

synthesis reactor, after transmission through a series of compressors and a heat exchanger to attain the desired temperature and pressure of the reactor. Boiling water in the shell side of the reactor is used to control the temperature of exothermic reactions. Afterwards, the reactor outlet is transported to a condenser to separate methanol and water, as the condensable gases from the unreacted gas. Some part of the unreacted gas is recycled to the reactor to increase conversion.

Very few studies have focused on the process model and increase of methanol production from carbon dioxide. Samimi *et al.* [215] investigated methanol production process from CO_2 via RWGS reaction (CAMERE process) in an industrial scale. The RWGS reactor operating conditions were optimized to achieve high methanol production rate. Furthermore, to minimize water formation, an H-SOD (hydroxy sodalite) membrane was used in the methanol synthesis reactor for removal of water during the reaction. This membrane is a zeolite-like material with excellent selectivity of water. The ultimate value of water permeation through H-SOD was published as $10-6$ mol/(s m^2Pa) for an ideal case [216 – 218]. The feasibility of the CAMERE process to produce methanol was compared with the conventional route (CR) of methanol synthesis by Samimi *et al.* [215]. These authors found that the methanol production rate increased by 88 ton/day in the CAMERE process compared to CR, however higher water production rate in the CAMERE process was not desired. This problem was solved with applying a water perm-selective membrane in which the water production was remarkably reduced.

2.13 Direct and indirect CO_2 hydrogenation to liquid fuels

Most research to date, not surprisingly, is focusing on the CO_2 hydrogenation to various C_1 feedstock (e.g., CH_4, CH_3OH, CO, HCOOH) [219 – 223], while few studies are focused on liquid fuels (C_{5+} hydrocarbons) due to the extreme inertness of CO_2 and a high C – C coupling barrier [224]. Production of hydrocarbons from CO_2 hydrogenation proceeds via two routes: direct and indirect routes. One promising route is the direct production of hydrocarbons, including both alkanes and olefins, which combines the reduction of CO_2 to CO by reverse water-gas shift reaction (Eq. 2.4) and subsequent hydrogenation of CO to hydrocarbons via modified Fischer-Tropsch synthesis process (Eq. 2.6) [225]. The indirect route is often performed by using different reactors with syngas and/or methanol intermediate formation [226 – 227]. Nonetheless, as compared with the indirect route, the direct route would be more economic and energy-efficient.
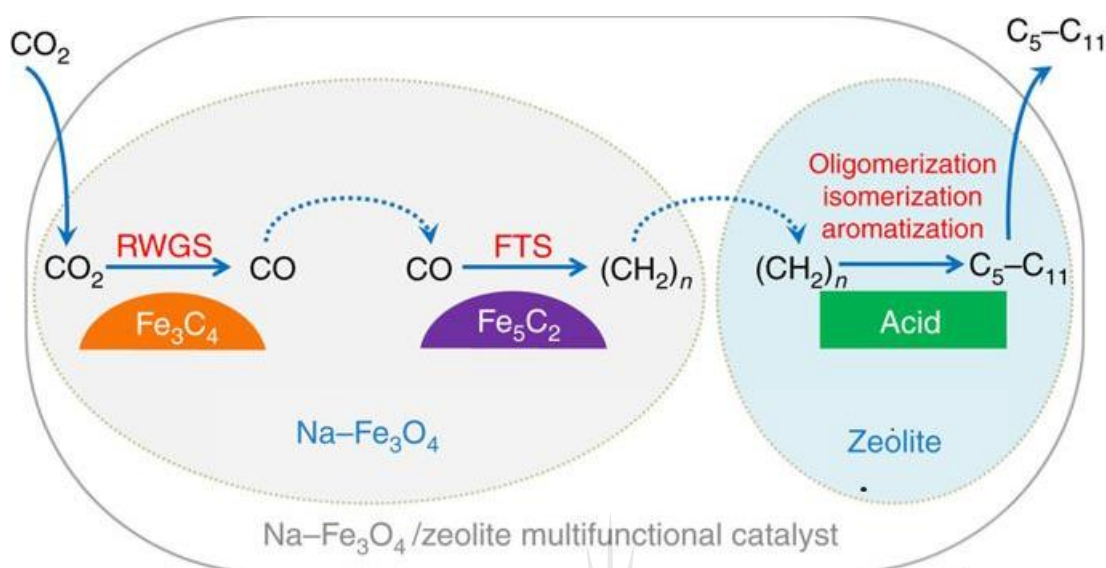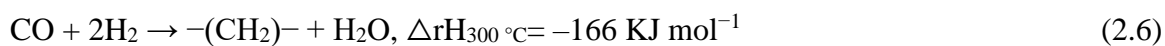
$$CO + 2H_2 \rightarrow -(CH_2)- + H_2O, \triangle rH_{300\,^\circ C} = -166 \text{ KJ mol}^{-1} \qquad (2.6)$$

Figure 2. 4: Reaction scheme for CO_2 hydrogenation to gasoline-range hydrocarbons [228].

Thermodynamically, as it is a slightly endothermic reaction, the conversion of CO_2 by RWGS is limited at low temperature. For that reason, many research groups studied the catalysts for CO_2 hydrogenation to hydrocarbons at high temperature (300 – 400 °C) [229 – 231]. To date, between the two industrially used FTS catalysts (Fe and Co), Fe is often selected for modified FTS using CO_2 since Co has been reported to perform as a methanation catalyst more than an FTS catalyst at high temperature [232 – 235]. This can explain why reports on CO_2 hydrogenation to hydrocarbons or alcohols using cobalt-based catalysts are limited. In traditional low temperature FTS (< 250 °C), cobalt-based catalysts are preferred for their high activity, high yields of long-chain hydrocarbons, high mechanical strength and high stability, compared to iron-based catalysts. In addition, cobalt catalysts are cheaper than noble metals such as Ru-based catalysts [236 – 237]. In recent times, Co-based catalysts have displayed a promising catalytic performance for CO_2 hydrogenation to light hydrocarbons and C_{2+} alcohols [238 – 239]. In addition, the incorporation of other metals like Cu, Pd, Pt and Ru to cobalt-based catalysts to improve CO production has not been adequately explored. Copper-based catalysts, the most popularly studied catalytic systems for the WGS reaction, have also been applied to the RWGS reaction [240]. Thus, the Co–Cu bimetallic catalyst can potentially be an efficient catalyst for CO_2 hydrogenation to hydrocarbons.

During CO_2 hydrogenation based on modified FTS process, the degree of hydrogenation of surface-adsorbed intermediates is higher because of the slower adsorption rate of CO_2 compared with CO hydrogenation, leading to much easier formation of CH_4 with a decreased chain growth [241]. For this reason, presently there remains a significant challenge to increase the chain growth and suppress the formation of methane. Akin *et al.* found that products of CO_2 hydrogenation contain about 70 C-mol% of methane over Co/Al_2O_3 catalyst [242]. Alkali metals like Na and K have been widely investigated as promoter of iron-based catalysts used for CO_2 hydrogenation [230, 234, 243 – 244]. They were found to suppress the formation of CH_4, increase the chain growth probability and improve the production of olefins. Additionally, their effects on the product selectivity have been found to be strongly dependent on their concentration.

2.14 CO_2 hydrogenation mechanism

$Cu/ZnO/Al_2O_3$ is the most commonly used industrial catalyst for synthesis of methanol from synthesis gas (syngas) containing CO and CO_2 [245–247]. The role and interaction of the different components in the catalyst under reaction conditions are under active discussion. Some researchers claim that the active phase depends on the Cu-Zn alloy formed under reaction conditions upon partial reduction of the ZnO phase [247, 248]. On the other hand, industrial catalysts were reported to contain a ZnO_X-overlayer on metallic Cu-nanoparticles [245]; recent experimental results display evidence of an improved catalytic activity of ZnO_X particles on Cu (111) relative to the conventional metal-on-oxide configuration [249 – 253]. These results strongly support the idea that the active sites in methanol synthesis catalysts correspond to the ZnO phase or to the ZnO-Cu interface [245 – 246, 249 – 250, 254 – 255]. In addition to their often-superior activity, inverse catalysts have become a valuable tool for investigating reaction mechanisms and the role of the oxide and the metal-oxide interface [256 – 259]. Likewise, recent density functional theory studies of supported oxide-clusters-models brought new understandings to the catalytic activity of $PtCo/TiO_2$ and $PtCo/ZrO_2$-catalysts concerning CO_2-hydrogenation [260]. The $CeO_X/Cu(111)$-system was reported to show an even superior performance compared to $ZnO_X/Cu(111)$, with the reaction mechanism consisting of a reverse water–gas shift (Eq. 2.4) followed by the CO hydrogenation (Eq. 2.7) [256].

$$CO + 2H_2 \rightarrow CH_3OH\ldots\ldots\ldots\ldots\ldots\ldots\ldots\ldots\ldots\ldots\ldots(2.7)$$

A similar reaction path was lately proposed on Cu supported ZrO_2 and on TiO_2 [261]. In contrast, most of theoretical and experimental investigations point to the fact that hydrogenation of CO_2 over Cu/ZnO catalysts does not proceed through a CO-intermediate [246, 250, 255, 262 – 263].

CO_2 also hydrogenates to hydrocarbons both directly and indirectly, that is, via synthesis gas and/or methanol production as intermediate [264]. Indirect routes include a multi-stage approach using separate reactors and a single-reactor-approach using hybrid catalysts to perform the multi-step transformation [265]. Lee *et al.* [266] proposed a reaction mechanism for hydrogenation of CO_2 to a hydrocarbon. CO_2 is reduced by iron (II) followed by H radical abstraction by the species adsorbed on the catalyst surface (Fig. 2.5). The residual H reacts with the carbonyl C to form OH, formic acid and CO. Fe-CH_2 radical forms in a similar manner as a carbon-carbon propagation species. Chain propagation represents the main reaction pathway since higher hydrocarbons are the main products. Higher α-olefin selectivity to paraffins is attributable to less H_2 uptake and no excess H_2 in this reaction system; therefore, the hydrogen dosing during the reaction is critical.
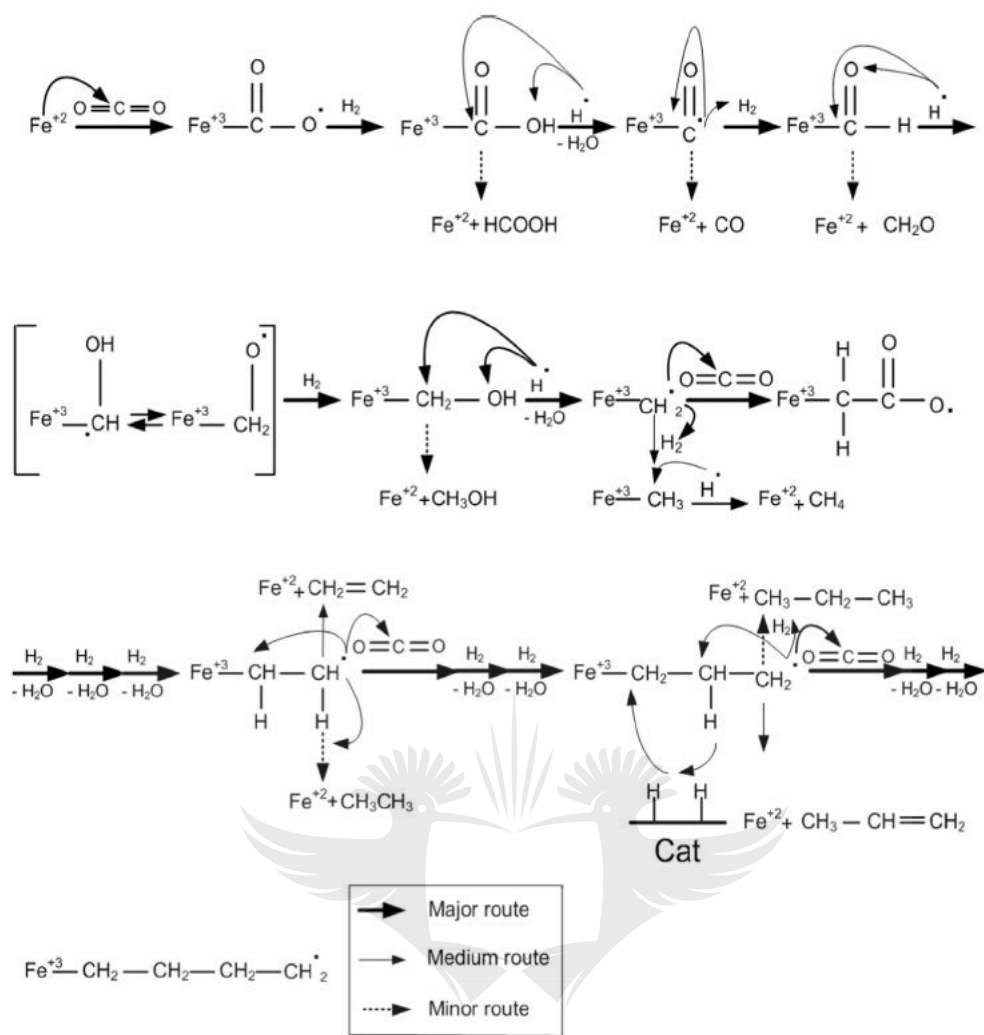
Figure 2. 5: Proposed overall reaction mechanism of CO_2 hydrogenation [266].

Lee *et al.* [267] explored H_2/CO_2 hydrogenation to hydrocarbon to investigate the deactivation route of Fe–K/γ-Al$_2$O$_3$ catalyst using XPS, HR-TEM, TPO, and Mossbauer spectroscopy. The iron-based catalysts deactivated considerably during CO_2 hydrogenation process as a result of catalyst poisoning and carbon deposition. The deactivated catalyst analyses provided knowledge on deactivation route as a function of time and catalyst position. The deactivation route differed with reactor position. As time progressed, hematite (Fe$_3$O$_4$) generated after H_2 reduction and was then gradually carbonized to χ-Fe$_5$C$_3$. Eventually, the χ-Fe$_5$C$_3$ phase was changed to χ-Fe$_3$C, which is not an active species for CO_2 hydrogenation. The main deactivation pathway in the inlet reactor region was phase transformation while the principal parameter at the reactor outlet region was coke deposits generated by secondary reactions.

Jacobs *et al.* [268] synthesized two kinds of Co$_3$O$_4$ catalysts by precipitation methods using nano-replicating technique to clarify mesoporosity effects of a Co$_3$O$_4$ catalysts. The

38

mesoporous Co_3O_4 indicated a proper initial activity with high mass-transfer rates of heavier FT products. These catalysts deactivated through changes in porosity and morphology due to coke deposition [259]. Van der Laan and Beenackers [269] determined the thermal stability and catalytic activity of zirconium phosphate (ZrP) supported-Co/ZrP/SiO_2 promoted with ruthenium during FTS reaction and found that phosphorous prevents cobalt particle aggregation and improves catalyst stability due to surface modifications. The thermal stability of these catalyst arises from the spatial confinement of cobalt particles [269].

2.15 Kinetic models for CO_2 hydrogenation over traditional FT catalysts

The kinetics for CO_2 hydrogenation reaction are extremely vital for industrial practices since they are required for process simulation, optimization and scale-up. Despite broad studies on FTS and WGS reactions kinetics [270 – 273]. The reaction mechanism for CO_2 hydrogenation to higher molecular weight hydrocarbons is complex with many reactions and species involved [274, 275 – 277].

Riedel *et al.* developed a non-Langmuir–Hinshelwood Hougen–Watson (LHHW) kinetic model using integration and regression features of ASPEN PLUS software for CO_2 hydrogenation on a potassium promoted iron catalyst [278]. Expressions for this kinetic model (LHHW) are given by Eqs. (2.8) – (2.11).

$$k_{SH} = \frac{\rho_{cat} R_g T k_{SH0} \exp\left[-E_{SH}/(R_g T)\right]}{[(CO + a_{SHH_2O}(H_2O) + b_{SHCO_2}(CO_2)]} \dots\dots\dots\dots\dots(2.8)$$

$$k_{SH} = \frac{\rho_{cat} R_g T k_{FT0} \exp\left[-E_{FT}/(R_g T)\right]}{[(CO + a_{FTH_2O}(H_2O) + b_{FTCO_2}(CO_2)]} \dots\dots\dots\dots(2.9)$$

$$k_{FTs} = \frac{\rho_{cat} R_g T k_{FTs0} \exp\left[-E_{FTs}/(R_g T)\right]}{[(CO + a_{FTsH_2O}(H_2O) + b_{FTsCO_2}(CO_2)]} \dots\dots\dots\dots(2.10)$$

$$K_{eq} = 10^{(2.029 - 2073/T)} \dots\dots\dots\dots\dots\dots(2.11)$$

where T is reaction temperature, Rg is universal rate constant, rcat is the catalyst density, which is defined as the mass of impregnated catalyst, Mc/bed volume. The kinetic constants k_{SH}, k_{FT} and k_{FTs} depend on the activation energies E_{SH}, E_{FT}, E_{FTs} for the RWGS, FT, and methanation reactions respectively. The parameters k_{SH0}, k_{FT0} and k_{FTs0} are the pre-exponential coefficients for the RWGS, FT, and methanation reactions respectively. The parameters a_{SHH_2O}, b_{SHCO_2},

a_{FTH_2O}, b_{FTCO_2}, a_{FTsH_2O}, b_{FTsCO_2} are the adsorption constants for the RWGS, FT, and methanation reactions respectively.

Willauer *et al.* used the kinetic model developed by Riedel *et al.* for comparison of experimental results obtained from CO_2 hydrogenation to higher hydrocarbons over Mn and K-promoted iron catalyst in fixed-bed and continuously stirred tank (CSTR) reactors [279]. They found that the maximum C_2–C_{5+} yield obtained in the fixed-bed experiments was 49% higher than that obtained in CSTR at lower gas hourly space velocity [279]. No kinetic models for CO_2 hydrogenation over cobalt-based catalysts were found in the literature.

2.16 Summary

Reports in the literature indicate that CO_2 can be hydrogenated directly (via modified Fischer – Tropsch synthesis) or indirectly (via methanol synthesis) into hydrocarbons. The reverse – water – gas – shift reaction is believed to be essential for transforming CO_2. Product produced during CO and CO_2 hydrogenation are reported to be different. For CO hydrogenation, typical FT products are obtained while methane has been reported to be the predominant product during CO_2 hydrogenation. In some instances, only traces of other short hydrocarbons (C_2 – C_4) were also observed when FT operating conditions and catalysts were modified. In addition, alkali promoters are reported to promote chain growth. They are reported to cause a charge transfer from alkali metals to catalyst surface, thereby inhibiting H_2 adsorption but enhancing CO_2 chemisorption and dissociation. CO_2 can also be converted to methanol. Two different synthesis routes for CO_2 conversion into methanol were proposed: direct and indirect hydrogenation. In the former, CO_2 and H_2 are directly converted into methanol, while in the latter, syngas is first produced by hydrogenation of CO_2 in a reverse water gas shift (RWGS) reactor and next the syngas is conveyed to a reactor as raw material to produce methanol.

REFERENCES

[1]. X. Xiaoding, J.A. Moulijn, "Mitigation of CO_2 by Chemical Conversion: Plausible Chemical Reactions and Promising Products", Energy & Fuels, 10, (1996) 305–325.

[2]. K. Stephenne, "Start-up of world's first commercial post-combustion coal fired CCS project: contribution of Shell Cansolv to SaskPower Boundary Dam ICCS project", Energy Procedia, 63, (2014) 6106–6110.

[3]. K.M.K. Yu, I. Curcic, J. Gabriel, S.C.E. Tsang, "Recent Advances in CO_2 Capture and Utilization", ChemSusChem: Chemistry & Sustainability Energy & Materials, 1, (2008) 893–899.

[4]. B. Anicic, P. Trop, D. Goricanec, "Comparison between two methods of methanol production from carbon dioxide", Energy, 77, (2014) 279–289.

[5]. M.K. Gnanamani, G. Jacobs, W.D. Shafer, D. Sparks, B.H. Davis, "Fischer–Tropsch synthesis: deuterium kinetic isotope study for hydrogenation of carbon oxides over cobalt and iron catalysts", Catalysis Letters, 141, (2011) 1420–1428.

[6]. H.Q. Tang, J.L. Li, "Performance of silica-nanotube-supported ruthenium catalysts for Fischer-Tropsch synthesis", Journal of fuel chemistry and technology, 39(8), (2011) 615–620.

[7]. M.A. Vannice, R.L. Garten, "Influence of the support on the catalytic behavior of ruthenium in CO/H_2 synthesis reactions", Journal of catalysis 63 (1980) 255–260.

[8]. A. Kogelbauer, J.G. Goodwin Jr, R.J. Oukaci, "Ruthenium Promotion of Co/Al_2O_3 Fischer–Tropsch Catalysts", Journal of Catalysis 160 (1996) 125.

[9]. Y. Yao, X. Liu, D. Hildebrandt, D. Glasser, "Fischer–Tropsch synthesis using $H_2/CO/CO_2$ syngas mixtures: A comparison of paraffin to olefin ratios for iron and cobalt based catalysts", Applied Catalysis A: General, 433–434, (2012) 58–68.

[10]. T. Riedel, H. Schulz, G. Schaub, K.W. Jun, J.S. Hwang, K.W. Lee, "Fischer–Tropsch on Iron with H_2/CO and H_2/CO_2 as Synthesis Gases: The Episodes of Formation of the Fischer–Tropsch Regime and Construction of the Catalyst", Topics in Catalysis, 26, (2003) 41–54.

[11]. A.N. Akin, M. Ataman, A.E. Aksoylu, Z.I. Onsana, "CO_2 fixation by hydrogenation over coprecipitated Co/Al_2O_3", Reaction Kinetics and Catalysis Letters, 76, (2002) 265-270.

[12]. R.W. Dorner, D.R. Hardy, F.W. Williams, H.D. Willauer, "Heterogeneous catalytic CO_2 conversion to value-added hydrocarbons", Energy & Environmental Science, 3, (2010) 884-890.

[13]. G.A. Olah, A. Goeppert, G.K.S. Prakash, "Beyond Oil and Gas: The Methanol Economy", Wiley-VCH Verlag GmbH and Co. KGaA: Weinheim, Germany, 2006.

[14]. A.Y. Khodakov, W. Chu, P. Fongarland, "Advances in the development of novel cobalt Fischer− Tropsch catalysts for synthesis of long-chain hydrocarbons and clean fuels", Chemical Reviews, 107, (2007) 1692-1744.

[15]. R.J. Madon, E. Iglesia, "The importance of olefin readsorption and H_2/CO reactant ratio for hydrocarbon chain growth on ruthenium catalysts", Journal of Catalysis, 139, (1993) 576-590.

[16]. R. B. Anderson, "The Fischer-Tropsch Synthesis", Academic Press: Orlando, FL, 1984.

[17]. X. Xiaoding, J.A. Moulijn, "Mitigation of CO_2 by chemical conversion: Plausible chemical reactions and promising products", Energy & Fuels, 10, (1996) 305–325.

[18]. W. Wang, S. Wang, X. Ma, "Recent advances in catalytic hydrogenation of carbon dioxide", Chemical Society Reviews, 40, (2011) 3703–3727.

[19]. F. Rohr, O.A. Lindvag, A. Holmen, E.A. Blekkan, "Fischer–Tropsch synthesis over cobalt catalysts supported on zirconia-modified alumina", Catalysis Today, 58, (2000) 247-254.

[20]. W.H. Zimmerman, D.B. Bukur, "Reaction kinetics over iron catalysts used for the fischer-tropsch synthesis", The Canadian journal of chemical engineering, 68, (1990) 292-301.

[21]. T. Riedel, M. Claeys, H. Schulz, G. Schaub, S.S. Nam, K.W. Jun, M.J. Choi, G. Kishan, K.W. Lee, "Comparative study of Fischer–Tropsch synthesis with H_2/CO and H_2/CO_2 syngas using Fe-and Co-based catalysts", Applied Catalysis A: General, 186, (1999) 201-213.

[22]. H. Schulz, G. Schaub, M. Claeys, T. Riedel, "Transient initial kinetic regimes of Fischer–Tropsch synthesis", Applied Catalysis A: General, 186, (1999) 215-227.

[23]. K.W. Jun, S.J. Lee, H. Kim, M.J. Choi, K.W. Lee, "Support effects of the promoted and unpromoted iron catalysts in CO_2 hydrogenation", Studies in Surface Science and Catalysis, 114, (1998) 345-350.

[24]. S.M. Kim, J.W. Bae, Y.J. Lee, K.W. Jun, "Effect of CO_2 in the feed stream on the deactivation of Co/γ-Al_2O_3 Fischer–Tropsch catalyst", Catalysis Communications, 9, (2008) 2269-2273.

[25]. D. Schanke, S. Vada, E.A. Blekkan, A.M. Hilmen, A. Hoff, A. Holmen, "Study of Pt-promoted cobalt CO hydrogenation catalysts", Journal of Catalysis, 156, (1995) 85-95.

[26]. T. Riedel, G. Schaub, "Low-Temperature Fischer–Tropsch Synthesis on Cobalt Catalysts—Effects of CO_2", Topics in Catalysis, 26, (2003) 145-156.

[27]. Y. Zhang, G. Jacobs, D.E. Sparks, M.E. Dry, B.H. Davis, "CO and CO_2 hydrogenation study on supported cobalt Fischer–Tropsch synthesis catalysts", Catalysis Today, 71, (2002) 411–418.

[28]. Y. Yao, D. Hildebrandt, D. Glasser, X. Liu, "Fischer− Tropsch synthesis using $H_2/CO/CO_2$ syngas mixtures over a cobalt catalyst", Industrial & Engineering Chemistry Research, 49, (2010) 11061–11066.

[29]. C.G. Visconti, L. Lietti, E. Tronconi, P. Forzatti, R. Zennaro, E. Finocchio, "Fischer–Tropsch synthesis on a Co/Al_2O_3 catalyst with CO_2 containing syngas", Applied Catalysis A: General, 355, (2009) 61–68.

[30]. M.K. Gnanamani, W.D. Shafer, D.E. Sparks, B.H. Davis, "Fischer–Tropsch synthesis: Effect of CO_2 containing syngas over Pt promoted $Co/\gamma\text{-}Al_2O_3$ and K-promoted Fe catalysts", Catalysis Communications, 12, (2011) 936-939.

[31]. B. Jongsomjit, J.G. Goodwin Jr., "Co-support compound formation in Co/Al_2O_3 catalysts: effect of reduction gas containing CO", Catalysis Today, 77, (2002) 191–204.

[32]. H.R. Azizi, A.A. Mirzaei, M. Kaykhaii, M. Mansouri, "Fischer–Tropsch synthesis: studies effect of reduction variables on the performance of Fe–Ni–Co catalyst", Journal of Natural Gas Science and Engineering, 18, (2014) 484–491.

[33]. M.E. Dry, "The Fischer–Tropsch process: 1950–2000", Catalysis Today, 72, (2002) 227 – 241.

[34]. H. Schulz, M. Claeys, S. Harms, "Effect of water partial pressure on steady state Fischer-Tropsch activity and selectivity of a promoted cobalt catalyst", Studies in Surface Science and Catalysis, 107, (1997) 193-200.

[35]. I.C. Yates, C.N. Satterfield, "Intrinsic kinetics of the Fischer-Tropsch synthesis on a cobalt catalyst", Energy & Fuels, 5, (1991) 168-173.

[36]. H.H. Kung, "Methanol synthesis", Catalysis Reviews—Science and Engmeering, 22, (1980) 235-259.

[37]. J.S. Lee, K.H. Lee, S.Y. Lee, Y.G. Kim, "A comparative study of methanol synthesis from CO_2/H_2 and CO/H_2 over a $Cu/ZnO/Al_2O_3$ catalyst", Journal of Catalysis, 144, (1993) 414-424.

[38]. G. Liu, D. Willcox, M. Garland, H.H. Kung, "The role of CO_2 in methanol synthesis on Cu-Zn oxide: An isotope labeling study", Journal of Catalysis, 96, (1985) 251-260.

[39]. G.A. Vedage, R.G. Herman, K. Klier, "Chemical trapping of surface intermediates in methanol synthesis by amines", Journal of Catalysis, 95 (1985) 423-434.

[40]. M.E. Dry, "Catalytic aspects of industrial Fischer-Tropsch synthesis", Journal of Molecular Catalysis, 17, (1982) 133–144.

[41]. S.R. Yan, K.W. Jun, J.S. Hong, M.J. Choi, K.W. Lee, "Promotion effect of Fe–Cu catalyst for the hydrogenation of CO_2 and application to slurry reactor", Applied Catalysis A: General, 194, (2000) 63–70

[42]. P.S. Prasad, J.W. Bae, K.W. Jun, K.W. Lee, "Fischer–Tropsch synthesis by carbon dioxide hydrogenation on Fe-based catalysts", Catalysis surveys from Asia, 12, (2008) 170–183.

[43]. T. Herranz, S. Rojas, F.J. Perez-Alonso, M. Ojeda, P. Terreros, J.L.G. Fierro, "Carbon oxide hydrogenation over silica-supported iron-based catalysts Influence of the preparation route", Applied Catalysis A: General, 308, (2006) 19–30.

[44]. R.W. Dorner, D.R. Hardy, F.W. Williams, H.D. Willauer, "Heterogeneous catalytic CO_2 conversion to value-added hydrocarbons", Energy & Environmental Science, 3, (2010) 884–890.

[45]. T. Riedel, G. Schaub, K.W. Jun, K.W. Lee, "Kinetics of CO_2 Hydrogenation on a K-Promoted Fe Catalyst", Industrial & Engineering Chemistry Research, 40, (2001) 1355–1363.

[46]. S.R. Yan, K.W. Jun, J.S. Hong, S.B. Lee, M.J. Choi, K.W. Lee, "Slurry-phase CO_2 hydrogenation to hydrocarbons over a precipitated Fe-Cu-Al/K catalyst: Investigation of reaction conditions", Korean Journal of Chemical Engineering, 16 (1999) 357–361.

[47]. C.G. Visconti, L. Lietti, E. Tronconi, P. Forzatti, R. Zennaro, E. Finocchio, "Fischer–Tropsch synthesis on a Co/Al_2O_3 catalyst with CO_2 containing syngas", Applied Catalysis A: General, 355, (2009) 61–68.

[48]. Y. Yao, D. Hildebrandt, D. Glasser, X. Liu, "Fischer−Tropsch Synthesis Using $H_2/CO/CO_2$ Syngas Mixtures over a Cobalt Catalyst", Industrial & Engineering Chemistry Research, 49, (2010) 11061–11066.

[49]. T. Riedel, M. Claeys, H. Schulz, G. Schaub, S.S. Nam, K.W. Jun, M.J. Choi, G. Kishan, K.W. Lee, "Comparative study of Fischer–Tropsch synthesis with H_2/CO and H_2/CO_2 syngas using Fe- and Co-based catalysts", Applied Catalysis A: general, 186, (1999) 201-213.

[50]. C.G. Visconti, L. Lietti, E. Tronconi, P. Forzatti, R. Zennaro, E. Finocchio, "Fischer–Tropsch synthesis on a Co/Al_2O_3 catalyst with CO_2 containing syngas", Applied Catalysis A: General, 355, (2009) 61–68.

[51]. M.K. Gnanamani, W.D. Shafer, D.E. Sparks, B.H. Davis, "Fischer–Tropsch synthesis: Effect of CO_2 containing syngas over Pt promoted $Co/\gamma-Al_2O_3$ and K-promoted Fe catalysts", Catalysis Communications, 12, (2011) 936-939.

[52]. T. Riedel, M. Claeys, H. Schulz, G. Schaub, S.S. Nam, K.W. Jun, M.J. Choi, G. Kishan, K.W. Lee, "Comparative study of Fischer–Tropsch synthesis with H_2/CO and H_2/CO_2 syngas using Fe-and Co-based catalysts" Applied Catalysis A: General, 186 (1999) 201-213.

[53]. Y. Yao, X. Liu, D. Hildebrandt, D. Glasser, "The effect of CO_2 on a cobalt-based catalyst for low temperature Fischer–Tropsch synthesis", Chemical engineering journal, 193, (2012) 318-327.

[54]. J.A. Díaz, A.R. de la Osa, P. Sánchez, A. Romero, J.L. "Valverde, Influence of CO_2 co-feeding on Fischer–Tropsch fuels production over carbon nanofibers supported cobalt catalyst", Catalysis Communications, 44, (2014) 57-61.

[55]. C.G. Visconti, M. Martinelli, L. Falbo, L. Fratalocchi, L. Lietti, "CO_2 hydrogenation to hydrocarbons over Co and Fe-based Fischer-Tropsch catalysts", Catalysis Today, 277, (2016) 161-170.

[56]. E.A. Blekkan, Ø. Borg, V. Frøseth, A. Holmen, "Fischer-Tropsch synthesis on cobalt catalysts: the effect of water", Catalysis, 20, (2007) 13–32.

[57]. M.E. Dry, "Chapter 3: Chemical concepts used for engineering purposes", Studies in Surface Science & Catalysis, 152, (2004) 196–257.

[58]. E. Zagli, J.L. Falconer, "Carbon dioxide adsorption and methanation on ruthenium", Journal of Catalysis, 69, (1981) 1-8.

[59]. J.L. Falconer, A.E. Zagli, "Adsorption and methanation of carbon dioxide on a nickel/silica catalyst", Journal of Catalysis, 62, (1980) 280-285.

[60]. G.D. Weatherbee, C.H. Bartholomew, "Hydrogenation of CO_2 on group VIII metals: IV. Specific activities and selectivities of silica-supported Co, Fe, and Ru", Journal of Catalysis, 87, (1984) 352-362.

[61]. G.D. Weatherbee, C.H. Bartholomew, "Hydrogenation of CO_2 on group VIII metals: II. Kinetics and mechanism of CO_2 hydrogenation on nickel", Journal of Catalysis, 77, (1982) 460-472.

[62]. Y. Zhang, G. Jacobs, D.E. Sparks, M.E. Dry, B.H. Davis, "CO and CO_2 hydrogenation study on supported cobalt Fischer–Tropsch synthesis catalysts", Catalysis Today, 71, (2002) 411-418.

[63]. S.M. Kim, J.W. Bae, Y.J. Lee, K.W. Jun, "Effect of CO_2 in the feed stream on the deactivation of Co/γ-Al_2O_3 Fischer–Tropsch catalyst", Catalysis Communications, 9, (2008) 2269-2273.

[64]. V.A. de la Pena O'Shea, S. Gonzalez, F. Illas, J.L.G. Fierro, "Evidence for spontaneous CO_2 activation on cobalt surfaces", Chemical Physics Letters, 454, (2008) 262–268.

[65]. Y. Zhang, G. Jacobs, D.E. Sparks, M.E. Dry, B.H. Davis, CO and CO_2 hydrogenation study on supported cobalt Fischer–Tropsch synthesis catalysts, Catalysis today, 71(3) (2002).411 – 418.

[66]. L. Xu, S. Bao, D.J. Houpt, S.H. Lambert, B.H. Davis, "Role of CO_2 in the initiation of chain growth and alcohol formation during the Fischer-Tropsch synthesis", Catalysis Today, 36, (1997) 347-355.

[67]. I.A. Fischer, A.T. Bell, "A Comparative Study of CO and CO_2 Hydrogenation over Rh/SiO_2", Journal of Catalysis, 162, (1996) 54-65.

[68]. A.M. Saib, D.J. Moodley, I.M. Ciobîca, M.M. Hauman, B.H. Sigwebela, C.J. Weststrate, J.W. Niemantsverdriet, J. van de Loosdrecht, "Fundamental understanding of deactivation and regeneration of cobalt Fischer–Tropsch synthesis catalysts", Catalysis Today, 154, (2010) 271–282.

[69]. E. van Steen, M. Claeys, "Fischer-Tropsch Catalysts for the Biomass-to-Liquid (BTL)-Process", Chemical Engineering & Technology: Industrial Chemistry-Plant Equipment-Process Engineering-Biotechnology, 31, (2008) 655–666.

[70]. K.W. Jun, S.J. Lee, H. Kim, M.J. Choi, K.W. Lee, "Support effects of the promoted and unpromoted iron catalysts in CO_2 hydrogenation", Studies in Surface Science & Catalysis, 114, (1998) 345-350.

[71]. T. Riedel, G. Schaub, K.W. Jun, K.W. Lee, Industrial Engineering Chemistry Research 40 (2001) 1255.

[72]. W.W. Russell, G.H. Miller, "Catalytic Hydrogenation of Carbon Dioxide to Higher Hydrocarbons", Journal of the American Chemical Society, 72, (1950) 2446–2454.

[73]. M.K. Gnanamani, G. Jacobs, R.A. Keogh, W.D. Shafer, D.E. Sparks, S.D. Hopps, G.A. Thomas, B.H. Davis, "Fischer-Tropsch synthesis: Effect of pretreatment conditions of cobalt on activity and selectivity for hydrogenation of carbon dioxide", Applied Catalysis A: General, 499, (2015) 39-46

[74]. R.E. Owen, J.P. O'Byrne, D. Mattia, P. Plucinski, S.I. Pascu, M.D. Jones, "Cobalt catalysts for the conversion of CO_2 to light hydrocarbons at atmospheric pressure", Chemical communications, 49, (2013) 11683-11685.

[75]. M.K. Gnanamani, H.H. Hamdeh, G. Jacobs, D. Qian, F. Liu, S.D. Hopps, G.A. Thomas, W.D. Shafer, Q. Xiao, Y. Hu, B.H. Davis, "Fischer–Tropsch synthesis: effect of Cu, Mn and Zn addition on activity and product selectivity of cobalt ferrite", RSC Advances, 6, (2016) 62356-62367.

[76]. J. Wei, J. Sun, Z. Wen, C. Fang, Q. Ge, H. Xu, "New insights into the effect of sodium on Fe_3O_4-based nanocatalysts for CO_2 hydrogenation to light olefins", Catalysis Science & Technology, 6, (2016) 4786-4793.

[77]. J. Zhang, S. Lu, X. Su, S. Fan, Q. Ma, T. Zhao, "Selective formation of light olefins from CO_2 hydrogenation over Fe–Zn–K catalysts", Journal of CO_2 Utilization, 12, (2015) 95–100.

[78]. C.G. Visconti, M. Martinelli, L. Falbo, A. Infantes-Molina, L. Lietti, P. Forzatti, G. Iaquaniello, E. Palo, B. Picutti, F. Brignoli, "CO_2 hydrogenation to lower olefins on a high surface area K-promoted bulk Fe-catalyst", Applied Catalysis B: Environmental, 200, (2017) 530-542.

[79]. M. Rafati, L. Wang, A. Shahbazi, "Effect of silica and alumina promoters on co-precipitated Fe–Cu–K based catalysts for the enhancement of CO_2 utilization during Fischer–Tropsch synthesis", Journal of CO_2 Utilization, 12, (2015) 34–42.

[80]. L. Gavrilović, J. Brandin, A. Holmen, H.J. Venvik, R. Myrstad, E.A. Blekkan, "Fischer-Tropsch synthesis—Investigation of the deactivation of a Co catalyst by exposure to aerosol particles of potassium salt", Applied Catalysis B: Environmental, 230, (2018) 203–209.

[81]. Z. Shi, H. Yang, P. Gao, X. Li, L. Zhong, H. Wang, H. Liu, W. Wei, Y. Sun, "Direct conversion of CO_2 to long-chain hydrocarbon fuels over K–promoted $CoCu/TiO_2$ catalysts", Catalysis Today, 311, (2018) 65-73.

[82]. R.C. Reuel, C.H. Bartholomew, "Effects of support and dispersion on the CO hydrogenation activity/selectivity properties of cobalt", Journal of Catalysis, 85, (1984) 78-88.

[83]. P. Munnik, P.E. de Jongh, K.P. de Jong, "Recent developments in the synthesis of supported catalysts", Chemical reviews, 115, (2015) 6687-6718.

[84]. G. Jacobs, T.K. Das, Y. Zhang, J. Li, G. Racoillet, B.H. Davis, "Fischer–Tropsch synthesis: support, loading, and promoter effects on the reducibility of cobalt catalysts", Applied Catalysis A: General, 233, (2002) 263-281.

[85]. Z. Shi, H. Yang, P. Gao, X. Chen, H. Liu, L. Zhong, H. Wang, W. Wei, Y. Sun, "Effect of alkali metals on the performance of $CoCu/TiO_2$ catalysts for CO_2 hydrogenation to long-chain hydrocarbons", Chinese Journal of Catalysis, 39, (2018) 1294–1302.

[86]. A.Y. Khodakov, W. Chu, P. Fongarland, "Advances in the development of novel cobalt Fischer− Tropsch catalysts for synthesis of long-chain hydrocarbons and clean fuels", Chemical Reviews, 107, (2007) 1692–1744.

[87]. C.G. Visconti, L. Lietti, E. Tronconi, P. Forzatti, R. Zennaro, E. Finocchio, "Fischer–Tropsch synthesis on a Co/Al_2O_3 catalyst with CO_2 containing syngas", Applied Catalysis A: General 355 (2009) 61–68.

[88]. F. Haga, T. Nakajima, H. Miya, S. Mishima, "Catalytic properties of supported cobalt catalysts for steam reforming of ethanol", Catalysis Letters, 48, (1997) 223–227.

[89]. S.S.Y. Lin, D.H. Kim, S.Y. Ha, "Hydrogen production from ethanol steam reforming over supported cobalt catalysts", Catalysis Letters, 122' (2008) 295–301.

[90]. R.C. Reuel, C.H. Bartholomew, "The stoichiometries of H_2 and CO adsorptions on cobalt: Effects of support and preparation", Journal of Catalysis, 85, (1984) 63–77.

[91]. T. Xiao, S. Ji, H. Wang, K.S. Coleman, M.L.H. Green, "Methane combustion over supported cobalt catalysts", Journal of Molecular Catalysis A: Chemical, 175, (2001) 111–123.

[92]. J. Liu, Z. Zhao, J. Wang, C. Xu, A. Duan, G. Jiang, Q. Yang, "The highly active catalysts of nanometric CeO_2-supported cobalt oxides for soot combustion", Applied Catalysis B: Environmental, 84, (2008) 185–195.

[93]. P. Ratnasamy, R.P. Mehrotra, A.V. Ramaswamy, "Interaction Between the Active Components and Support in $Co-MO-Al_2O_3$ Systems", Journal of Catalysis, 32, (1974) 63–71.

[94]. L.E. Gomez, I.S. Tiscornia, A.V. Boix, E.E. Miro, "Co/ZrO_2 catalysts coated on cordierite monoliths for CO preferential oxidation", Applied Catalysis A: General, 401, (2011) 124–133.

[95]. C.H. Bartholomew, R.C. Reuel, "Cobalt-support interactions: Their effects on adsorption and carbon monoxide hydrogenation activity and selectivity properties", Industrial & Engineering Chemistry Product Research and Development, 24, (1985) 56–61.

[96]. F.M.T. Mendes, C.A.C. Perez, F.B. Noronha, M. Schmal, "TPSR of CO hydrogenation on Co/Nb_2O_5/Al_2O_3 catalysts", Catalysis Today, 101, (2005) 45–50.

[97]. Y. Brik, M. Kacimi, M. Ziyad, F. Bozon-Verduraz, "Titania-Supported Cobalt and Cobalt–Phosphorus Catalysts: Characterization and Performances in Ethane Oxidative Dehydrogenation", Journal of Catalysis, 202, (2001) 118–128.

[98]. H. Xiong, Y. Zhang, K. Liew, J. Li, "Catalytic performance of zirconium-modified Co/Al_2O_3 for Fischer–Tropsch synthesis", Journal of Molecular Catalysis A: Chemical, 231, (2005) 145–151.

[99]. H.Y. Wang, E. Ruckenstein, "CO_2 reforming of CH_4 over Co/MgO solid solution catalysts — effect of calcination temperature and Co loading", Applied Catalysis A: General, 209, (2001) 207–215.

[100]. L.G.A. van de Water, G.L. Bezemer, J.A. Bergwerff, M. Versluijs, M. Versluijs-Helder, B.M. Weckhuysen, K.P. de Jong, "Spatially resolved UV–vis microspectroscopy on the preparation of alumina-supported Co Fischer–Tropsch catalysts: Linking activity to Co distribution and speciation", Journal of Catalysis, 242, (2006) 287–298.

[101]. T. Das, G. Deo, "Synthesis, characterization and in situ DRIFTS during the CO2 hydrogenation reaction over supported cobalt catalysts", Journal of Molecular Catalysis A: Chemical, 350, (2011) 75–82.

[102]. T. Das, G. Deo, "Effects of metal loading and support for supported cobalt catalyst", Catalysis today, 198, (2012) 116-124.

[103]. E.V. Suslova, S.A. Chernyak, A.V. Egorov, S.V. Savilov, V.V. Lunin, "CO_2 hydrogenation over cobalt-containing catalysts", Kinetics & Catalysis, 56, (2015) 646-654.

[104]. R.E. Owen, P. Plucinski, D. Mattia, L. Torrente-Murciano, V.P. Ting, M.D. Jones, "Effect of support of Co-Na-Mo catalysts on the direct conversion of CO_2 to hydrocarbons", Journal of CO_2 Utilization, 16, (2016) 97-103.

[105]. L. Torrente-Murciano, A.A. Lapkin, D. Chadwick, Synthesis of high aspect ratio titanate nanotubes Journal of Materials Chemistry, 20, (2010) 6484-6489.

[106]. M. Fujiwara, H. Ando, M. Matsumoto, Y. Matsumura, M. Tanaka, Y. Souma, "Hydrogenation of carbon dioxide over Fe-ZnO/zeolite composite catalysts", Chemistry Letters, 24, (1995) 839-840.

[107]. S. Saeidi, N.A.S. Amin, M.R. Rahimpour, "Hydrogenation of CO_2 to value-added products—A review and potential future developments", Journal of CO_2 Utilization, 5, (2014) 66-81.

[108]. R.W. Dorner, D.R. Hardy, F.W. Williams, B.H. Davis, H.D. Willauer, "Influence of Gas Feed Composition and Pressure on the Catalytic Conversion of CO_2 to Hydrocarbons Using a Traditional Cobalt-Based Fischer−Tropsch Catalyst", Energy & Fuel, 23, (2009) 4190-4195.

[109]. R.E. Owen, J.P. O'Byrne, D. Mattia, P. Plucinski, S.I. Pascu, M.D. Jones, "Cobalt catalysts for the conversion of CO_2 to light hydrocarbons at atmospheric pressure", Chemical Communications, 49, (2013) 11683-11685.

[110]. J.P. den Breejen, P.B. Radstake, G.L. Bezemer, J.H. Bitter, V. Frøseth, A. Holmen, K.P. de Jong, "On the origin of the cobalt particle size effects in Fischer− Tropsch catalysis", Journal of the American Chemical Society, 131, (2009) 7197-7203.

[111]. S. Vada, A. Hoff, E. Adnanes, D. Schanke, A. Holmen, "Fischer-Tropsch synthesis on supported cobalt catalysts promoted by platinum and rhenium", Topics in Catalysis, 2, (1995) 155–162.

[112]. T.K. Das, G. Jacobs, B.H. Davis, "Fischer–Tropsch synthesis: Deactivation of promoted and unpromoted cobalt–alumina catalysts", Catalysis Letters, 101, (2005) 187–190.

[113]. G.E. Batley, A. Ekstrom, D.A. Johnson, "Studies of topochemical heterogeneous catalysis: 3. Catalysis of the reduction of metal oxides by hydrogen", Journal of Catalysis, 34, (1974) 368– 375.

[114]. S.D. Rossi, G. Ferraris, S. Fermiotti, A. Cimino, V. Indovina, "Propane dehydrogenation on chromia/zirconia catalysts", Applied Catalysis A: General, 81, (1992) 113–132.

[115]. J. Cheng, P. Hu, P. Ellis, S. French, G. Kelly, C.M. Lok, "Chain growth mechanism in Fischer− Tropsch synthesis: A DFT study of C− C coupling over Ru, Fe, Rh, and Re surfaces", Journal of Physical Chemistry C, 112, (2008) 6082–6086.

[116]. R. Hammami, A. Dhouib, S. Fernandez, C. Minot, "CO_2 adsorption on (001) surfaces of metal monoxides with rock-salt structure", Catalysis Today, 139, (2008) 227–233.

[117]. D. Mendes, A. Mendes, L.M. Madeira, A. Iulianelli, J.M. Sousa, A. Basile, "The water-gas shift reaction: from conventional catalytic systems to Pd-based membrane reactors—a review", Asia-Pacific Journal of Chemical Engineering, 5, (2010) 111-137.

[118]. A. Ranjbar, A. Irankhah, S.F. Aghamiri, "Reverse water gas shift reaction and CO_2 mitigation: nanocrystalline MgO as a support for nickel based catalysts", Journal of Environmental Chemical Engineering, 6, (2018) 4945–4952.

[119]. Y.A. Daza, J.N. Kuhn, "CO_2 conversion by reverse water gas shift catalysis: comparison of catalysts, mechanisms and their consequences for CO_2 conversion to liquid fuels", RSC Advances, 6(55), (2016) 49675-49691.

[120]. A. Goguet, F.C. Meunier, D. Tibiletti, J.P. Breen, R. Burch, "Spectrokinetic investigation of reverse water-gas-shift reaction intermediates over a Pt/CeO_2 catalyst", Journal of Physical Chemistry B, 108, (2004) 20240–20246.

[121]. A. Goguet, F. Meunier, J.P. Breen, R. Burch, M.I. Petch, A.F. Ghenciu, "Study of the origin of the deactivation of a Pt/CeO_2 catalyst during reverse water gas shift (RWGS) reaction", Journal of Catalysis, 226, (2004) 382–392.

[122]. D. Tibiletti, A. Goguet, F.C. Meunier, J.P. Breen, R. Burch, "On the importance of steady-state isotopic techniques for the investigation of the mechanism of the reverse water-gas-shift reaction", Chemical Communications, 14, (2004) 1636–1637.

[123]. S. Ando, Y. Koyama, S. Miyata, S. Sato, S. Kanehashi, K. Nagai, "Synthesis and characterization of ABA-type triblock copolymers derived from polyimide and poly (2-methyl-2-adamantyl methacrylate, Polymer International", 63, (2014) 1634–1642.

[124]. D. Baudouin, U. Rodemerck, F. Krumeich, A. de Mallmann, K.C. Szeto, H. Menard, L. Veyre, J.P. Candy, P.B. Webb, C. Thieuleux, C. Coperet, "Particle size effect in the low temperature reforming of methane by carbon dioxide on silica-supported Ni nanoparticles", Journal of Catalysis, 297, (2013) 27–34.

[125]. F.V. Vazquez, P. Pfeifer, J. Lehtonen, P. Piermartini, P. Simell, V. Alopaeus, "Catalyst screening and kinetic modeling for CO production by high pressure and temperature reverse water gas shift for Fischer-Tropsch applications", Industrial & Engineering Chemistry Research, 56, (2017) 13263–13273.

[126]. M.T. Rodrigues, P.C. Zonetti, O.C. Alves, E.F. Sousa-Aguiar, L.E.P. Borges, L.G. Appel, "RWGS reaction employing Ni/Mg(Al,Ni)O - the role of the O vacancies", Applied Catalysis A: General, 543, (2017) 98–103.

[127]. F. Bustamante, R.M. Enick, A.V. Cugini, R.P. Killmeyer, B.H. Howard, K.S. Rothenberger, M.V. Ciocco, B.D. Morreale, "High-temperature kinetics of the homogeneous reverse water-gas shift reaction", AlChE Journal, 50, (2004) 1028–1041.

[128]. C.S. Chen, W.H. Cheng, S.S. Lin, "Study of iron-promoted Cu/SiO_2 catalyst on high temperature reverse water gas shift reaction", Applied Catalysis A: General, 257, (2004) 97–106.

[129]. C.S. Chen, W.H. Cheng, S.S. Lin, "Study of reverse water gas shift reaction by TPD, TPR and CO_2 hydrogenation over potassium-promoted Cu/SiO_2 catalyst", Applied Catalysis A: General, 238, (2003) 55–67.

[130]. M.J.L. Gines, A.J. Marchi, C.R. Apesteguia, "Kinetic study of the reverse water-gas shift reaction over $CuO/ZnO/Al_2O_3$ catalysts", Applied Catalysis A: General, 154, (1997) 155–171.

[131]. D. Waller, D. Stirling, F.S. Stone, M.S. Spencer, "Copper-zin oxide catalysts – activity in relation to precursor structure and morphology", Faraday Discussions of the Chemical Society, 87, (1989) 107–120.

[132]. C.S. Chen, W.H. Cheng, S.S. Lin, "Mechanism of CO formation in reverse water-gas shift reaction over Cu/Al_2O_3 catalyst", Catalysis Letters, 68, (2000) 45–48.

[133]. H.T. Xu, Y.S. Li, X.K. Luo, Z.L. Xu, J.P. Ge, "Monodispersed gold nanoparticles supported on a zirconium-based porous metal-organic framework and their high catalytic ability for the reverse water-gas shift reaction", Chemical Communications, 53, (2017) 7953–7956.

[134]. R. Carrasquillo-Flores, I. Ro, M.D. Kumbhalkar, S. Burt, C.A. Carrero, A.C. Alba-Rubio, J.T. Miller, I. Hermans, G.W. Huber, J.A. Dumesic, "Reverse water-gas shift on interfacial sites formed by deposition of oxidized molybdenum moieties onto gold nanoparticles", Journal of American Chemical Society, 137, (2015) 10317–10325.

[135]. M. Manzoli, A. Chiorino, F. Vindigni, F. Boccuzzi, "Hydrogen interaction with gold nanoparticles and clusters supported on different oxides: a FTIR study", Catalysis Today, 181, (2012) 62–67.

[136]. Z.S. Fishman, Y.L. He, K.R. Yang, A.W. Lounsbury, J.Q. Zhu, T.M. Tran, J.B. Zimmerman, V.S. Batista, L.D. Pfefferle, "Hard templating ultrathin polycrystalline hematite nanosheets: effect of nano-dimension on CO_2 to CO conversion via the reverse water-gas shift reaction", Nanoscale, 9, (2017) 12984–12995.

[137]. G.W. Roberts, P. Chin, X.L. Sun, J.J. Spivey, "Preferential oxidation of carbon monoxide with Pt/Fe monolithic catalysts: interactions between external transport and the reverse water-gas-shift reaction", Applied Catalysis B: Environmental, 46, (2003) 601–611.

[138]. R. Merkache, I. Fechete, M. Maamache, M. Bernard, P. Turek, K. Al-Dalama, F. Garin, "3D ordered mesoporous Fe-KIT-6 catalysts for methylcyclopentane (MCP) conversion and carbon dioxide (CO_2) hydrogenation for energy and environmental applications", Applied Catalysis A: General, 504, (2015) 672–681.

[139]. R.C. Baliban, J.A. Elia, C.A. Floudas, "Optimization framework for the simultaneous process synthesis, heat and power integration of a thermochemical hybrid biomass, coal, and natural gas facility", Computers & Chemical Engineering, 35, (2011) 1647–1690.

[140]. G. Pekridis, K. Kalimeri, N. Kaklidis, E. Vakouftsi, E.F. Iliopoulou, C. Athanasiou, G.E. Marnellos, "Study of the reverse water gas shift (RWGS) reaction over Pt in a solid oxide fuel cell (SOFC) operating under open and closed-circuit conditions", Catalysis Today, 127, (2007) 337–346.

[141]. T. Yoshida, D.L. Thorn, T. Okano, J.A. Ibers, S. Otsuka, "Hydration and reduction of carbon-dioxide by rhodium hydride compounds - preparation and reactions of rhodium bicarbonate and formate complexes, and the molecular-structure of $RhH_2(O_2COH)(P(i-PR)_3)_2$", Journal of the American Chemical Society, 101, (1979) 4212–4221.

[142]. K.-I. Tominaga, Y. Sasaki, T. Watanabe, M. Saito, "Ethylene oxide-mediated reverse water-gas shift reaction catalyzed by ruthenium complexes", Energy, 22, (1997) 169–176.

[143]. K. Tsuchiya, J.D. Huang, K. Tominaga, "Reverse water-gas shift reaction catalyzed by mononuclear Ru complexes", ACS Catalysis, 3, (2013) 2865–2868.

[144]. W. Li, S. Guo, L. Guo, "Theoretical investigation of reverse water gas shift reaction catalyzed by ruthenium halogen carbonyl complexes", Catalysis Surveys from Asia, 21, (2017) 185–197.

[145]. R. Franke, D. Selent, A. Börner, "Applied hydroformylation", Chemical Reviews, 112, (2012) 5675–5732.

[146]. C. Bianchini, D.G. Burnaby, J. Evans, P. Frediani, A. Meli, W. Oberhauser, R. Psaro, L. Sordelli, F. Vizza, "Preparation, characterization, and performance of tripodal polyphosphine rhodium catalysts immobilized on silica via hydrogen bonding", Journal of the American Chemical Society, 121, (1999) 5961–5971.

[147]. G.J.H. Buisman, P.C.J. Kamer, P. Vanleeuwen, "Rhodium catalyzed asymetric hydroformylation with Chiral diphosphite ligands", Tetrahedron: Asymmetry, 4, (1993) 1625–1634.

[148]. T. Hanaoka, H. Arakawa, T. Matsuzaki, Y. Sugi, K. Kanno, Y. Abe, "Ethylene hydroformylation and carbon monoxide hydrogenation over modified and unmodified silica supported rhodium catalysts", Catalysis Today, 58, (2000) 271–280.

[149]. K. Tominaga, Y. Sasaki, "Biphasic hydroformylation of 1-hexene with carbon dioxide catalyzed by ruthenium complex in ionic liquids", Chemistry Letters, 33, (2004) 14–15.

[150]. K. Tominaga, Y. Sasaki, "Ruthenium-catalyzed one-pot hydroformylation of alkenes using carbon dioxide as a reactant", Journal of Molecular Catalysis A: Chemical, 220, (2004) 159–165.

[151]. K. Tominaga, Y. Sasaki, "Ruthenium complex-catalyzed hydroformylation of alkenes with carbon dioxide", Catalysis Communications, 1, (2000) 1–3.

[152]. Y. Liu, Z. Li, H. Xu, Y. Han, "Reverse water–gas shift reaction over ceria nanocube synthesized by hydrothermal method", Catalysis Communications, 76, (2016) 1–6.

[153]. B. Dai, G. Zhou, S. Ge, H. Xie, Z. Jiao, G. Zhang, X. Zhang, "CO_2 reverse water-gas shift reaction on mesoporous M-CeO_2 catalysts", Canadian Journal of Chemical Engineering, 95, (2017) 634–642.

[154]. L. Wang, H. Liu, Y. Chen, R. Zhang, S. Yang, "K-promoted Co-CeO_2 catalyst for the reverse water–Gas shift reaction", Chemistry Letters, 42, (2013) 682–683.

[155]. W. Luhui, L. Hui, L. Yuan, C. Ying, Y. Shuqing, "Influence of preparation method on performance of Ni-CeO_2 catalysts for reverse water-gas shift reaction", Journal of Rare Earths, 31, (2013) 559–564.

[156]. C.S. Chen, W.H. Cheng, S.S. Lin, "Mechanism of CO formation in reverse water–gas shift reaction over Cu/Al_2O_3 catalyst", Catalysis Letters, 68, (2000) 45–48.

[157]. M. Lortie, "Reverse Water Gas Shift Reaction Over Supported Cu-Ni Nanoparticle Catalysts", Doctoral dissertation Université d'Ottawa/University of Ottawa, 2014.

[158]. Y. Sun, G. Yang, C. Wen, L. Zhang, Z. Sun, "Artificial neural networks with response surface methodology for optimization of selective CO_2 hydrogenation using K promoted iron catalyst in a microchannel reactor", Journal of CO_2 Utilization, 24, (2018) 10–21.

[159]. A.G. Kharaji, A. Shariati, M.A. Takassi, "A novel γ-Alumina supported Fe-Mo bimetallic catalyst for reverse water gas shift reaction", Chinese Journal of Chemical Engineering, 21, (2013) 1007–1014.

[160]. A. Wolf, A. Jess, C. Kern, "Syngas production via reverse water-gas shift reaction over a Ni-Al_2O_3 catalyst-Catalyst stability, reaction kinetics and reactor modeling", Chemical Engineering & Technology, 39, (2016) 1040–1048.

[161]. C.S. Chen, J.H. Lin, J. You, K.H. Yang, "Effects of potassium on Ni−K/Al_2O_3 catalysts in the synthesis of carbon nanofibers by catalytic hydrogenation of CO_2", Journal of Physical Chemistry A, 114, (2009) 3773–3781.

[162]. D.J. Pettigrew, D.L. Trimm, N.W. Cant, "The effects of rare earth oxides on the reverse water-gas shift reaction on palladium/alumina", Catalysis Letters, 28, (1994) 313–319.

[163]. C.S. Chen, W.H. Cheng, "Study on the mechanism of CO formation in reverse water gas shift reaction over Cu/SiO_2 catalyst by pulse reaction, TPD and TPR", Catalysis Letters, 83, (2002) 121–126.

[164]. H.C. Wu, Y.C. Chang, J.H. Wu, J.H. Lin, I.K. Lin, C.S. Chen, "Methanation of CO_2 and reverse water gas shift reactions on Ni/SiO_2 catalysts: the influence of particle size on selectivity and reaction pathway", Catalysis Science & Technology, 5, (2015) 4154–4163.

[165]. I. Ro, R. Carrasquillo-Flores, J.A. Dumesic, G.W. Huber, "Intrinsic kinetics of plasmon enhanced reverse water gas shift on Au and Au–Mo interfacial sites supported on silica", Applied Catalysis A: General, 521, (2016) 182–189.

[166]. C.S. Chen, W.H. Cheng, S.S. Lin, "Study of reverse water gas shift reaction by TPD, TPR and CO2 hydrogenation over potassium-promoted Cu/SiO_2 catalyst", Applied Catalysis A: General, 238, (2003) 55–67.

[167]. B. Liang, H. Duan, X. Su, X. Chen, Y. Huang, X. Chen, T. Zhang, "Promoting role of potassium in the reverse water gas shift reaction on Pt/mullite catalyst", Catalysis Today, 281, (2017) 319–326.

[168]. C.S. Chen, W.H. Cheng, S.S. Lin, "Study of iron-promoted Cu/SiO_2 catalyst on high temperature reverse water gas shift reaction", Applied Catalysis A: General, 257, (2004) 97–106.

[169]. B. Lu, K. Kawamoto, "Direct synthesis of highly loaded and well-dispersed NiO/SBA-15 for producer gas conversion", RSC Advances, 2, (2012) 6800–6805.

[170]. X. Zhang, X. Zhu, L. Lin, S. Yao, M. Zhang, X. Liu, D. Ma, "Highly dispersed copper over β-Mo_2C as efficient and stable catalysts for RWGS reaction", ACS Catalysis, 7, (2016) 912–918.

[171]. M.D. Porosoff, S. Kattel, W. Li, P. Liu, J.G. Chen, "Identifying trends and descriptors for selective CO_2 conversion to CO over transition metal carbides", Chemical Communications, 51, (2015) 6988–6991.

[172]. M.T. Rodrigues, P.C. Zonetti, O.C. Alves, E.F. Sousa-Aguiar, L.E. Borges, L.G. Appel, "RWGS reaction employing Ni/Mg (Al, Ni) O the role of the O vacancies", Applied Catalysis A: General, 543, (2017) 98–103.

[173]. M.R. Gogate, R.J. Davis, "Comparative study of CO and CO_2 hydrogenation over supported Rh–Fe catalysts", Catalysis Communications, 11, (2010) 901–906.

[174]. J.C. Matsubu, V.N. Yang, P. Christopher, "Isolated metal active site concentration and stability control catalytic CO_2 reduction selectivity", Journal of the American Chemical Society, 137, (2015) 3076–3084.

[175]. V. Lebarbier, R. Dagle, A. Datye, Y. Wang, "The effect of PdZn particle size on reverse water gas shift reaction", Applied Catalysis A: General, 379, (2010) 3–6.

[176]. K. Oshima, T. Shinagawa, Y. Nogami, R. Manabe, S. Ogo, Y. Sekine, "Low temperature catalytic reverse water gas shift reaction assisted by an electric field", Catalysis Today, 232, (2014) 27–32.

[177]. Q. Sun, J. Ye, C.J. Liu, Q. Ge, "In_2O_3 as a promising catalyst for CO_2 utilization: A case study with reverse water gas shift over In_2O_3", Greenhouse Gases: Science & Technology, 4, (2014) 140–144.

[178]. F.M. Sun, C.F. Yan, C.Q. Guo, S.L. Huang, "Ni/Ce–Zr–O catalyst for high CO_2 conversion during reverse water gas shift reaction (RWGS)", International Journal of Hydrogen Energy, 40, (2015) 15985–15993.

[179]. W. Wang, Y. Zhang, Z. Wang, J.M. Yan, Q. Ge, C.J. Liu, "Reverse water gas shift over In_2O_3–CeO_2 catalysts", Catalysis Today, 259, (2016) 402–408.

[180]. L.D.R. Silva-Calpa, P.C. Zonetti, C.P. Rodrigues, O.C. Alves, L.G. Appel, R.R. de Avillez, "The $Zn_xZr_{1-x}O_{2-y}$ solid solution on m-ZrO_2: creating O vacancies and improving the m-ZrO_2 redox properties", Journal of Molecular Catalysis A: Chemical, 425, (2016) 166–173.

[181]. D.H. Kim, J.L. Park, E.J. Park, Y.D. Kim, S. Uhm, "Dopant effect of barium zirconate-based perovskite-type catalysts for the intermediate-temperature reverse water gas shift reaction", ACS Catalysis, 4, (2014) 3117–3122.

[182]. Y.A. Daza, R.A. Kent, M.M. Yung, J.N. Kuhn, "Carbon dioxide conversion by reverse water–gas shift chemical looping on perovskite-type oxides", Industrial & Engineering Chemistry Research, 53, (2014) 5828–5837.

[183]. B.J. Hare, D. Maiti, Y.A. Daza, V.R. Bhethanabotla, J.N. Kuhn, "Enhanced CO_2 conversion to CO by silica-supported perovskite oxides at low temperatures", ACS Catalysis, 8, (2018) 3021–3029.

[184]. J.R. Rostrup-Nielsen, K. Pedersen, J. Sehested, "High temperature methanation sintering and structure sensitivity", Applied Catalysis A: General, 330, (2007) 134–138.

[185]. S. Rönsch, J. Schneider, S. Matthischke, M. Schlüter, M. Götz, J. Lefebvre, P. Prabhakaran, S. Bajohr, "Review on methanation – from fundamentals to current projects", Fuel, 166, (2016) 276–296.

[186]. G. Centi, E.A. Quadrelli, S. Perathoner, "Catalysis for CO_2 conversion: a key technology for rapid introduction of renewable energy in the value chain of chemical industries", Energy & Environmental Science, 6, (2013) 1711–1731.

[187]. K.M.K. Yu, I. Curcic, J. Gabriel, S.C.E. Tsang, "Recent advances in CO_2 capture and utilization", ChemSusChem: Chemistry & Sustainability Energy & Materials, 1(11), (2008) 893–899.

[188]. M.A.A. Aziz, A.A. Jalil, S. Triwahyono, A. Ahmad, "CO_2 methanation over heterogeneous catalysts: recent progress and future prospects", Green Chemistry, 17, (2015) 2647–2663.

[189]. K. Jalama, "Carbon dioxide hydrogenation over nickel-, ruthenium-, and copper based catalysts: review of kinetics and mechanism", Catalysis Reviews, 59, (2017) 95–164.

[190]. B. Miao, S.S.K. Ma, X. Wang, H. Su, S.H. Chan, "Catalysis mechanisms of CO_2 and CO methanation", Catalysis Science & Technology, 6, (2016) 4048–4058.

[191]. P.A.U. Aldana, F. Ocampo, K. Kobl, B. Louis, F. Thibault-Starzyk, M. Daturi, P. Bazin, S. Thomas, A.C. Roger, "Catalytic CO_2 valorization into CH_4 on Ni-based ceria-zirconia. Reaction mechanism by operando IR spectroscopy", Catalysis Today, 215, (2013) 201–207.

[192]. Q. Pan, J. Peng, T. Sun, S. Wang, S. Wang, "Insight into the reaction route of CO_2 methanation: promotion effect of medium basic sites", Catalysis Communications, 45, (2014) 74–78.

[193]. M. Behrens, "Heterogeneous catalysis of CO_2 conversion to methanol on copper surfaces", Angewandte Chemmie International Edition, 53, (2014) 12022–12024.

[194]. E. Frei, A. Schaadt, T. Ludwig, H. Hillebrecht, I. Krossing, "The influence of the precipitation/ageing temperature on a $Cu/ZnO/ZrO_2$ catalyst for methanol synthesis from H_2 and CO_2", ChemCatChem, 6, (2014) 1721–1730.

[195]. J. Burger, V. Papaioannou, S. Gopinath, G. Jackson, A. Galindo, C.S. Adjiman, "A hierarchical method to integrated solvent and process design of physical CO_2 absorption using the SAFT-c Mie approach", AIChE Journal, 61, (2015) 3249–3269.

[196]. A. Goeppert, M. Czaun, J.-P. Jones, G.K.S. Prakash, G.A. Olah, "Recycling of carbon dioxide to methanol and derived products – closing the loop", Chemical Society Reviews, 43, (2014) 7995–8048.

[197]. M.D. Porosoff, B. Yan, J.G. Chen, "Catalytic reduction of CO_2 by H_2 for synthesis of CO, methanol and hydrocarbons: challenges and opportunities", Energy & Environmental Science, 9, (2016) 62–73.

[198]. M. Soltanieh, K.M. Azar, M. Saber, "Development of a zero emission integrated system for co-production of electricity and methanol through renewable hydrogen and CO_2 capture", International Journal of Greenhouse Gas Control, 7, (2012) 145–152.

[199]. M.K. Gnanamani, G. Jacobs, R.A. Keogh, W.D. Shafer, D.E. Sparks, S.D. Hopps, G.A. Thomas, B.H. Davis, "Fischer–Tropschsynthesis: effect of pretreatment conditions of cobalt on activity and selectivity for hydrogenation of carbon dioxide", Applied Catalysis A:General, 499, (2015) 39–46.

[200]. S.G. Jadhav, P.D. Vaidya, BM. Bhanage, J.B. Joshi, "Catalytic carbon dioxide hydrogenation to methanol: a review of recent studies", Chemical Engineering Research & Design, 92, (2014) 2557–2567.

[201]. P.G. Jessop, F. Joó, C.C. Tai, "Recent advances in the homogeneous hydrogenation of carbon dioxide", Coordination Chemistry Reviews, 248, (2004) 2425–2442.

[202]. S. Arab, J.M. Commenge, J.F. Portha, L. Falk, "Methanol synthesis from CO_2 and H_2 in multi-tubular fixed-bed reactor and multi-tubular reactor filled with monoliths" Chemical Engineering Research & Design, 92, (2014) 2598–2608.

[203]. M. Farsi, A. Jahanmiri, "Application of water vapor and hydrogen-permselective membranes in an industrial fixed-bed reactor for large scale methanol production", Chemical Engineering Research & Design, 89, (2011) 2728–2735.

[204]. I. González-Aparicio, Z. Kapetaki, E. Tzimas, "Wind energy and carbon dioxide utilisation as an alternative business model for energy producers: a case study in Spain", Applied Energy, 222, (2018) 216–227.

[205]. F. Samimi, S. Kabiri, M.R. Rahimpour, "The optimal operating conditions of a thermally double coupled, dual membrane reactor for simultaneous methanol synthesis, methanol dehydration and methyl cyclohexane dehydrogenation", Journal of Natural Gas Science & Engineering, 19, (2014) 175–189.

[206]. F. Samimi, M.R. Rahimpour, A. Shariati, "Development of an efficient methanol production process for direct CO_2 hydrogenation over a $Cu/ZnO/Al_2O_3$ Catalyst", Catalysts, 7, (2017) 332.

[207]. J. Skrzypek, M. Lachowska, M. Grzesik, J. Słoczýnski, P. Nowak, "Thermodynamics and kinetics of low pressure methanol synthesis", Chemical Engineering Journal & Biochemical Engineering Journal, 58, (1995) 101–108.

[208]. M.J. Bos, D.W.F. Brilman, "A novel condensation reactor for efficient CO_2 to methanol conversion for storage of renewable electric energy", Chemical Engineering Journal, 278, (2015) 527–532.

[209]. N. Karim, S.K. Kamarudin, "An overview on non-platinum cathode catalysts for direct methanol fuel cell", Applied Energy, 103, (2013) 212–220.

[210]. F. Samimi, S. Kabiri, A. Mirvakili, M.R. Rahimpour, "The concept of integrated thermally double coupled reactor for simultaneous production of methanol, hydrogen and gasoline via differential evolution method", Journal of Natural Gas Science & Engineering, 14, (2013) 144–157.

[211]. M. Sahibzada, "Pd-promoted Cu/ZnO catalyst systems for methanol synthesis from CO_2/H_2", Chemical Engineering Research & Design, 78, (2000) 943–946.

[212]. O.S. Joo, K.D. Jung, I. Moon, A.Y. Rozovskii, G.I. Lin, S.H. Han, S.J. Uhm, "Carbon dioxide hydrogenation to form methanol via a reverse-water-gas-shift reaction (the CAMERE process)", Industrial & Engineering Chemistry Research, 38, (1999) 1808–1812.

[213]. S.W. Park, O.S. Joo, K.D. Jung, H. Kim, S.H. Han, "Development of ZnO/Al_2O_3 catalyst for reverse-water-gas-shift reaction of CAMERE (carbon dioxide hydrogenation to form methanol via a reverse-water-gas-shift reaction) process", Applied Catalysis A: General, 211, (2001) 81–90.

[214]. S.W. Park, O.S. Joo, K.D. Jung, H. Kim, S.H. Han, "ZnO/Cr_2O_3 catalyst for reverse-water-gas-shift reaction of CAMERE process", Korean Journal of Chemical Engineering, 17, (2000) 719–722.

[215]. F. Samimi, D. Karimipourfard, M.R. Rahimpour, "Green methanol synthesis process from carbon dioxide via reverse water gas shift reaction in a membrane reactor", Chemical Engineering Research and Design, 140, (2018) 44–67.

[216]. G. Bercic, J. Levec, "Intrinsic and global reaction rate of methanol dehydration over gamma-alumina pellets", Industrial & Engineering Chemistry Research, 31, (1992) 1035–1040.

[217]. S. Khajavi, J.C. Jansen, F. Kapteijn, "Application of a sodalite membrane reactor in esterification — coupling reaction and separation", Catalysis Today, 156, (2010) 132–139.

[218]. M. Rohde, G. Schaub, S. Khajavi, J. Jansen, F. Kapteijn, "Fischer–Tropsch synthesis with in situ H_2O removal — directions of membrane development", Microporous & Mesoporous Materials, 115, (2008) 123–136.

[219]. S. Scire, C. Crisafulli, R. Maggiore, S. Minico, S. Galvagno, "Influence of the support on CO_2 methanation over Ru catalysts: an FT-IR study", Catalysis Letters, 51 (1998) 41–45.

[220]. C.S. Chen, J.H. Lin, J.H. You, C.R. Chen, "Properties of Cu(thd)$_2$ as a Precursor to Prepare Cu/SiO$_2$ Catalyst Using the Atomic Layer Epitaxy Technique", Journal of the American Chemical Society, 128, (2006) 15950–15951.

[221]. S. Moret, P.J. Dyson, G. Laurenczy, "Direct synthesis of formic acid from carbon dioxide by hydrogenation in acidic media", Nature Communications, 5, (2014) 4017.

[222]. F. Studt, I. Sharafutdinov, F. Abild-Pedersen, C.F. Elkjaer, J.S. Hummelshoj, S. Dahl, I. Chorkendorff, J.K. Norskov, "Discovery of a Ni-Ga catalyst for carbon dioxide reduction to methanol", Nature Chemistry, 6, (2014) 320–324.

[223]. S. Xiao, Y. Zhang, P. Gao, L. Zhong, X. Li, Z. Zhang, H. Wang, W. Wei, Y. Sun, "Highly efficient Cu-based catalysts via hydrotalcite-like precursors for CO$_2$ hydrogenation to methanol", Catalysis Today, 281, (2017) 327–336.

[224]. P. Gao, S. Li, X. Bu, S. Dang, Z. Liu, H. Wang, L. Zhong, M. Qiu, C. Yang, J. Cai, W. Wei, "Direct conversion of CO$_2$ into liquid fuels with high selectivity over a bifunctional catalyst", Nature Chemistry, 9, (2017) 1019–1024.

[225]. R.W. Dorner, D.R. Hardy, F.W. Williams, H.D. Willauer, "Heterogeneous catalytic CO$_2$ conversion to value-added hydrocarbons", Energy & Environmental Science, 3, (2010) 884–890.

[226]. S. Abello, D. Montane, "Exploring Iron-based Multifunctional Catalysts for Fischer–Tropsch Synthesis: A Review", ChemSusChem, 4, (2011) 1538–1556.

[227]. N. Meiri, R. Radus, M. Herskowitz, "Simulation of novel process of CO$_2$ conversion to liquid fuels", Journal of CO$_2$ Utililization, 17, (2017) 284–289.

[228]. W. Li, H. Wang, X. Jiang, J. Zhu, Z. Liu, X. Guo, C. Song, "A short review of recent advances in CO$_2$ hydrogenation to hydrocarbons over heterogeneous catalysts", RSC Advances, 8, (2018) 7651-7669.

[229]. U. Rodemerck, M. Holena, E. Wagner, Q. Smejkal, A. Barkschat, M. Baerns, Catalyst Development for CO$_2$ Hydrogenation to Fuels", ChemCatChem, 5, (2013) 1948–1955.

[230]. J. Wei, J. Sun, Z. Wen, C. Fang, Q. Ge, H. Xu, "New insights into the effect of sodium on Fe$_3$O$_4$-based nanocatalysts for CO$_2$ hydrogenation to light olefins", Catalysis Science & Technology, 6, (2016) 4786–4793.

[231]. S. Hu, M. Liu, F. Ding, C. Song, G. Zhang, X. Guo, "Hydrothermally stable MOFs for CO$_2$ hydrogenation over iron-based catalyst to light olefins", Journal of CO$_2$ Utilization, 15, (2016) 89–95.

[232]. R. Satthawong, N. Koizumi, C.S. Song, P. Prasassarakich, "Comparative Study on CO_2 Hydrogenation to Higher Hydrocarbons over Fe-Based Bimetallic Catalysts", Topics in Catalysis, 57, (2014) 588–594.

[233]. P. Kangvansura, L.M. Chew, W. Saengsui, P. Santawaja, Y. Poo-arporn, M. Muhler, H. Schulz, A. Worayingyong, "Product distribution of CO_2 hydrogenation by K-and Mn-promoted Fe catalysts supported on N-functionalized carbon nanotubes", Catalysis Today, 275, (2016) 59–65.

[234]. J. Zhang, S. Lu, X. Su, S. Fan, Q. Ma, T. Zhao, "Selective formation of light olefins from CO_2 hydrogenation over Fe–Zn–K catalysts", Journal of CO_2 Utilization, 12, (2015) 95–100.

[235]. M. Albrecht, U. Rodemerck, M. Schneider, M. Bröring, D. Baabe, E.V. Kondratenko, "Unexpectedly efficient CO_2 hydrogenation to higher hydrocarbons over non-doped Fe_2O_3", Applied Catalysis B: Environmental, 204, (2017) 119–126.

[236]. B. Zeng, B. Hou, L. Jia, J. Wang, C. Chen, D. Li, Y. Sun, "The intrinsic effects of shell thickness on the Fischer–Tropsch synthesis over core–shell structured catalysts", Catalysis Science & Technology, 3, (2013) 3250–3255.

[237]. R. Xie, H. Wang, P. Gao, L. Xia, Z. Zhang, T. Zhao, Y. Sun, "Core@shell Co_3O_4@C-m-SiO_2 catalysts with inert C modified mesoporous channel for desired middle distillate", Applied Catalysis A: General, 492, (2015) 93–99.

[238]. M.K. Gnanamani, G. Jacobs, R.A. Keogh, W.D. Shafer, D.E. Sparks, S.D. Hopps, G.A. Thomas, B.H. Davis, "Fischer-Tropsch synthesis: Effect of pretreatment conditions of cobalt on activity and selectivity for hydrogenation of carbon dioxide", Applied Catalysis A: General, 499, (2015) 39–46.

[239]. R.E. Owen, J.P. O'Byrne, D. Mattia, P. Plucinski, S.I. Pascu, M.D. Jones, "Cobalt catalysts for the conversion of CO_2 to light hydrocarbons at atmospheric pressure", Chemical Communications, 49, (2013) 11683–11685.

[240]. W. Wang, S. Wang, X. Ma, J. Gong, "Recent advances in catalytic hydrogenation of carbon dioxide", Chemical Society Reviews, 40, (2011) 3703–3727.

[241]. T. Riedel, M. Claeys, H. Schulz, G. Schaub, S.S. Nam, K.W. Jun, M.J. Choi, G.Kishan, K.W. Lee, "Comparative study of Fischer–Tropsch synthesis with H_2/CO and H_2/CO_2 syngas using Fe- and Co-based catalysts", Applied Catalysis A: General, 186, (1999) 201–213.

[242]. A.N. Akin, M. Ataman, A.E. Aksoylu, Z.I. Onsan, "CO_2 fixation by hydrogenation over coprecipitated Co/Al_2O_3", Reaction Kinetics & Catalysis Letters, 76, (2002) 265–270.

[243]. C.G. Visconti, M. Martinelli, L. Falbo, A. Infantes-Molina, L. Lietti, P. Forzatti, G. Iaquaniello, E. Palo, B. Picutti, F. Brignoli, "CO_2 hydrogenation to lower olefins on a high surface area K-promoted bulk Fe-catalyst", Applied Catalysis B: Environmental, 200, (2017) 530–542.

[244]. M. Rafati, L. Wang, A. Shahbazi, "Effect of silica and alumina promoters on co-precipitated Fe–Cu–K based catalysts for the enhancement of CO_2 utilization during Fischer–Tropsch synthesis", Journal of CO_2 Utilization, 12, (2015) 34–42.

[245]. T. Lunkenbein, J. Schumann, M. Behrens, R. Schlögl, M.G. Willinger, "Formation of a ZnO overlayer in industrial $Cu/ZnO/Al_2O_3$ catalysts induced by strong metal–support interactions", Angewandte Chemie International Edition, 54, (2015) 4544–4548.

[246]. M. Behrens, F. Studt, I. Kasatkin, S. Kühl, M. Hävecker, F. Abild-Pedersen, S. Zander, F. Girgsdies, P. Kurr, B.-L. Kniep, M. Tovar, R.W. Fischer, J.K. Nørskov, R. Schlögl, "The active site of methanol synthesis over $Cu/ZnO/Al_2O_3$ industrial catalysts", Science, 336, (2012) 893–897.

[247]. S. Kuld, M. Thorhauge, H. Falsig, C.F. Elkjær, S. Helveg, I. Chorkendorff, J. Sehested, Quantifying the promotion of Cu catalysts by ZnO for methanol synthesis, Science 352, (2016) 969–974.

[248]. M.M.J. Li, Z. Zeng, F. Liao, X. Hong, S.C.E. Tsang, "Enhanced CO_2 hydrogenation to methanol over CuZn nanoalloy in Ga modified Cu/ZnO catalysts", Journal of Catalysis, 343, (2016) 157–167.

[249]. S.D. Senanayake, P.J. Ramirez, I. Waluyo, S. Kundu, K. Mudiyanselage, Z. Liu, Z. Liu, S. Axnanda, D.J. Stacchiola, J. Evans, J.A. Rodriguez, "Hydrogenation of CO_2 to methanol on $CeO_x/Cu(111)$ and $ZnO/Cu(111)$ catalysts: Role of the metal–oxide interface and importance of Ce^{3+} sites", Journal of Physical Chemistry C, 120, (2016) 1778–1784.

[250]. S. Kattel, P.J. Ramírez, J.G. Chen, J.A. Rodriguez, P. Liu, "Active sites for CO_2 hydrogenation to methanol on Cu/ZnO catalysts", Science, 355, (2017) 1296–1299.

[251]. L. Martínez-Suárez, J. Frenzel, D. Marx, "Cu/ZnO nanocatalysts in response to environmental conditions: surface morphology, electronic structure, redox state and CO_2 activation", Physical Chemistry Chemical Physics, 16, (2014) 26119–26136.

[252]. L. Martínez-Suárez, N. Siemer, J. Frenzel, D. Marx, "Reaction network of methanol synthesis over Cu/ZnO Nanocatalysts", ACS Catalysis, 5, (2015) 4201–4218.

[253]. K. Larmier, W.C. Liao, S. Tada, E. Lam, R. Verel, A. Bansode, A. Urakawa, A. Comas-Vives, C. Copéret, "CO_2-to-methanol hydrogenation on zirconia-supported copper

nanoparticles: Reaction intermediates and the role of the metal–support interface", Angewandte Chemie International edition, 129, (2017) 2358–2363.

[254]. R. Naumann d'Alnoncourt, X. Xia, J. Strunk, E. Loffler, O. Hinrichsen, M. Muhler, "The influence of strongly reducing conditions on strong metal-support interactions in Cu/ZnO catalysts used for methanol synthesis", Physical Chemistry Chemical Physics, 8, (2006) 1525–1538.

[255]. F. Studt, M. Behrens, E.L. Kunkes, N. Thomas, S. Zander, A. Tarasov, J. Schumann, E. Frei, J.B. Varley, F. Abild-Pedersen, J.K. Nørskov, R. Schlögl, "The mechanism of CO and CO_2 hydrogenation to methanol over Cu-based catalysts", ChemCatChem, 7, (2015) 1105–1111.

[256]. J. Graciani, K. Mudiyanselage, F. Xu, A.E. Baber, J. Evans, S.D. Senanayake, D.J. Stacchiola, P. Liu, J. Hrbek, J.F. Sanz, J.A. Rodriguez, "Highly active copper-ceria and copper-ceria-titania catalysts for methanol synthesis from CO_2", Science, 345, (2014) 546–550.

[257]. J. Graciani, A.B. Vidal, J.A. Rodriguez, J.F. Sanz, "Unraveling the nature of the oxide–metal interaction in ceria-based noble metal inverse catalysts", Journal of Physical Chemistry C, 118, (2014) 26931–26938.

[258]. J.A. Rodriguez, S. Ma, P. Liu, J. Hrbek, J. Evans, M. Pérez, "Activity of CeO_x and TiO_x nanoparticles grown on Au(111) in the water-gas shift reaction", Science, 318, (2007) 1757–1760.

[259]. J.A. Rodriguez, J. Hrbek, "Inverse oxide/metal catalysts: a versatile approach for activity tests and mechanistic studies", Surface Science, 604, (2010) 241–244.

[260]. S. Kattel, W. Yu, X. Yang, B. Yan, Y. Huang, W. Wan, P. Liu, J.G. Chen, "CO_2 hydrogenation over oxide-supported PtCo catalysts: The role of the oxide support in determining the product selectivity", Angewandte Chemie International Edition, 55, (2016) 7968–7973.

[261]. S. Kattel, B. Yan, Y. Yang, J.G. Chen, P. Liu, "Optimizing binding energies of key intermediates for CO_2 hydrogenation to methanol over oxide-supported copper", Journal of the American Chemical Society, 138, (2016) 12440–12450.

[262]. E.L. Kunkes, F. Studt, F. Abild-Pedersen, R. Schlögl, M. Behrens, "Hydrogenation of CO_2 to methanol and CO on $Cu/ZnO/Al_2O_3$: Is there a common intermediate or not?", Journal of Catalysis, 328, (2015) 43–48.

[263]. Y. Yang, J. Evans, J.A. Rodriguez, M.G. White, P. Liu, "Fundamental studies of methanol synthesis from CO_2 hydrogenation on Cu(111), Cu clusters, and Cu/ZnO(0001)", Physical Chemistry Chemical Physics, 12, (2010) 9909–9917.

[264]. L.B. Backman, A. Rautiainen, M. Lindblad, O. Jylha, A.O.I. Krause, "Characterisation of Co/SiO_2 catalysts prepared from $Co(acac)_3$ by gas phase deposition", Applied Catalysis A: General, 208, (2001) 223-234

[265]. S. Ho, M. Houalla, D.M. Hercules, "Effect of particle size on carbon monoxide hydrogenation activity of silica supported cobalt catalysts", Journal of Physical Chemistry, 94, (1990) 6396-6399.

[266]. E. Iglesia, "Design, synthesis, and use of cobalt-based Fischer-Tropsch synthesis catalysts", Applied Catalysis A: General, 161, (1997) 59-78.

[267]. J.H. Cho, J.H. Park, T.S. Chang, G. Seo, C.H. Shin, "Reductive amination of 2-propanol to monoisopropylamine over $Co/\gamma-Al_2O_3$ catalysts", Applied Catalysis A: General, 417–418, (2012) 313-319.

[268]. G. Jacobs, P.M. Patterson, T.K. Das, M. Luo, B.H. Davis, "Fischer–Tropsch synthesis: effect of water on Co/Al_2O_3 catalysts and XAFS characterization of reoxidation phenomena", Applied Catalysis A: General, 270, (2004) 65-76.

[269]. G.P. Van Der Laan , A.A.C.M. Beenackers , "Kinetics and selectivity of the Fischer–Tropsch synthesis: a literature review", Catalysis Reviews, 41, (1999) 255–318.

[270]. B. Deng , X. Pang , "Variations of optic properties of water under action of static magnetic field", Chinese Science Bulletin, 52, (2007) 3179–3182.

[271]. S.H. Kwack, M.J. Park, J. Bae, K.S. Ha, K.W. Jun, "Development of a kinetic model of the Fischer–Tropsch synthesis reaction with a cobalt-based catalyst", Reaction Kinetics, Mechanism & Catalysis, 104, (2011) 483–502.

[272]. B.T. Teng, J. Chang, J. Yang, G. Wang, C.H. Zhang, Y.Y. Xu, H.W. Xiang, Y.W. Li, "Water gas shift reaction kinetics in Fischer–Tropsch synthesis over an industrial Fe–Mn catalyst", Fuel, 84, (2005) 917–926.

[273]. N. Fischer, R. Henkel, B. Hettel, M. Iglesias, G. Schaub, M. Claeys, "Hydrocarbons via CO_2 Hydrogenation Over Iron Catalysts: The Effect of Potassium on Structure and Performance", Catalysis Letters, 146, (2016) 509–517.

[274]. A.N. Pour, M.R. Housaindokht, S.F. Tayyari, J. Zarkesh, "Effect of nano-particle size on product distribution and kinetic parameters of Fe/Cu/La catalyst in Fischer-Tropsch synthesis", Journal of Natural Gas Chemistry, 19, (2010) 107–116.

64

[275]. M. Iglesias, R. Edzang, G. Schaub, "Combinations of CO/CO_2 reactions with Fischer–Tropsch synthesis", Catalysis Today, 215, (2013) 194–200.

[276]. A.N. Pour, H. Khodabandeh, M. Izadyar, M.R. Housaindokht, "Detailed kinetics of Fischer–Tropsch synthesis on a precipitated iron catalyst", Reaction Kinetics, Mechanism & Catalysis, 111, (2014) 29–44.

[277]. A.N. Pour, Z. Keyvanloo, M. Izadyar, S.M. Modaresi, "Dissociative hydrogen adsorption on the cubic cobalt surfaces: A DFT study", International Journal of Hydrogen Energy, 40, (2015) 7064–7071.

[278]. T. Riedel, G. Schaub, K.W. Jun, K.W. Lee, "Kinetics of CO_2 Hydrogenation on a K-Promoted Fe Catalyst", Industrial & Engineering Chemistry Research, 40, (2001) 1355–1363.

[279]. H.D. Willauer, R. Ananth, M.T. Olsen, D.M. Drab, D.R. Hardy, F.W. Williams, "Modeling and kinetic analysis of CO_2 hydrogenation using a Mn and K-promoted Fe catalyst in a fixed-bed reactor", Journal of CO_2 Utilization, 3–4, (2013) 56–64.
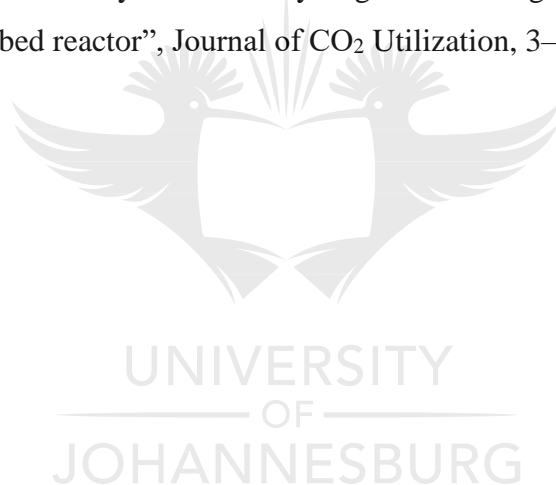
CHAPTER 3: RESEARCH APPROACH AND METHODOLOGY

3.1 Introduction

The main objective of this chapter is to outline the general techniques that were followed to achieve the objectives of this project. Several experiments were conducted, and this section will only provide the general procedures followed and details on the equipment used. The specific experimental details are provided in their respective chapters.

This project involves the preparation of several alumina-supported catalysts that were characterized using several techniques and tested for modified Fischer-Tropsch reactions that converted CO_2 into synthetic fuel. Research activities covered in this project include catalysts synthesis, characterization and evaluation for CO_2 hydrogenation.

3.2 Materials and chemicals used

3.2.1 Gases

All gases used in this study were of high purity and supplied by AFROX. The composition of all gasses used in the study are outlined below.

a)   Calibration gas mixture

This gas mixture was used to calibrate the gas chromatograph (GC) and has the following molar composition:

C_2H_4: 0.98%

C_2H_6: 0.98%

CO_2: 4.8%

CH_4: 5.2%

CO: 24.0%

N_2: 10.4%

H_2: Bal

b) Special feed gas

The feed gas was used for modified FT runs. It contained 10% N_2, 22.5% CO_2 with H_2 balance.

c) Nitrogen

Nitrogen was used to purge and flush the system and for pressurizing the system to check for leaks before starting the reaction.

d) Carrier gases for the GC

Pure Ar was used as carrier gas for the thermal conductivity detector (TCD) connected to a carboxen 1000 column.

Pure H_2 and air were used as flame gases and H_2 was also used as carrier gas for the flame ionization detector (FID) connected to a fused silica capillary column 30m long with 0.32mm diameter.

e) Gases used as reducing agents:

5%H_2/Ar was used to perform temperature programmed reduction (TPR).

10%CO_2/He was used to perform temperature programmed desorption (TPD).

3.2.2 Chemicals

Cobalt nitrate hexahydrate ($Co(NO_3)_2 \cdot 6H_2O$) was used as precursor for the Al_2O_3 supported catalyst. Potassium nitrate (KNO_3) was used to load potassium on the prepared 15%Co/Al_2O_3 catalyst. Copper nitrate trihydrate ($CuN_2O_6 \cdot 3H_2O$), Palladium nitrate hydrate ($PdN_2O_6 \cdot 2H_2O$) and ruthenium nitrosyl nitrate ($HN_4O_{10}Ru$) solutions were used to load copper, palladium and ruthenium respectively on the prepared 15%Co-6%K/Al_2O_3 catalyst. All chemicals used in this project were supplied by Sigma-Aldrich.

3.3 Equipment

Various equipment were used to achieve the objective of this project. A drying oven was used to dry both the blank support and various support samples impregnated by metal precursor solution before calcination to remove moisture from the samples. A calcination oven was used

to remove moisture in both blank support and impregnated supports and to decompose metal precursor in the catalyst to either their oxide or metallic forms.

Several characterization equipment were employed in this project. X-Ray diffractometer (Rigaku Ultima IV) was used to determine the structure of the catalyst. Figure 3.1 shows the X-ray diffractometer that was used to perform XRD analysis for this study.

Figure 3. 1: X-ray diffractometer

Micrometritics ASAP 2460 apparatus was used to perform N_2 adsorption using the Brunauer-Emmett-Teller (BET) method. The analysis was done on the Micrometritics Tristar apparatus shown in Figure 3.2.

Figure 3. 2: Micrometritics Tristar apparatus (ASAP 24600)

Temperature programmed reduction (TPR) was conducted using the apparatus constructed at the University. The analysis was conducted on equipment shown in Figure 3.3.

Figure 3. 3: TPR apparatus

SPECS PHOIBOS 150 hemispherical analyzer was used to perform X-ray photoelectron spectroscopy (XPS) analysis to obtain information on the oxidation state of the various species on the catalyst surface. SPECS PHOIBOS 150 hemispherical used to perform XPS is shown in Figure 3.4 below.
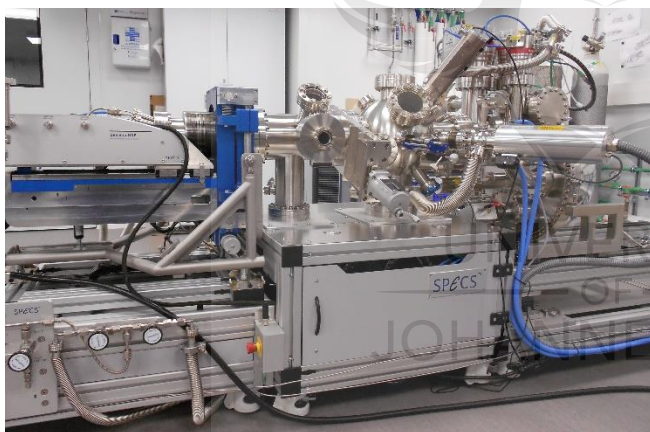
Figure 3. 4: SPECS PHOIBOS 150 hemispherical

The prepared catalysts were tested for CO_2 hydrogenation using a fixed-bed tubular reactor constructed at the university. The reactor used was 400 mm long with an internal diameter of 15 mm. The reactor gas products were analyzed using a DANI Master GC. Pictures showing the GC and the FT rig used in this study are shown in Figure 3.5.
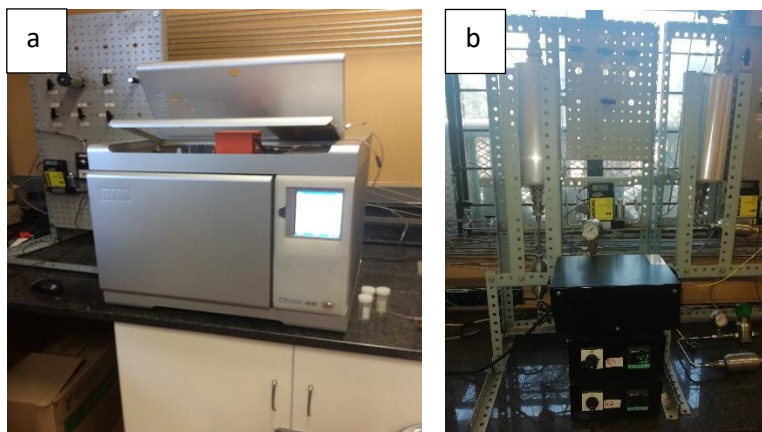
Figure 3. 5: a) Dani master GC and b) fixed bed reactor setup

3.4 Experimental procedure

The various steps followed to meet the objectives of this project are detailed in this section and include catalyst synthesis, characterization and testing.

3.4.1 Catalyst synthesis

The catalysts used in this study were synthesized using an incipient wetness impregnation of the support with nitrate solutions. All catalysts were supported on γ-alumina and promoted with potassium (0-8%) and/or 0-3% of either copper, ruthenium or palladium. The support was prepared by mixing γ-alumina with distilled water and dried in air at 120 $^{\circ}$C for 24 hours. The support was then calcined in air at 500 $^{\circ}$C for 10 hours. The blank calcined support was then impregnated with aqueous solution of cobalt nitrate hexahydrate ($CoN_2O_6.6H_2O$). The impregnating solution was added to the γ-alumina to give a cobalt loading of 15% by mass. The impregnated support was dried in air at 120 $^{\circ}$C and calcined in air at 500 $^{\circ}$C for 10 hours to decompose and convert cobalt nitrate to cobalt oxide. The catalysts promoted with potassium were prepared by consecutive incipient wetness impregnation step using potassium nitrate solution. The catalysts were prepared to give the weight percentage of potassium to be 0, 1, 3, 5, 6 and 8 wt.% respectively. The promoted catalysts were also dried in air overnight at 120 $^{\circ}$C and then calcined in air at 500 $^{\circ}$C for 10 hours. The second promoters (i.e noble metal Ru or Pd and other metals such as Cu) were also added using the same method. The catalysts were prepared to give the weight percentage of potassium to be 6 wt.% and the second promoter weight percentage of 0 – 3 wt.% respectively.

70

3.4.2 Catalyst characterization

XRD, BET, XPS, TPR, and CO_2 TPD analyses were used to characterize the catalyst.

3.4.2.1. X-ray diffraction (XRD) analyses

XRD analysis was conducted using the Rigaku Ultima IV diffractometer using Cu-Kα radiation (30 mA,0 kV). The scan was taken from $2\theta = 10°$ to $2\theta = 90°$ with a step width of $2\theta = 0.03°$.

3.4.2.2 Brunauer – Emmett – Teller (BET) analyses

Surface area and porosity are significant features, capable of influencing the quality and usefulness of various materials. As a result, it is essential to define and manipulate them perfectly. Equally, understanding of porosity and surface area are often vital keys in understanding the structure, formation and possible uses of different natural materials. BET was employed to determine catalyst surface area and pore distribution in the catalyst. Nitrogen gas was used in all the BET surface area measurements using Micrometritics ASAP 2460 apparatus. N_2 adsorption-desorption was performed at -196 ºC.

3.4.2.3 X-ray photoelectron spectroscopy (XPS) analyses

X-ray photoelectron spectroscopy (XPS) analysis was performed on a SPECS PHOIBOS 150 hemispherical analyzer to obtain information on the oxidation state of the various species on the catalyst surface. The X – ray source was a monochromatised Al Ka at 1486.71 eV. The total experimental resolution was of the order of 0.6 to 0.7 eV. A low energy electron flood gun was used to counteract charging of the sample. The parameters of the flood gun were 2.0 to 2.5 eV and 20 µA. The binding energies were corrected by setting the oxidic O1s binding energy to 531.5 eV [1].

3.4.2.4 Temperature programmed reduction (TPR) analyses

TPR was performed on an apparatus constructed at the University to compare the behavior of unpromoted and promoted Co catalysts during reduction in the presence of H_2. The analyses were performed with a gas mixture containing 5% H_2 in Ar. 100 mg of calcined catalyst samples were initially loaded in a stainless-steel tube reactor and degassed using pure helium gas (30 ml/min) at 300 °C for 60 min and cooled to room temperature. The catalyst was subsequently exposed to a continuous flow of a reducing gas mixture (5% H_2 in Ar) while the reactor temperature was elevated to 700 °C with a heating rate of 10 ºC. The flow-rate of the

reducing gas was kept at 30 ml/min for all the analyses and a thermal conductivity detector (TCD) was located at the reactor outlet to detect changes in H_2 concentration.

3.4.2.5 CO_2 - Temperature programmed desorption (TPD) analyses

CO_2 temperature programed desorption (CO_2-TPD) analyses were performed to determine catalyst basicity, using the same equipment used to perform H_2-TPR analysis. The analysis was performed on a reduced and passivated catalyst sample. Catalyst reduction was performed as described in section 3.4.3. Catalyst passivation was performed by exposing the reduced catalyst to a flow of 5% O_2/He for 2 hours at room temperature. 200 mg of reduced and passivated catalyst were then loaded into the tube reactor, which was flushed with pure He at 300 $^\circ$C (30 ml/min) for 1 hour. After cooling to room temperature, TPR was conducted with 5%H_2/Ar at 350 $^\circ$C for 30 minutes at a heating rate of 10 $^\circ$C/min. The sample was then exposed to a flow of pure He at 350 $^\circ$C (30 ml/min) for 30 min before cooling to 50 $^\circ$C. The sample was maintained at this temperature for 10 minutes before switching the gas to 10%CO_2/He for 60 minutes. After this step, the gas was switched back to pure He to remove all molecules physically adsorbed on the sample. Once the TCD signal was stable, CO_2-TPD was performed, under the flow of He, by increasing the temperature from 50 $^\circ$C to 700 $^\circ$C at a heating rate of 5 $^\circ$C/min and holding at 700 $^\circ$C for 30 minutes [2].

3.4.3 Catalyst testing

The catalysts were tested for carbon dioxide hydrogenation using a fixed-bed tubular reactor constructed at the university. 0.5 g of the catalyst was loaded in the reactor and various parameters such as the operating pressure, temperature, potassium loading and promotion with a second metal were evaluated. P&ID diagram for the experimental set-up is given in fig 3.6.
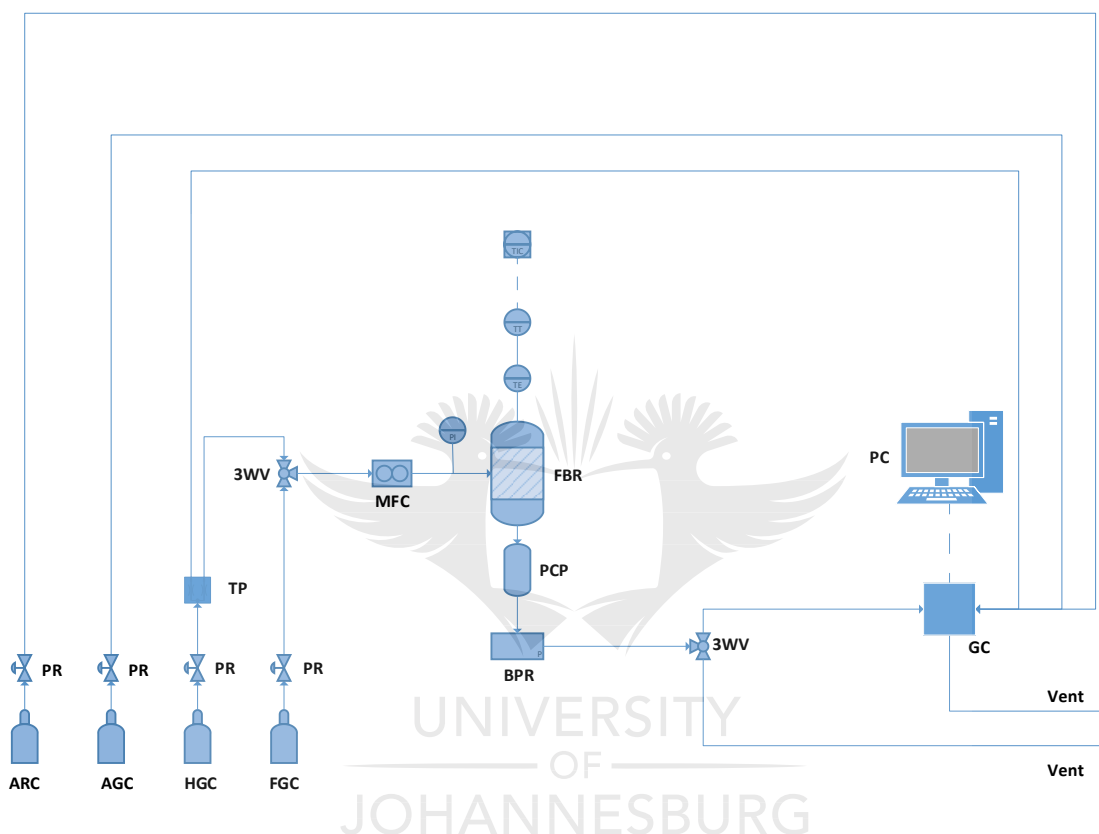
Figure 3. 6: P&ID for experimental set up

Where:

AGC – Air gas cylinder

ARC – Argon gas cylinder

BPR – Back pressure regulator

FBR – Fixed bed reactor

FGC – Feed gas cylinder

GC – Gas Chromatograph

HGC – Hydrogen gas cylinder

MFC – Mass flow-controller

PC – Personal computer

PCP – Product collection pot

PI – Pressure indicator

PR – Pressure regulator
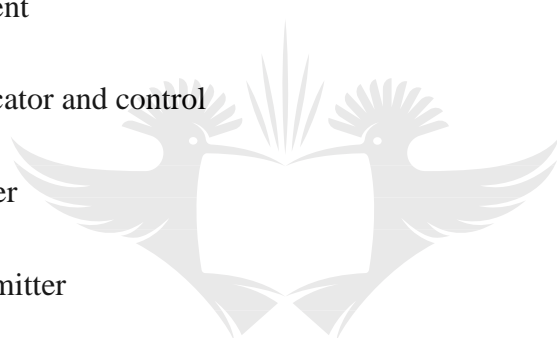
TE – Temperature element

TIC – Temperature indicator and control

TP – T-piece flow divider

TT – Temperature transmitter

3WV – Three –way valve

The reactor was constructed using a stainless–steel tube with the internal diameter of 16 mm and the length of 220 mm. The catalyst was loaded in the central part of the tube and the remaining space was filled with glass wool. The catalyst was fixed in one position in the reactor using a thin layer of glass wool to avoid catalyst loss. The system was pressurized to 20 bar using pure nitrogen to test for leaks. The catalysts were activated by reducing with pure H_2 for 17 hours to convert cobalt oxide to metallic cobalt. The flow rate of the reducing gas mixture was set to 30 ml/min at atmospheric pressure. Inlet reducing gas flow-rate was adjusted to 30 ml/min using an Aalborg GFC17 mass-flow controller and the flow was confirmed using a bubble flow-meter located at the reactor outlet. The temperature was elevated from room temperature to 350 ºC at a rate of 10 ºC per minute and kept there for 17 hours. The reactor was heated using a heating coil and the temperature was measured and monitored using Thermon type "K" thermocouple with the length of 400 mm and 1.5 mm diameter and controlled using a Unitemp temperature control unit. After reduction, the system was cooled to

room temperature under the flow of the reducing gas before switching to feed gas used for hydrogenation.

Once switching to feed gas, the reactor was pressurized (if necessary) and the feed gas was allowed to flow for at 1 hour under room temperature. The flow was adjusted to 10 ml/min and the temperature was increased at a heating rate of 10 $^{\circ}$C/min. CO_2 hydrogenation runs were performed using a feed containing 10%N_2, 22.5%CO_2 and 67.5%H_2. The outlet gas products were analyzed using a Dani master GC equipped with TCD and an FID.

Examples of FID and TCD chromatograms for calibration mixture and a reactor exit sample are given in Figure 3.7 – 3.10 below.
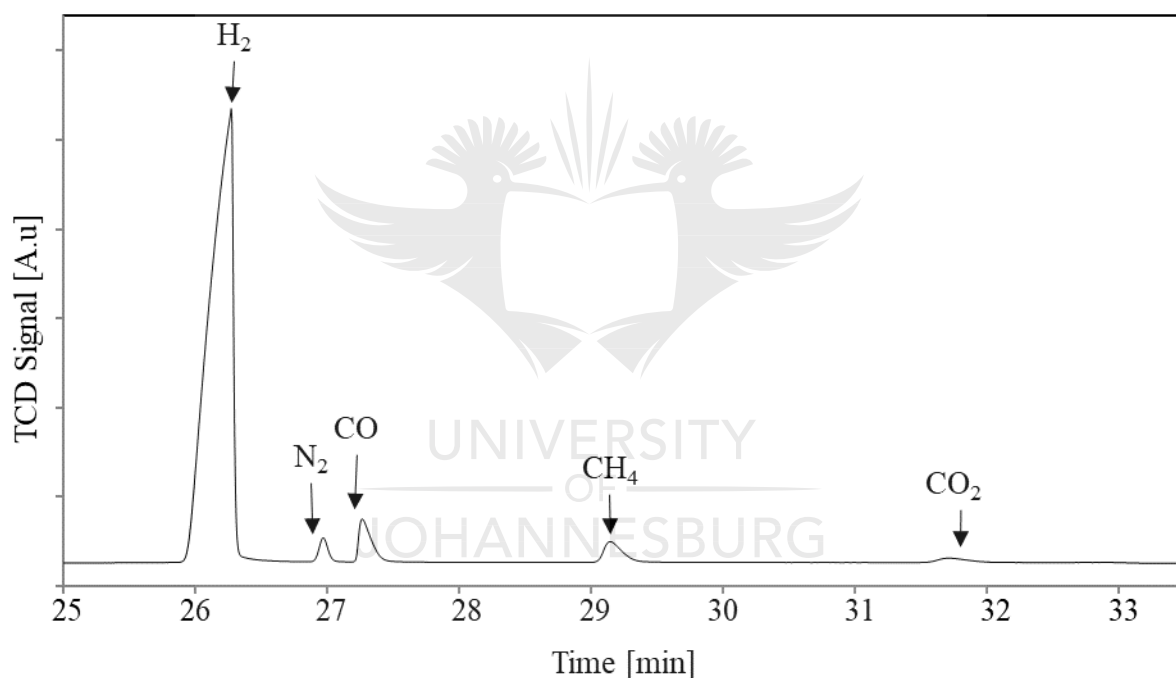
Figure 3. 7: GC chromatogram for calibration mixture on TCD
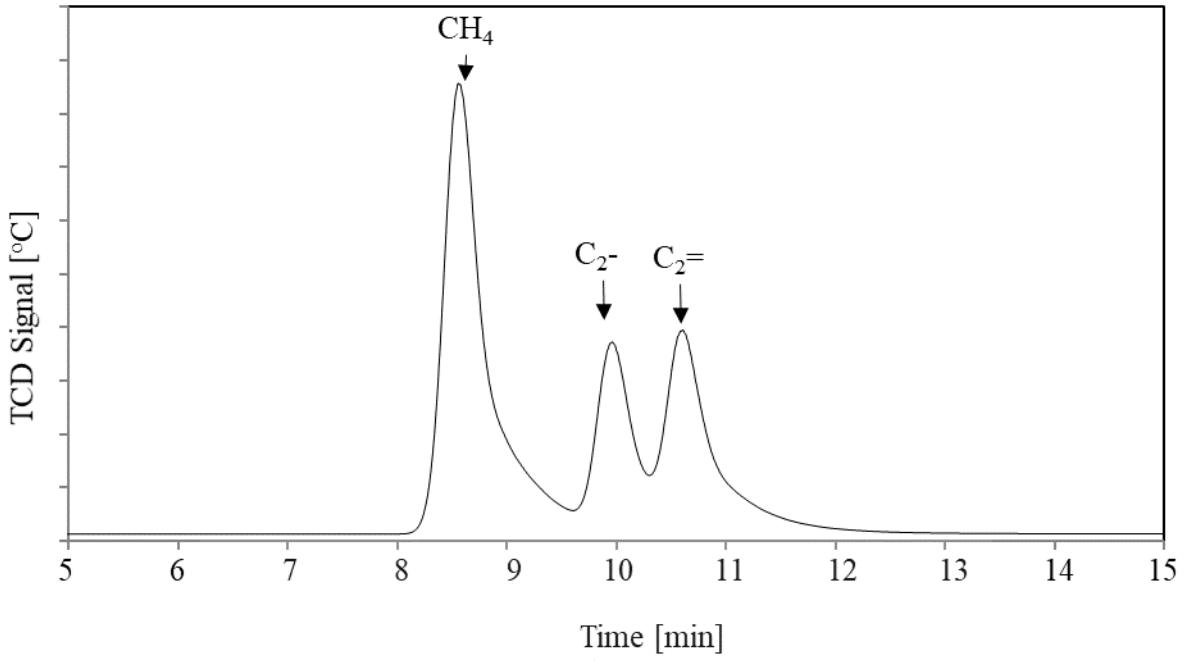
Figure 3. 8: GC chromatogram for calibration mixture on FID
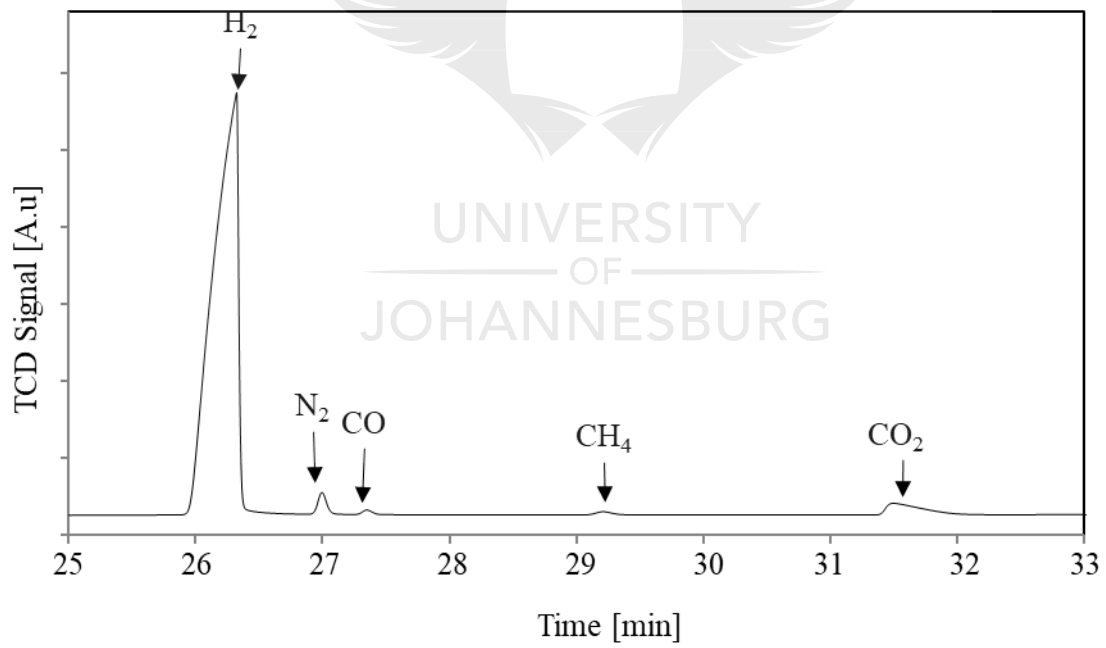
Figure 3. 9: GC chromatogram for reactor outlet on TCD

76
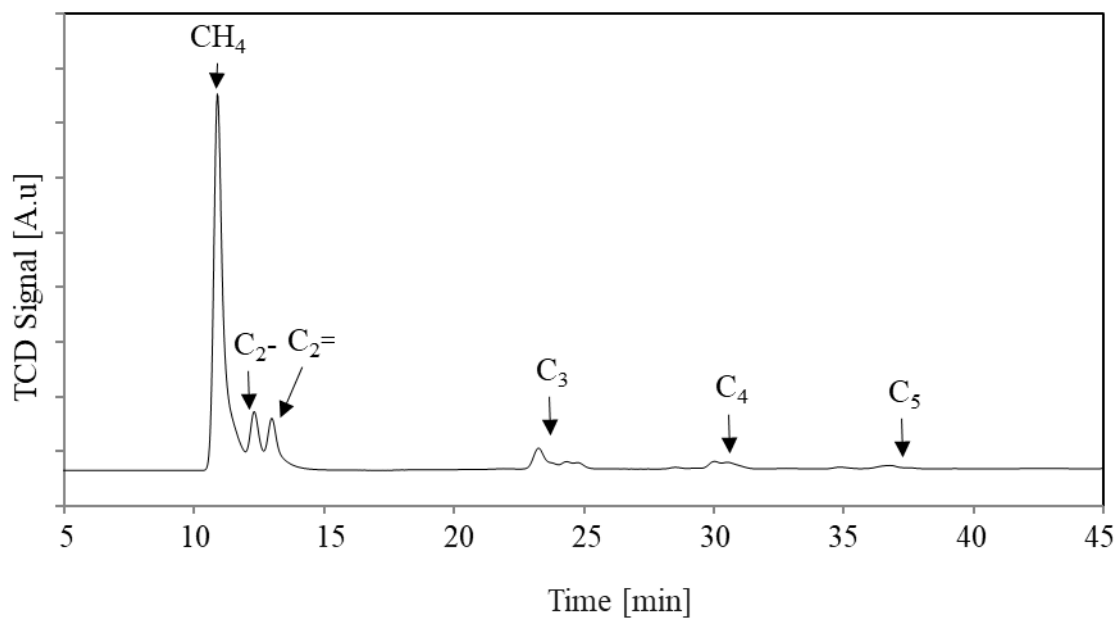
Figure 3. 10: GC chromatogram for reactor outlet sample on FID
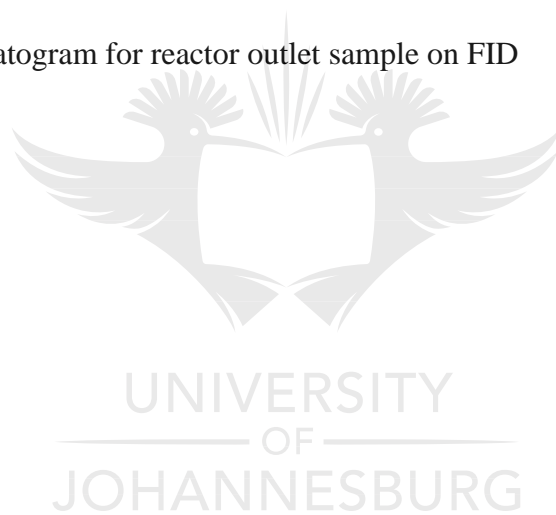
3.4.4 Data collection and processing

3.4.4.1 TPR and TPD

The equipment used was equipped with the TCD, which was connected to the personal computer on which all the information provided by the TCD was recorded using Pico station software (TCD signal (a.u) as a function of time (s). The data was exported to text file and then to excel spreadsheet. Time in seconds was divided by 60 and multiplied by the heating rate (either 10 or 5 ^oC/min) to convert time into the corresponding temperature based on the programme that was entered on the temperature control unit.

3.4.4.2 BET

Micromeritics' innovative MicroActive software was used to process the isotherm data from Micromeritics ASAP. The program installed on the machine automatically generate the results using BET and BJH model. An example of a machine printouts is available in Appendix C.

3.4.4.3 XRD

XRD data was processed using PDxL software program and the quantification of the sample was done using Reference Internal Ratio (RIR). The software allowed for the data to be exported into excel and the XRD patterns were replotted. The software also generated the peak list as excel file and this was used to identify different peaks. The average size of cobalt particles was calculated according to the Scherrer equation:

$$d = \frac{k\lambda}{\beta Cos\theta} \dots\dots\dots\dots\dots\dots\dots\dots\dots\dots\dots\dots\dots\dots\dots\dots\dots\dots.(3.1)$$

where:

d is the average crystallite diameter;

λ is the wavelength of X-ray, and;

β is the full width at half maximum in radian.

3.4.4.4 XPS

XPS data was exported as XY file and the file was opened as text file using the personal computer. The data was then transferred into an excel file and replotted. The data was corrected by setting the oxidic O1s binding energy to 531.5 eV.

3.4.4.5 Catalyst testing

The reactor outlet products were analyzed using the GC and the results were recorded using Clarity Apex GC software. The software allowed for data to be integrated and the area under the peaks were captured on the excel spreadsheet. The GC was calibrated with the premixed gas in which all the molar fractions for gases were known. The calibration mixture contained CH_4, C_2H_4, C_2H_6, CO, CO_2, H_2 and N_2 and its composition is given in section 3.2.1. The C_1 and C_2 hydrocarbons were calibrated directly, and the remaining hydrocarbons in the gas phase were calculated using the calibration for C_2 and the corresponding response factors. The response factors for hydrocarbons are given in Table 3.1 below.

Table 3. 1: Hydrocarbons response factors [3].

Carbon Number	Olefin	Paraffin
2	1.00	1.00
3	0.70	0.74
4	0.55	0.55
5	0.47	0.47
6	0.40	0.40
7	0.35	0.35
8	0.32	0.32
9	0.28	0.28
10	0.24	0.24
11	0.21	0.21
12	0.19	0.19
13	0.18	0.18
14	0.17	0.17
15	0.15	0.15

3.4.4.6 Mass balance calculations

The configuration of the experimental set-up used in this study allows setting the inlet volumetric flowrate, from which the outlet flow rate can be calculated. N_2 (10%) was present in the reaction feed as an internal standard used for accurate calculations of the CO_2 conversion.

The N_2 balance is shown in equation 3.2

$$\dot{n}_{T_{in}} \times \%N_{2_{in}} = \dot{n}_{T_{out}} \times \%N_{2_{out}} \dots\dots\dots\dots\dots\dots\dots\dots\dots\dots\dots\dots\dots\dots\dots.(3.2)$$

Where $\dot{n}_{T_{in}}$ and $\dot{n}_{T_{out}}$ are the total molar flow rates entering and leaving the reactor and $\%N_{2in}$ and $\%N_{out}$ are the percentages of N_2 flowing in and out respectively.

The $\%CO_2$ conversion was calculated as follows:

$$\%CO_2 \text{ conversion} = \frac{\dot{n}_{CO_{2reacted}}}{\dot{n}_{CO_{2in}}} \times 100\% = \frac{\dot{n}_{CO_{2in}} - \dot{n}_{CO_{2out}}}{\dot{n}_{CO_{2in}}} \times 100\% \dots\dots\dots\dots..(3.3)$$

Where

$$\dot{n}_{CO_{2in}} = \dot{n}_{T_{in}} \times \%CO_{2_{in}} \dots\dots\dots\dots\dots\dots\dots\dots\dots\dots\dots\dots\dots\dots\dots...\dots (3.4)$$

$$\dot{n}_{CO_{2out}} = \dot{n}_{T_{out}} \times \%CO_{2_{out}} \dots\dots\dots\dots\dots\dots\dots\dots\dots\dots\dots\dots. \dots\dots..\dots\dots\dots(3.5)$$

$$\dot{n}_{T_{out}} = \dot{n}_{T_{in}} \times \frac{\%N_{2in}}{\%N_{2out}} \dots\dots\dots\dots\dots\dots\dots\dots..\dots\dots\dots\dots\dots\dots\dots\dots\dots.....(3.6)$$

After substitution of equations 3.4, 3.5 and 3.6 in equation 3.3, the % CO_2 conversion was calculated as

$$\%CO_2 \text{ conversion} = \frac{\%CO_{2in} - \left(\frac{\%N_{2in}}{\%N_{2out}}\right) \times \%CO_{2out}}{\%CO_{2in}} \times 100\% \dots\dots\dots\dots\dots\dots\dots.(3.7)$$

The rate of CO_2 conversion was calculated as:

$$-rCO_2 = \dot{n}_{T_{in}} \times \%CO_{2_{in}} \times \frac{\%CO_2 \text{ Conversion}}{100} \dots\dots\dots\dots\dots\dots\dots\dots\dots\dots\dots\dots\dots.(3.8)$$

The rate of CH_4 production was calculated as:

$$rCH_4 = \dot{n}_{T_{out}} \times \frac{\%CH_{4_{out}}}{100} \ \dots\dots\dots\dots\dots\dots\dots\dots\dots\dots\dots\dots\dots\dots\dots\dots..\dots(3.9)$$

The selectivity of CH_4 was expressed as follows:

$$CH_4 \ selectivity = \frac{rCH_4}{-rCO_2} \times 100\% \ \dots\dots\dots\dots\dots\dots\dots\dots\dots\dots\dots..\dots.......(3.10)$$

The selectivity of C_2-C_4 was calculated using the following expression

$$C_n selectivity = \frac{[(rC_nH_{n+1}+rC_nH_{n+2})\times n]}{-rCO_2} \times 100\% \ \dots\dots\dots\dots\dots\dots\dots\dots\dots...(3.11)$$

Where n is the number of carbons

The rate of CO production was calculated as:

$$rCO = \dot{n}_{T_{out}} \times \frac{\%CO_{out}}{100} \ \dots\dots\dots\dots\dots\dots\dots\dots\dots\dots\dots\dots\dots\dots..\dots(3.12)$$

The selectivity of CO was expressed as follows:

$$CO \ selectivity = \frac{rCO}{-rCO_2} \times 100\% \ \dots\dots\dots\dots\dots\dots\dots\dots\dots\dots\dots\dots.......(3.13)$$

The selectivity of C_{5+} was calculated as follows:

$$C_{5+}selectivity = 100\% - CH_4selectivity - \sum(C_2 + C_3 + C_4) \ selectivity - CO \ selectivity$$
$$\dots\dots\dots\dots\dots\dots\dots\dots\dots\dots\dots\dots\dots\dots\dots\dots\dots\dots\dots\dots\dots\dots\dots\dots\dots\dots\dots....(3.14)$$

The C_{2+} selectivity was calculated as follows:

$$C_{2+}selectivity = \sum(C_2 + C_3 + C_4) \ selectivity + C_{5+}selectivity \ \dots\dots\dots..\dots(3.15)$$

The C_{2+} yield was calculated as follows:

$$C_{2+}yield = \frac{CO_{2_{conversion}} \times C_{2+}selectivity}{100\%} \ \dots\dots\dots\dots\dots\dots\dots\dots\dots\dots\dots..(3.16)$$

The CH_4 yield was calculated as:

$$CH_4yield = \frac{CO_{2_{conversion}} \times CH_4 selectivity}{100\%} \ \dots\dots\dots\dots\dots\dots\dots\dots\dots..\dots..(3.17)$$

The C$_{5+}$ yield was calculated as:

$$C_{5+}\text{yield} = \frac{CO_{2_{conversion}} \times C_{5+} selectivity}{100\%}$$ ……………………………..……..(3.18)

REFERENCES

[1]   M. Jacquemin, M.J. Genet, E.M. Gaigneaux, D.P. Debecker, "Calibration of the X Ray Photoelectron Spectroscopy Binding Energy Scale for the Characterization of Heterogeneous catalysis: Is everything really under control?", Chem PhysChem, 14 (15), (2013) 3618-3626.

[2]   Z. Shi, H. Yang, P. Gao, X. Li, L. Zhong, H. Wang, H. Liu, W. Wei, Y. Sun, "Direct conversion of CO_2 to long-chain hydrocarbon fuels over K–promoted CoCu/TiO_2 catalysts", Catalysis Today, 311, (2018) 65-73.

[3]   K. Jalama, "Fischer Tropsch synthesis over supported cobalt catalysts: effect of ethanol addition, precursors and gold doping", (2008), (Doctoral thesis).

CHAPTER 4: RESULTS AND DISCUSSIONS

4.1 Effect of operating temperature, pressure and potassium loading on CO_2 hydrogenation

4.1.1 Introduction

The aim of this study was to investigate the effect of operating temperature (190 – 345 ºC), pressure (up to 20 bar) and promotion of Co/Al_2O_3 catalyst with potassium (0 – 8%) on CO_2 hydrogenation. The catalysts were prepared by incipient wetness impregnation method and characterized by BET, CO_2-TPD, TPR, XRD and XPS as described in chapter 3.

4.1.2 Catalyst characterization

4.1.2.1 Brunauer – Emmett and Teller (BET) analyses

BET analyses were performed on both potassium–promoted and unpromoted calcined fresh catalysts. The BET surface area, total pore volume and average pore sizes for $15\%Co/Al_2O_3$ catalysts with different potassium loadings are reported in Table 4.1.

Table 4. 1: Summary of BET results

Catalyst	BET surface area [m²/g]	Pore volume [cm³/g]	Pore size [nm]
$15\%Co/Al_2O_3$	124.2	0.193	6.20
$15\%Co-1\%K/Al_2O_3$	107.2	0.176	6.56
$15\%Co-3\%K/Al_2O_3$	105.1	0.174	6.61
$15\%Co-5\%K/Al_2O_3$	72.2	0.129	7.12
$15\%Co-6\%K/Al_2O_3$	56.2	0.101	7.17
$15\%Co-8\%K/Al_2O_3$	28.2	0.013	1.88

The BET surface area and pore volume of the calcined $15\%Co/Al_2O_3$ catalysts decreased with the addition of potassium. Linear regression was applied to the data (figure 4.1) and the summary of ANOVA and regression statistics are reported in Appendix B.
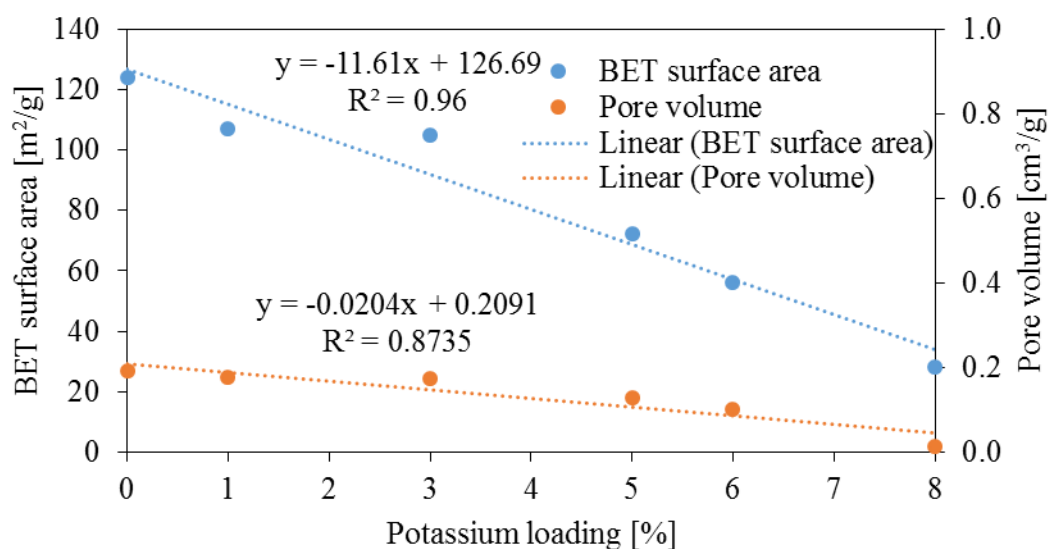
Figure 4. 1: BET surface area and pore volume as function of potassium loading.

At 95% level of confidence, the confidence interval for the slope related to the change of the BET surface area with potassium loading is (-15.06, -8.17). Since the slope of the linear trendline (-11.61) falls in this interval, there is a significant negative relationship between the BET surface area and potassium loading. 96 % ($R^2 = 0.96$) of the change in BET surface area can be explained by the change in potassium loading. Similarly, the pore volume of the catalyst linearly decreases with an increasing potassium loading. However, at 8% potassium loading, a significant drop in pore volume is noticed.

This was most likely the result of the partial coverage of the surface by potassium [1]. On the other hand, the average pore size was found to increase with potassium loading from 6.20 nm in the case of the unpromoted catalyst to 7.17 nm in the case of 6 wt.% potassium loading. This could indicate that some pores collapsed during the subsequent calcination step used to decompose potassium nitrate added to the catalyst. Further increase in potassium loading resulted in severe pore blockage in the catalyst as indicated by significant and concomitant drop in BET surface area, pore volume and pore size.

4.1.2.2 X – Ray Diffraction analyses

XRD analyses were performed on calcined freshly activated and spent catalysts. The results are presented in Figure 4.2 below.
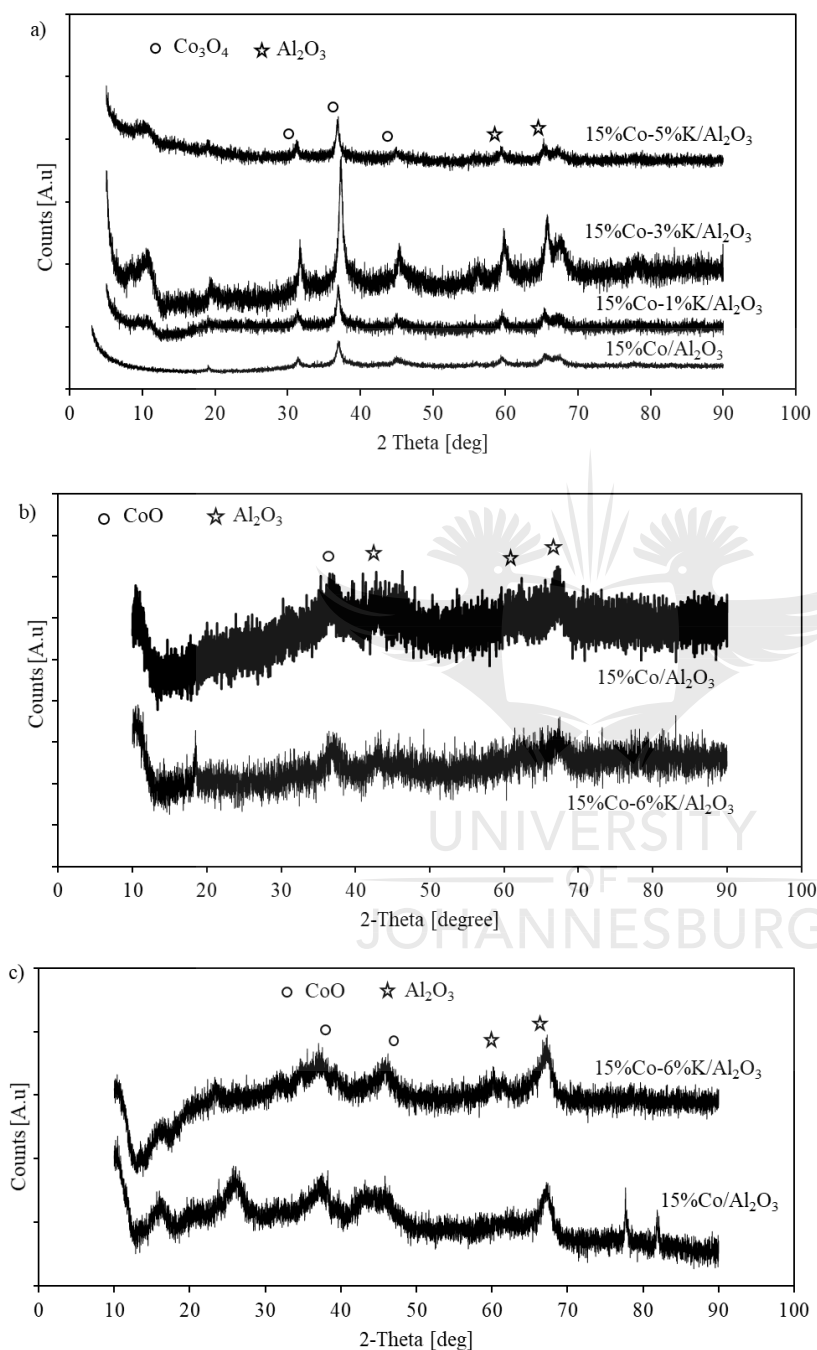
Figure 4. 2: XRD profiles for a) fresh-calcined, b) reduced and passivated, and c) spent catalysts.

For calcined fresh catalyst sample (Figure 4.2a), the diffraction peaks corresponding to Co_3O_4 are observed at angle 2θ of around 31°, 37° and 45°. No diffraction peaks associated with potassium were detected from the samples. This could possibly be due to low concentration and good dispersion [2]. The average particle size (Table 4.2) of Co_3O_4 was calculated using the most intense peaks associated to Co_3O_4, around 37°, by Scherrer. The particle size for the catalysts increased slightly with the introduction of potassium. For the unpromoted calcined catalyst, the average Co_3O_4 particle size was 9.4 nm; it increased to 13.2, 13.4 and 15.6 nm respectively after adding 1, 3 and 5% of potassium on the catalyst. For the reduced catalysts, Figure 4.2b, the XRD pattern displayed three peaks at around 37°, 42° and 67° with the most intensive peak associated to cobalt at 37°. The most intensive peak corresponding to cobalt crystallite was observed at about 37°. For spent catalysts, Figure 4.2c (300 ^{o}C, 5 bar, H_2/CO_2 = 3.0), the diffraction peaks were observed at 37.2^o and 44.0^o for the unpromoted catalyst and 36.8^o and 45.6^o for 6% potassium–promoted catalyst. The particle sizes were 2.6 and 2.1 nm for unpromoted and 6% potassium–promoted catalysts accordingly. This was significantly low as compared to their respective fresh calcined catalysts.

Table 4. 2: Cobalt particle size as estimated by XRD

Catalysts	Particle Size [nm]		
	Fresh catalyst (Co_3O_4)	Reduced catalyst (CoO)	Spent catalysts (CoO)
15%Co/Al$_2$O$_3$	9.4	8.8	2.6
15%Co-1%K/Al$_2$O$_3$	13.2	-	-
15%Co-3%K/Al$_2$O$_3$	13.4	-	-
15%Co-5%K/Al$_2$O$_3$	15.6	-	-
15%Co-6%K/Al$_2$O$_3$	-	13.2	2.1

A direct relationship between cobalt particle size, CO_2 conversion and product selectivity has been reported. During traditional FT synthesis, methane production usually increases with cobalt particle size decrease and larger particles tend to favour the production of high molecular weight hydrocarbons [3]. The authors explained that higher selectivity to methane associated with small Co particles is primarily due to their higher hydrogen coverages relative to larger Co particles.

4.1.2.3 H$_2$ - Temperature Programmed Reduction (TPR) analyses

Temperature programmed reduction analyses were performed on 15%Co/Al$_2$O$_3$ catalysts with different potassium loading to study the catalysts reduction behaviour in presence of pure H$_2$; the results are shown in Figure 4.3.
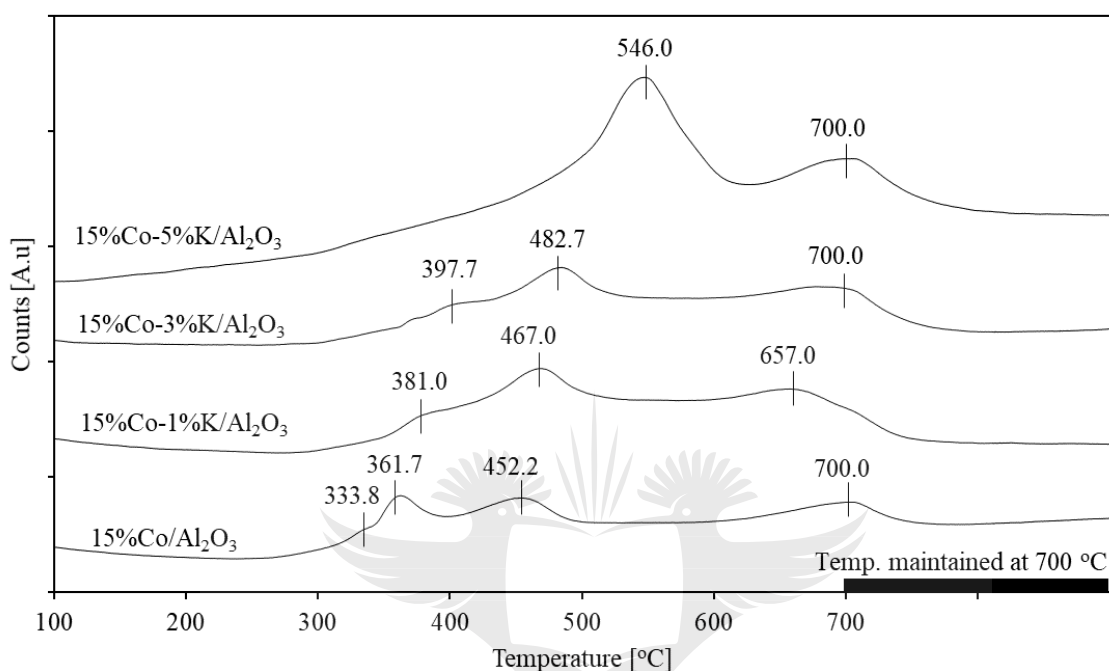
Figure 4. 3: TPR profiles for a) unpromoted, b) 1% K-promoted, c) 3% K-promoted and d) 5% K-promoted 15%Co/Al$_2$O$_3$ catalysts

It can be observed that all the TPR profiles show several overlapping broader reduction peaks, which are associated with several reduction steps. For the unpromoted catalyst, the first reduction peak started at ca. 278.3 ^{o}C and reached its maximum at 333.8 ^{o}C when the second peak started to appear, reaching its maximum at ca. 361.7 ^{o}C. This peak decreased until 400.7 ^{o}C when the third peak started to appear, reaching its maximum at ca. 452.2 ^{o}C. This peak decreased until the baseline was established at ca. 501.8 ^{o}C. The last peak started to appear at ca. 652.5 ^{o}C, reaching its maximum at 700 ^{o}C. These reduction peaks were identified as follows: first peak: decomposition of CoN$_2$O$_6$ [4]; peak 2: reduction of Co$_3$O$_4$, peak 3: reduction of CoO and peak 4: reduction of CoO in strong interaction with Al$_2$O$_3$.

The first major peak, which appear at lower temperature (333.8 ^{o}C) can be linked to decomposition of CoN$_2$O$_6$. The second and third major peaks, which appears at the temperatures 361.7 and 452.2 ^{o}C, can be ascribed to the two-step reduction of highly dispersed

cobalt oxide species to CoO and Co^0 respectively. The last peak, which appear at higher temperature (700 ^{o}C), can be linked to the reduction of cobalt species that strongly interacts with the support and are difficult to reduce. These species require more active H_2 for reduction to take place and can only be reduced at elevated temperatures. It was also observed that, as the amount of potassium promoter was increased in the catalysts, the reduction temperature shifted to higher values. For example, comparing the reduction behaviour of K-free catalyst with 5%K-promoted catalyst. For unpromoted catalyst, the first two major peak, which are associated with the two-step reduction of highly dispersed cobalt oxide to CoO and Co^0 were observed at 361.7 and 452.2 ^{o}C respectively. The last peak representing the reduction of cobalt species, which strongly interact with the support, was observed at 700 ^{o}C. For 5.wt% K-promoted catalyst, the peak linked to the two-step reduction was observed at 546 ^{o}C. The last peak associated to the reduction of cobalt species in strong interaction with the support was observed at 700 ^{o}C.

Supported with XPS data, that will be discussed in section 4.1.2.5, this observation can be linked to metal-support interaction, which has been reported to increase with increasing potassium loading, inhibiting the reducibility of the catalyst to some extent [1].

4.1.2.4 CO$_2$ - Temperature Programmed Desorption (CO$_2$ - TPD) analyses

CO$_2$ – TPD analyses were performed to determine the surface basicity for unpromoted and 6 wt.% K–promoted catalysts. The results are reported in Figure 4.4.
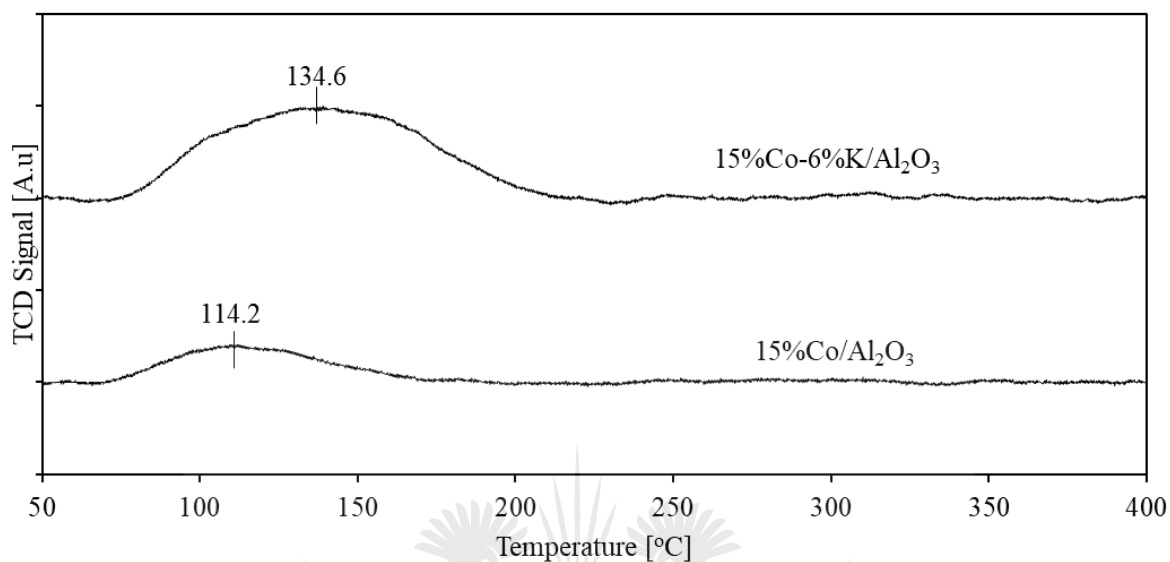
Figure 4. 4: CO$_2$ - TPD profiles of reduced catalysts

It was observed that, a broad peak was present in both TPD profiles at 114.2 ^{o}C and 134.6 ^{o}C for K-free and K-promoted catalysts respectively. For the unpromoted catalyst, the desorption peak started at ca. 71.5 ^{o}C. This peak extended until it reached its maximum at ca. 114.2 ^{o}C, when it started to decrease, reaching the baseline at ca. 171.6 ^{o}C. The K-promoted catalyst displayed a desorption peak starting at ca. 76.7 ^{o}C and extending until it reached its maximum at ca. 134.6 ^{o}C before decreasing until the baseline was established at ca. 210.4 ^{o}C. It displayed a much broader and bigger peak, which originated from the desorption of CO$_2$ that strongly interacts with the surface basic sites, compared to the unpromoted catalyst, suggesting that potassium significantly enhanced the surface basicity of the catalyst [2].

4.1.2.5 X-ray photoelectron spectroscopy (XPS) analyses

The Co2p binding energies for the unpromoted and K-promoted catalysts are shown in Figure 4.5. The data for C 1s, K 2p and Al 2p are reported in Appendix A.
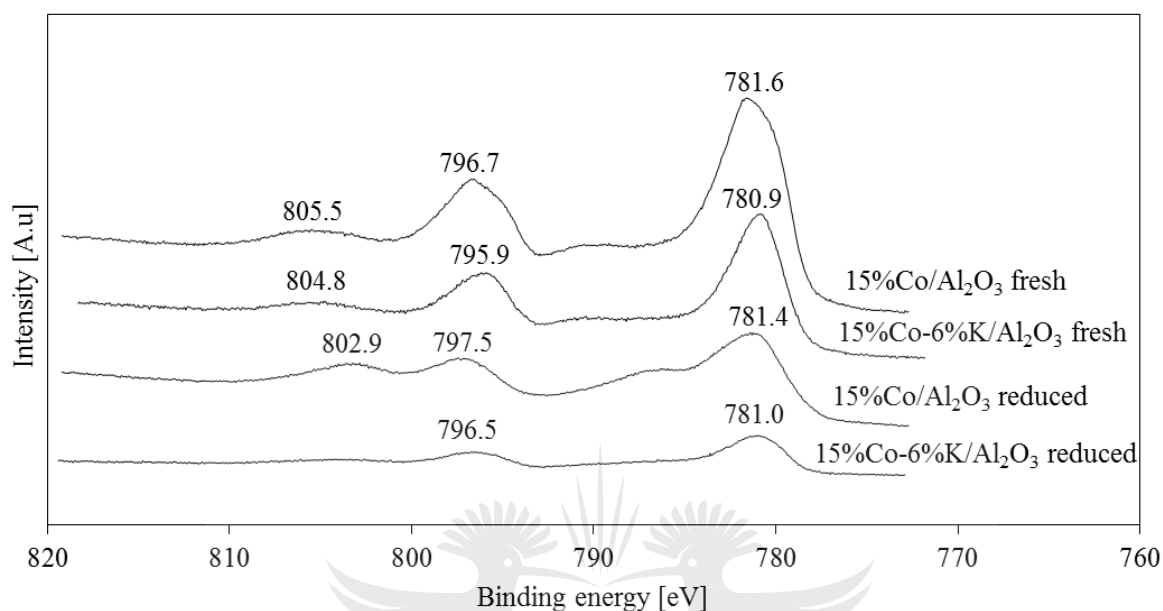
Figure 4. 5: XPS profiles (Co 2p) for unpromoted and K-promoted catalysts.

These data were corrected by setting the binding energy of oxidic O 1s at 531.5 eV [5]. For fresh calcined and unreduced catalyst samples, the binding energies of Co 2p slightly shifted to lower values with the addition of K. As can be seen, for the unpromoted catalyst, the binding energies were 781.6 and 796.7 eV for Co $2P_{3/2}$ and Co $2P_{1/2}$ respectively. They respectively shifted to 780.9 and 795.9 eV when potassium was added. Likewise, for the reduced catalysts, a similar trend was observed. For the unpromoted catalyst, the binding energies of Co 2P decreased with potassium addition, from 781.4 and 797.5 eV to 781.0 and 796.5 eV for Co $2P_{3/2}$ and Co $2P_{1/2}$ respectively. This suggests an electronic modification of cobalt species in the catalyst by K [2].

4.1.3 Catalyst evaluation

4.1.3.1 Effect of reaction temperature

The effect of reaction temperature (195 – 345 °C) on CO_2 hydrogenation was studied over a 15%Co-5%K/Al_2O_3 catalyst, at 1 bar. The results are presented in Figure 4.6.
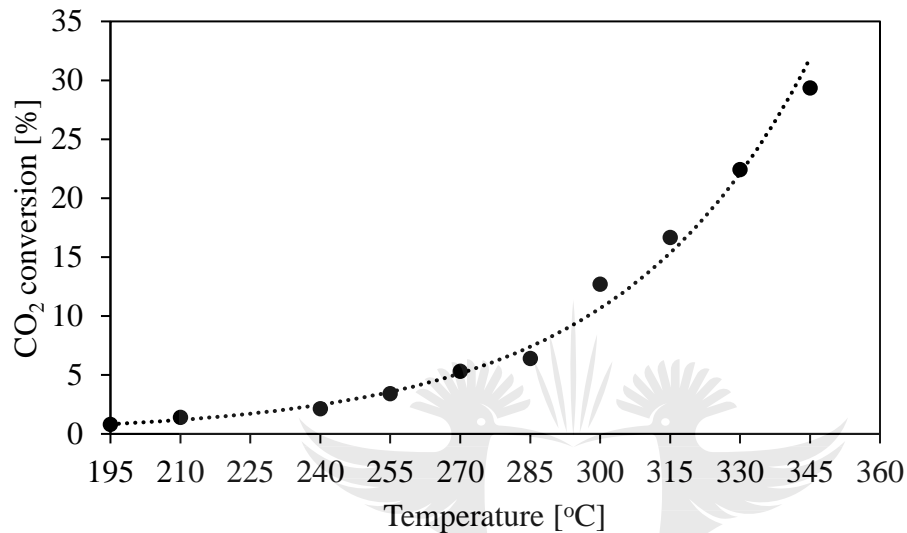
Figure 4. 6: Effect of reaction temperature on CO_2 conversion

As the temperature was increased, the CO_2 conversion also increased. At higher temperatures (beyond 285 °C), this influence was significant. For instance, when the temperature was increased from 285 to 300 °C, the CO_2 conversion increased from 5.5 to 12.7%. The trend line clearly shows an exponential relationship between the CO_2 conversion and the temperature.

The activation energy of the CO_2 hydrogenation was determined using the Arrhenius plot (figure 4.7). The Arrhenius equation expresses the relationship between the temperature, reaction rate, and activation energy as follows:

$$k(T) = k_0 e^{\frac{E_a}{RT}} \dots\dots\dots\dots\dots\dots\dots\dots\dots\dots\dots\dots\dots\dots\dots\dots\dots\dots\text{Eq.(4.1)}$$

where k_0 is the pre-exponential factor, Ea is the activation energy, R is the gas constant, T is the reaction temperature, k(T) is the rate constant. The exponential term is dimensionless. In

the Arrhenius plot, where ln [k(T)] is plotted versus $\frac{1}{T}$, the slope of the curve is $-\frac{E_a}{R}$ and the y-intercept is ln(k₀).
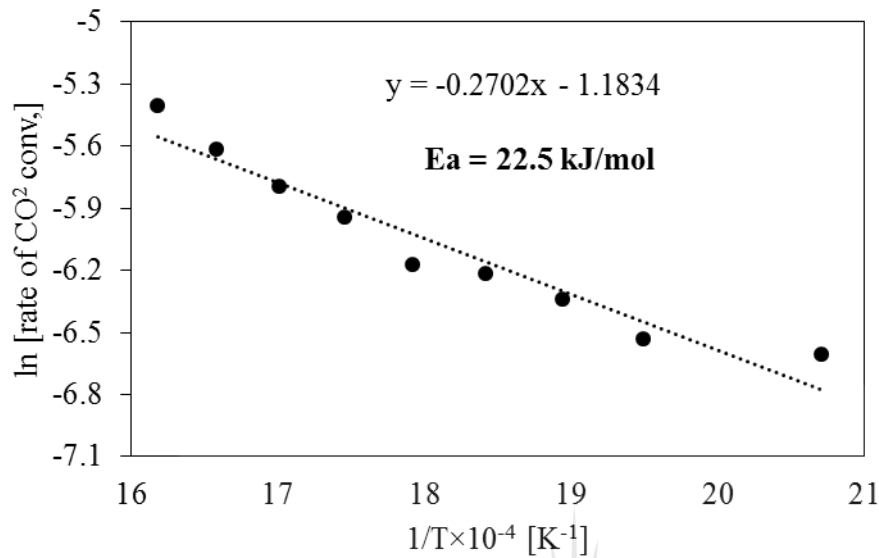
Figure 4. 7: Arrhenius plot for 15%Co-5%K/Al$_2$O$_3$ catalyst

The activation energy for this study was found to be 22.5 kJ/mol. This is significantly lower compared to 77 kJ/mol reported by Mutscler *et al.* [6]. This could be due to a different temperature range of 480 – 510 K and feed gas (H$_2$:CO$_2$) ratio of 4.1 used in their study.

Figure 4.8 shows the effect of temperature on the product selectivity.
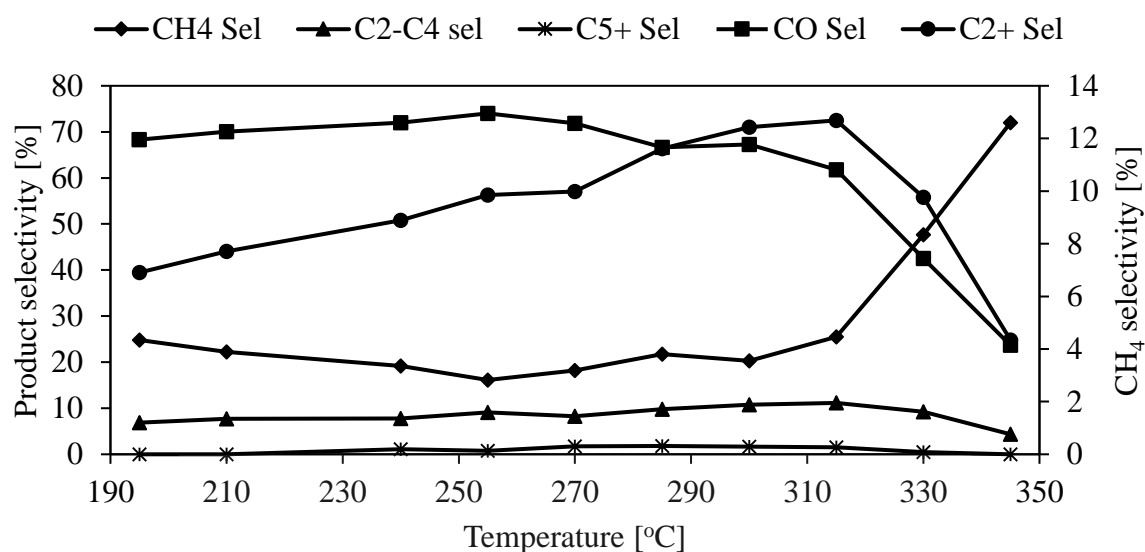
Figure 4. 8: Effect of reaction temperature on product selectivity (Catalyst: 15%Co-5%K/Al$_2$O$_3$; Pressure: atmospheric; space velocity: 1.2 nl/gCat/hr)

As the reaction temperature was increased from 195 to 255 °C, the CO selectivity also increased from 68.3 to 74.0%. Further increase in temperature caused the CO selectivity to decrease, reaching 23.7% at ca. 345 °C. In contrast, as the temperature was increased from 195 to 255 °C, the CH$_4$ selectivity decreased from 24.8 to 16.1%. Further temperature increase resulted in the CH$_4$ selectivity increase reaching 71.2% at ca. 345 °C. On the other hand, the C$_2$ – C$_4$ selectivity increased from 6.9 to 11.1% when the temperature was increased from 195 to 315 °C, before decreasing to 4.3% at ca. 345 °C. Moreover, no C$_{5+}$ hydrocarbons were observed below 240 °C. The selectivity to C$_{5+}$ hydrocarbons increased from 1.1 to 1.8% as the reaction temperature was increased from 240 to 285 °C before decreasing to 0.5% at ca. 330 °C. Further increase in the reaction temperature to 345 °C suppressed the formation of C$_{5+}$. Nonetheless, the C$_{2+}$ selectivity was observed to increase from 6.9 to 12.7% as the temperature was increased from 195 to 315 °C, before decreasing to 4.3% at ca. 345 °C.

Various CO$_2$ hydrogenation reaction mechanisms have been proposed in literature. The type of catalysts involved have been reported to play a significant role in the mechanism. On cobalt-based catalysts, it is generally believed that CO$_2$ hydrogenation proceed in a two-step reaction mechanism [2]. CO$_2$ is converted to hydrocarbon through CO as an intermediate product, which is then converted to hydrocarbons through FT synthesis. At higher temperatures, the rate of reaction also increases [7] resulting in the CO formed in the reverse-water-gas-shift reaction

94

(RWGS) being converted to hydrocarbons rapidly leading to the CO selectivity decreasing and the selectivity of other hydrocarbons improves. At this point, the selectivity of CH_4 increases while the C_2-C_4 and C_{5+} selectivities declined as the temperature increases. The reaction tends to favor CH_4 formation at higher temperatures. It has been reported in earlier studies that according to Anderson-Schulz-Flory model, the chain growth probability decreases and methane formation increases at elevated temperatures [8 – 9]. Based on these observations it can be seen that higher temperatures play a positive role in converting the intermediate CO but at the same time negatively affect the formation of longer chained hydrocarbons while favoring the formation of methane. Therefore, it becomes useful to determine the amount of carbon from CO_2 that does not end up in CH_4. This is achieved by calculating the products yields.

Figure 4.9 shows the yield of CH_4 and hydrocarbons other than methane (C_{2+}).
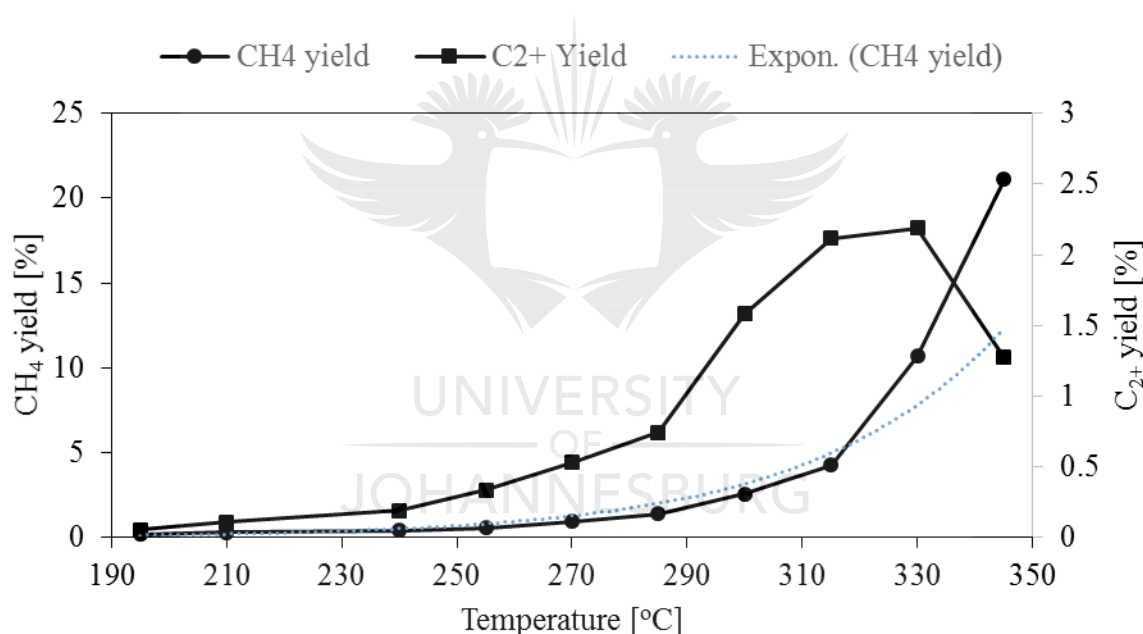
Figure 4. 9: Effect of reaction temperature on CH_4 and C_{2+} yield during CO_2 hydrogenation.

The methane yield almost exponentially increased with an increase in temperature. For example, as the temperature was increased from 285 to 330 ^{o}C, the methane yield increased at a faster rate from 0.88 to ca. 11 %. However, the C_{2+} yield was found to increase with the temperature, reaching its maximum of 2.19% at 330 ^{o}C. Further increase in temperature to 345 ^{o}C negatively affected the C_{2+} yield as it dropped significantly by almost half to 1.28%.

The increase in C_{2+} yield with the temperature is explained by a concomitant increase in CO_2 conversion (figure 4.6) and C_{2+} selectivity (figure 4.8) from 190 to 315 ^{o}C. Beyond this

temperature, the selectivity to C_{2+} products started to decrease, while CO_2 conversion kept increasing. This resulted in a decrease in C_{2+} yield beyond 330 ºC. Since the increase in C_{2+} yield with temperature was very low in the range from 190 to 290 ºC and that the largest change was recorded when the temperature was increased from 290 to 300 ºC, the latter was selected for the rest of the experiments in this study.

4.1.3.2 Effect of reaction pressure

The effect of pressure (from 1 bar to 20 bar) was evaluated using 15%Co-5%K/Al$_2$O$_3$ catalyst at 300 ºC. The data are reported in figure 4.10.
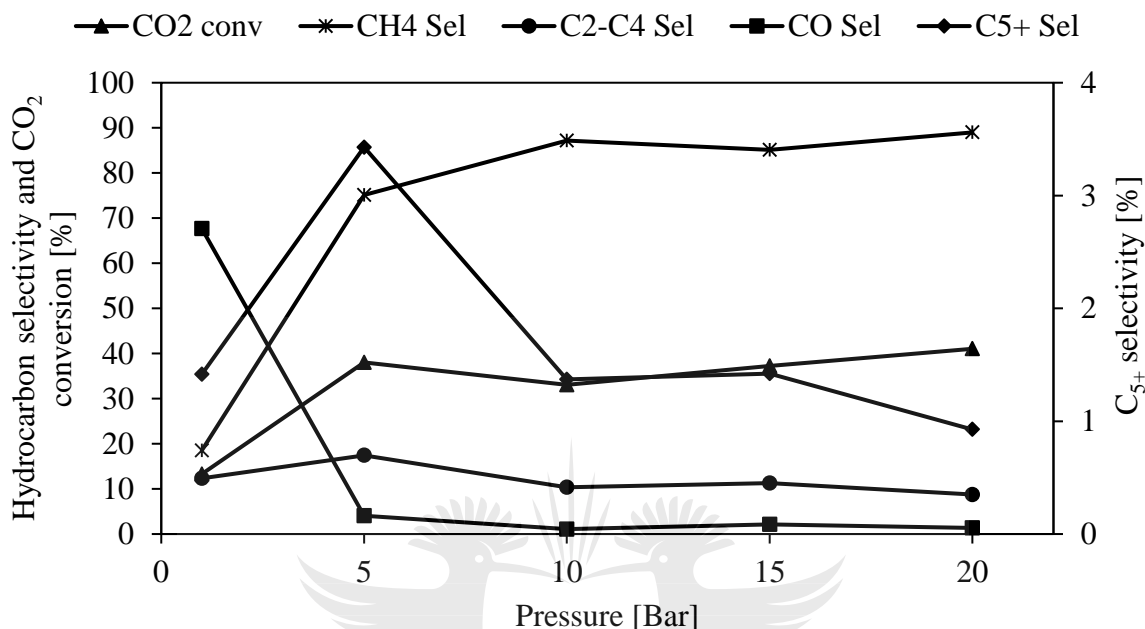
Figure 4. 10: Effect of reaction pressure on product selectivity and CO$_2$ conversion

By increasing the pressure from 1 to 5 bar, the CO$_2$ conversion significantly increased from 13.3 to 38.0 %. This was expected and can be explained by an increase in reactants partial pressures in the reactor. The CH$_4$, C$_2$-C$_4$ and C$_{5+}$ selectivities also increased significantly from 18.5, 12.4 and 1.4 to 75.1, 17.4 and 3.4% respectively. At the same time, the selectivity of CO significantly decreased from 67.7 to 4.0%. As the operating pressure was further increased beyond 5 bar, the CO$_2$ conversion did not significantly change and was limited at 41.0% at 20 bar. While the CH$_4$ selectivity continued to increase, reaching its highest value of 88.9% at 20 bar, the CO, C$_2$-C$_4$ and C$_{5+}$ selectivities respectively decreased to reach 1.3, 8.8 and 0.93% at 20 bar. The data suggests that higher pressures enhances the methanation ability of the catalyst.

The data in figure 4.11 shows an increase in CH_4 yield with increasing pressure, while the C_{2+} yield, C_{2+} selectivity and the chain growth probability, α, increased from 1 bar to 5 bar before decreasing at higher pressures.
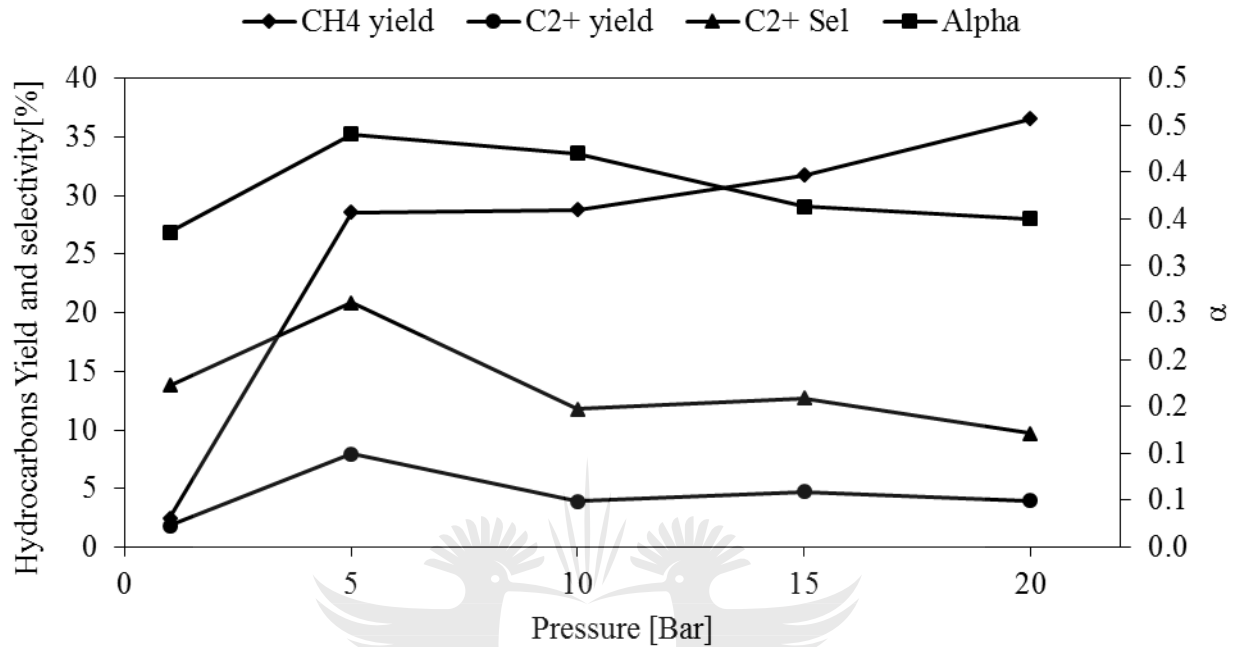
Figure 4. 11: Effect of pressure on CH_4, C_{2+} yield, C_{2+} selectivity and chain growth probability (α)

For example, as the pressure was increased from 1 to 5 bar, the CH_4 yield increased from 2.5 to 28.6%. It continued to increase with pressure, up to 36.5% at 20 bar. On the other hand, the C_{2+} yield first increased from 1.83% to 7.9% when the pressure was increased from 1 to 5 bar, before decreasing to values between 3.8 and 4.7% at operating pressures beyond 5 bar. For this reason, 5 bar was selected as the operating pressure for the rest of the experiments in this study.

4.1.3.3 Effect of potassium loading

Various amounts of potassium were added to the 15%Co/Al$_2$O$_3$ catalyst in order to determine the optimal loading of potassium in the catalyst that will maximize the yield of hydrocarbon products other than methane (C$_{2+}$) during CO$_2$ hydrogenation. The results obtained are presented in Table 4.3.

Table 4. 3: Effect of potassium promoter loading on 15%Co/Al$_2$O$_3$ catalyst performance during CO$_2$ hydrogenation (Temperature: 300 °C, 5 bar and 1.2 nl/gCat./hr)

Catalyst	CO$_2$ conv. (%)	CH$_4$ sel. (%)	C$_2$ - C$_4$ sel. (%)	C$_{5+}$ Sel. (%)	CO Sel. (%)	CH$_4$ yield (%)	C$_{2+}$ Sel. (%)	C$_{2+}$ Yield (%)	Alpha*
15%Co/Al$_2$O$_3$	33.8	97.0	1.7	0.0	1.3	32.8	1.7	0.6	-
15%Co-1%K/Al$_2$O$_3$	34.2	96.4	2.0	0.1	1.6	32.9	2.1	0.7	0.475
15%Co-3%K/Al$_2$O$_3$	33.7	91.9	3.2	0.0	4.9	31.0	3.2	1.1	-
15%Co-5%K/Al$_2$O$_3$	38.0	75.1	17.4	3.4	4.0	28.6	20.9	7.9	0.440
15%Co-6%K/Al$_2$O$_3$	42.3	67.6	22.3	1.9	8.2	28.6	24.2	10.2	0.412
15%Co-8%K/Al$_2$O$_3$	12.2	15.9	50.6	0.0	33.5	2.0	50.6	6.2	-

*up to C$_6$

The product generated was predominantly methane, C_{2+} hydrocarbons and CO. Supported cobalt-based catalysts are commonly used in a traditional FT synthesis with syngas as the feed [10]. Nonetheless, when changing from syngas to CO_2-containing syngas feed (where CO is replaced with CO_2), the reaction tends to shift towards a methanation process. As the potassium promoter content was increased from 0 to 3% on the catalyst, the CO_2 conversion did not change much as it was about 34%. Further increase of potassium content to 5 and 6% resulted in CO_2 conversion increase to 38.0 and 42.3% respectively. The CO_2 conversion then decreased to 12.2% when potassium content was increased to 8%. In contrast, the CH_4 selectivity significantly decreased from 97.0 to 15.9% when potassium content was increased from 0 to 8%. On the other hand, the $C_2 - C_4$ selectivity significantly increased from 1.7 to 50.6% when the potassium loading was increased from 0 to 8%. The C_{5+} selectivity did not show a clear trend, but the highest selectivity was 3.43% at potassium loading of 5%. The CO selectivity increased from a minimum value of 1.3 to 33.5% when the potassium loading was increased from 0 to 8%. Moreover, the C_{2+} selectivity increased from 1.7 to 50.6% when the potassium loading was increased from 0 to 8%. At the same time, the CH_4 yield significantly decreased from 32.8 to 2.0% when the potassium content was increased from 0 to 8%. Nonetheless, the C_{2+} yield increased from 0.6 to 10.2% when potassium content was increased from 0 to 6%, before decreasing to 6.2% when potassium content was increased to 8%. No clear trend was observed for chain growth probability, α. The chain growth probability was 0.475, 0.440 and 0.412 when potassium content was 1, 5 and 6% respectively.

Based on these observations, we believe that during CO_2 hydrogenation over 15%Co/Al_2O_3 catalysts promoted with different potassium content, CO_2 is first converted to CO through the reverse–water–gas–shift (RWGS) reaction, followed by a subsequent hydrogenation of CO to hydrocarbons via modified FT synthesis. In addition, the unpromoted catalyst performed as a methanation catalyst rather than FT catalyst as the selectivity of CH_4 was found to be 97% when this catalyst was employed [11 – 12]. These results indicate that an appropriate quantity of potassium is required to enhance the catalytic performance for CO_2 hydrogenation to longer chain hydrocarbons. During traditional FT synthesis, potassium is known to promote chain growth probability, and the products lean towards heavy molecular weight hydrocarbons [13]. In our case, the chain growth probability did not show good trend, which makes it difficult to conclude. The optimum potassium loading was found to be 6 wt.% because it produced the highest C_{2+} yield; it was selected for the rest of our study.

100

In summary, potassium decreased catalyst reducibility and improved product selectivity by shifting product towards the formation of hydrocarbons other than methane (C_{2+}). CO_2 is first converted to CO through reverse–water–gas–shift (RWGS) reaction, followed by a subsequent hydrogenation of CO to hydrocarbons via modified FT synthesis. The unpromoted catalyst performed as a methanation catalyst rather than FT catalyst.

4.2 Effect of Ru, Cu and Pd as reduction promoter of 6% K-promoted Co/Al₂O₃ catalyst

4.2.1 Introduction

As discussed in section 4.1, potassium decreased the catalyst reducibility. The aim of this study was to investigate the effect of ruthenium, palladium and copper as a second catalyst promoter of 6% K-promoted Co/Al₂O₃ catalyst during CO_2 hydrogenation. This was done to improve the catalyst reducibility and production of CO because cobalt is not active for WGS and RWGS reactions [14 – 16]. Ru and Pd are known to improve cobalt catalyst reducibility and therefore it will be vital to explore their effect on the performance of 6%K-promoted 15%Co/Al₂O₃ catalyst and product distribution during CO_2 hydrogenation. To the best of our knowledge, no studies have been conducted with the combination of potassium and Ru or Pd on CO_2 hydrogenation to hydrocarbons using cobalt-based catalyst. On the other hand, copper-based catalysts have been reported to promote RWGS reaction [2]. The catalysts were prepared by incipient wetness impregnation method and characterized by XRD, BET and TPR as described in chapter 3.
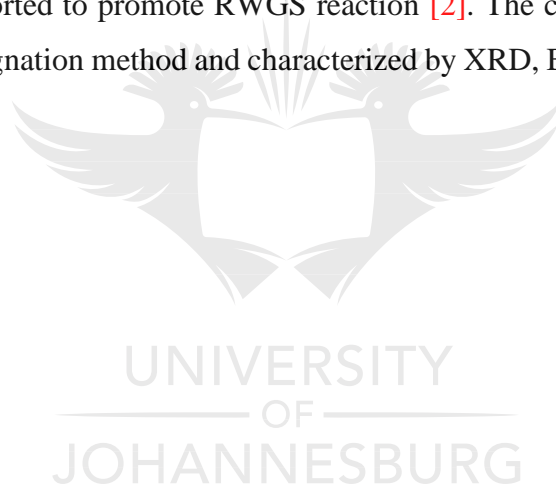
4.2.2 Catalyst characterization

4.2.2.1 XRD analyses

XRD data for 15%Co-6%K/Al_2O_3 promoted with a second metal are summarized in Figure 4.12.
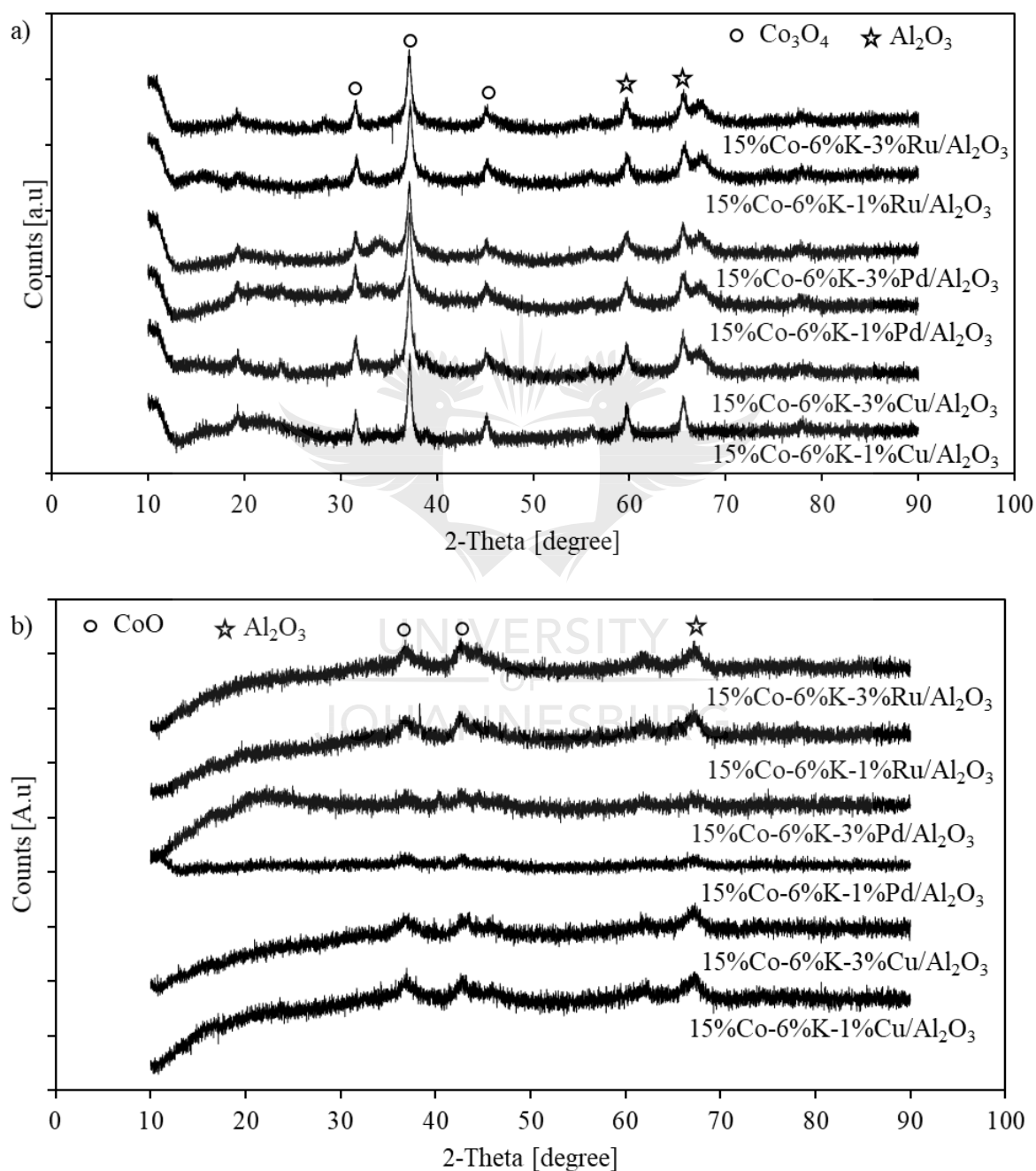
Figure 4. 12: XRD pattern of 15%Co-6%K/Al_2O_3 catalyst with a second promoter (Cu, Pd, Ru): a) calcined and unreduced and b) reduced catalysts.

103

For fresh unreduced catalysts, diffraction peaks corresponding to Co_3O_4 particles are observed at 31.5°, 37.1° and 45.2° in all spectrum of catalysts [17 – 18]. The most intensive peak of Co_3O_4 in the XRD profile of all catalyst samples was observed at about 37.1°. Due to low amounts of K, Ru, Cu and Pd promoters in the promoted catalysts, no diffraction peak for these metals and their oxides was observed. For the reduced catalysts, the diffraction peaks corresponding to CoO were observed at about 37° and 42°. The most intensive peak corresponding to CoO was at about 37°. No diffraction lines corresponding to either K, Cu, Pd or Ru were observed. The average particle sizes of cobalt species in fresh and reduced catalysts are reported in Table 4.4 below.

Table 4. 4: Cobalt species particle size as estimated by XRD

Catalysts	Particle size (nm)	
	Unreduced Catalyst [Co_3O_4]	Reduced Catalyst [Co^0]
15%Co-6%K/Al$_2$O$_3$	13.20	2.10
15%Co-6%K-1%Cu/Al$_2$O$_3$	18.07	5.05
15%Co-6%K-3%Cu/Al$_2$O$_3$	14.00	1.85
15%Co-6%K-1%Pd/Al$_2$O$_3$	16.90	2.60
15%Co-6%K-3%Pd/Al$_2$O$_3$	16.69	13.68
15%Co-6%K-1%Ru/Al$_2$O$_3$	13.35	1.65
15%Co-6%K-3%Ru/Al$_2$O$_3$	13.82	5.29

As can be seen from Table 4.4, for unreduced catalysts, Pd and Ru do not have any effect on the particle size, within an experimental error. Only Cu tends to decrease the average crystallite size of cobalt species in both the unreduced and reduced catalyst samples. This suggest that copper increased the dispersion of cobalt in the catalyst. There are limited reports published in the literature on the influence of Cu as promoter for Co-based catalysts. A study on the effect of small amounts of Group 11 metals on the FT activity of Group 11 (Cu, Ag, Au) promotion of 15%Co/Al$_2$O$_3$ [19] indicates that Group 11 promoters are well dispersed and possibly in surface contact with the cobalt oxide crystallites. This proximity would allow Group 11 promoter to reduce and help reducing the cobalt, possibly via H_2 dissociation and spillover

mechanism. Nevertheless, once reduced, Group 11 promoter agglomerates to a metal particle. The study also suggested that the formation of the metal particle leads to a decrease in the promoter–cobalt surface interaction.

In contrast, Pd and Ru caused the cobalt particles sizes to increase in the reduced catalysts, except for 1%Ru-promoted catalyst where the particle size decreased. Our results contradict with Xu *et al.* [18]. They found that cobalt dispersion improved when Co/Al_2O_3 catalyst was promoted with Ru and Pd. In our case, cobalt dispersion decreased since particle size increased. Based on H_2-chemisorption results, Hosseini *et al.* [20] also found that promotion with Ru led to improved cobalt dispersion. Interestingly, they also observed a significant cobalt particle size decrease when Ru was added. These findings agree with Kogelbauer *et al.* [21]. It is worth noting that the data reported on the literature [18, 20 – 21] were for catalysts with only Ru or Pd as a promoter, while the catalysts used in this study were promoted with potassium and Ru or Pd. Vosoughi *et al.* [22] reported that the cobalt dispersion and degree of reduction significantly increased when Ru was added to mesoporous alumina supported cobalt catalysts.

4.2.2.2 Brunauer – Emmett and Teller (BET) analyses

The BET analyses was performed on the fresh calcined $15\%Co/Al_2O_3$ catalysts promoted with 6 wt% potassium and 0 – 3% of x (copper, ruthenium or palladium) as the second promoter. The BET surface area, total pore volume and pore sizes are summarized in Table 4.5.

Table 4. 5: Summary of BET analysis for promoted Co/Al_2O_3 catalysts promoted with K and a second metal (Cu, Pd, Ru).

Catalyst	BET surface area [m^2/g]	Pore volume [cm^3/g]	Pore size [nm]
$15\%Co-6\%K/Al_2O_3$	56.2	0.101	7.17
$15\%Co-6\%K-1\%Cu/Al_2O_3$	77.0	0.135	7.01
$15\%Co-6\%K-3\%Cu/Al_2O_3$	57.4	0.102	7.09
$15\%Co-6\%K-1\%Pd/Al_2O_3$	81.6	0.138	6.78
$15\%Co-6\%K-3\%Pd/Al_2O_3$	76.7	0.197	10.30
$15\%Co-6\%K-1\%Ru/Al_2O_3$	70.6	0.119	6.75
$15\%Co-6\%K-3\%Ru/Al_2O_3$	64.6	0.110	6.83

The BET surface area of the catalysts increased with the addition of a second promoter (Cu, Pd or Ru) relative to the catalyst promoted with potassium only. The surface area declined when the second promoter content was increased from 1 to 3 wt.% for all catalysts tested. The total pore volume increased when the second promoter was introduced for all catalysts and decreased slightly when the content of these promoters was increased to 3 wt.%, with the exception of palladium where the pore volume increased with its content in the catalyst. The decrease in the surface area and the total pore volume when the second promoter content was increased could be the result of some pores being obstructed due to the second promoter being deposited inside the pores of the catalyst. Except for the 15%Co-6%K-3%Pd/Al$_2$O$_3$ where both pore volume and pore size increased with Pd content, no other significant difference in the pore volume and pore sizes were observed.

4.2.2.3 Temperature Programmed Reduction (TPR) analyses

The catalyst reduction behavior was studied using TPR analysis under hydrogen atmosphere. The results are shown in Figure 4.13 below.
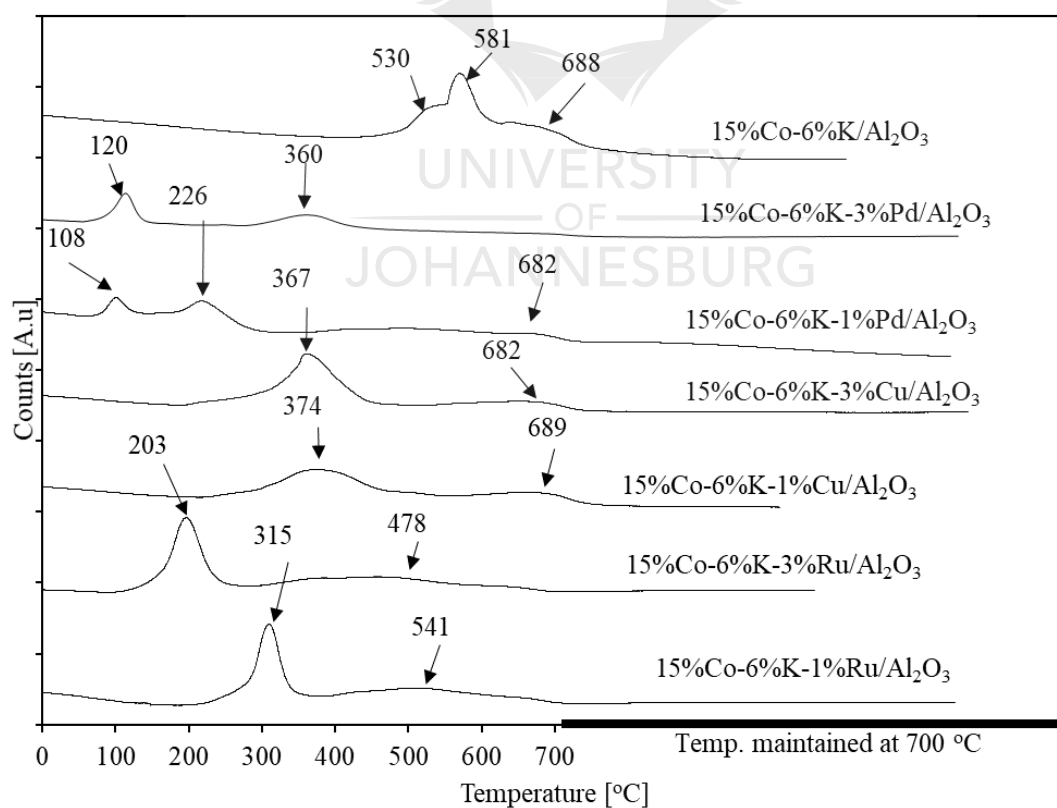
Figure 4. 13: TPR profiles for 15%Co-6%K/Al$_2$O$_3$ promoted with a second promoter x (1 to 3wt.% of Cu, Pd, and Ru).

106

For the catalyst promoted with potassium only, the first reduction peak was observed at ca. 472 $^{\circ}$C and reached its maximum at 530 $^{\circ}$C when the second peak started to appear. This peak was extended until it reached its maximum at ca. 581 $^{\circ}$C. This peak started to decrease until 623 $^{\circ}$C when the last peak started to appear and was extended until reaching its maximum at 688 $^{\circ}$C. When Pd was introduced to $15\%Co-6\%K/Al_2O_3$ catalyst, two main reduction peaks were observed in all catalyst samples. When 1%-Pd was added to the catalyst, the first reduction peak was observed at ca.81 $^{\circ}$C, reaching its maximum at ca.108 $^{\circ}$C. This peak then started to decrease until the base line was established at ca.136 $^{\circ}$C. The second peak was observed at ca.188 $^{\circ}$C and reached its maximum at ca.226 $^{\circ}$C. This peak started to decrease until the baseline was established at ca.305 $^{\circ}$C. For 3%-Pd promoted catalyst, the first peak started at ca.84 $^{\circ}$C and was extended, reaching its maximum at ca.120 $^{\circ}$C. This peak started to decrease and reached the baseline at ca.144 $^{\circ}$C. The second peak was observed at ca.298 $^{\circ}$C, reaching its maximum at 360 $^{\circ}$C. This peak then started to decrease until ca.434 $^{\circ}$C when the third peak started to appear. This peak was broad and bigger and was extended until ca.682 $^{\circ}$C. When 1% of Cu was added to the catalyst, the reduction peak started at ca.250 $^{\circ}$C, reaching it maximum at ca.374 $^{\circ}$C. The peak then decreased until the baseline was established at ca.500 $^{\circ}$C. The last peak started to appear at ca.613 $^{\circ}$C, reaching its maximum at ca.689 $^{\circ}$C. For 3% Cu promoted catalyst, the reduction peak started at ca.235 $^{\circ}$C and was extended until its maximum at ca.367 $^{\circ}$C when it started to decrease until the baseline was established at ca.466 $^{\circ}$C. The second peak was also observed, reaching maximum at ca.682 $^{\circ}$C. When Ru was introduced to the catalyst, two major reduction peaks were observed. When 1% of Ru was added to the catalyst, the reduction peak started at ca. 230 $^{\circ}$C, reaching its maximum at 315 $^{\circ}$C. This peak started to decrease until the baseline was established at ca. 364 $^{\circ}$C, when the second peak started to appear. This peak reached its maximum at ca.541 $^{\circ}$C. When 3% Ru was added to the catalyst, the reduction peak started at ca.125 $^{\circ}$C and was extended until it reached its maximum at ca.203 $^{\circ}$C. The second peak started to appear at ca.305 $^{\circ}$C, reaching its maximum at ca.478 $^{\circ}$C.

For $15\%Co-6\%K/Al_2O_3$ catalyst, the first two peaks can be ascribed to the reduction of Co_3O_4 to CoO and the subsequent reduction of CoO to Co^0. The third peak at higher temperature can be linked to the presence of well – dispersed small cobalt particles, which interact strongly with the support and are difficult to reduce. When the second promoter (Ru, Pd or Cu) was added to the catalyst, the reduction shifted to lower temperature as the promoter loading was increased. These observations are opposite from what was observed with potassium loading only (section 4.1.2.3) where the reduction temperature was observed to increase with potassium content.

Promoters such as Pd, Ru and Cu are known to influence reduction temperature by shifting it towards lower temperatures and enhances the cobalt clusters dispersion [20 – 21, 23]. These results indicate that the addition of these second catalyst promoters improved the catalyst reducibility with palladium shifting the reduction to lower temperature followed by ruthenium and copper respectively. There are two central explanations to clarify the promoting effect by these noble metals: (i) noble metals dissociate H_2 and the dissociated H_2 from the noble metal spillover to nucleate reduced sites in cobalt oxides [23 – 25], and (ii) a chemical promotion such as an electronic effect from alloying.

4.2.3 Catalyst evaluation

4.2.3.1 Effect of promotion with Ru

The effect of second promoter (1 – 3wt.% of Cu, Pd or Ru) on the catalytic performance of 15%Co-6 wt.%K/Al_2O_3 catalysts during CO_2 hydrogenation to hydrocarbons was evaluated at 300 ^{o}C and 5 bar.
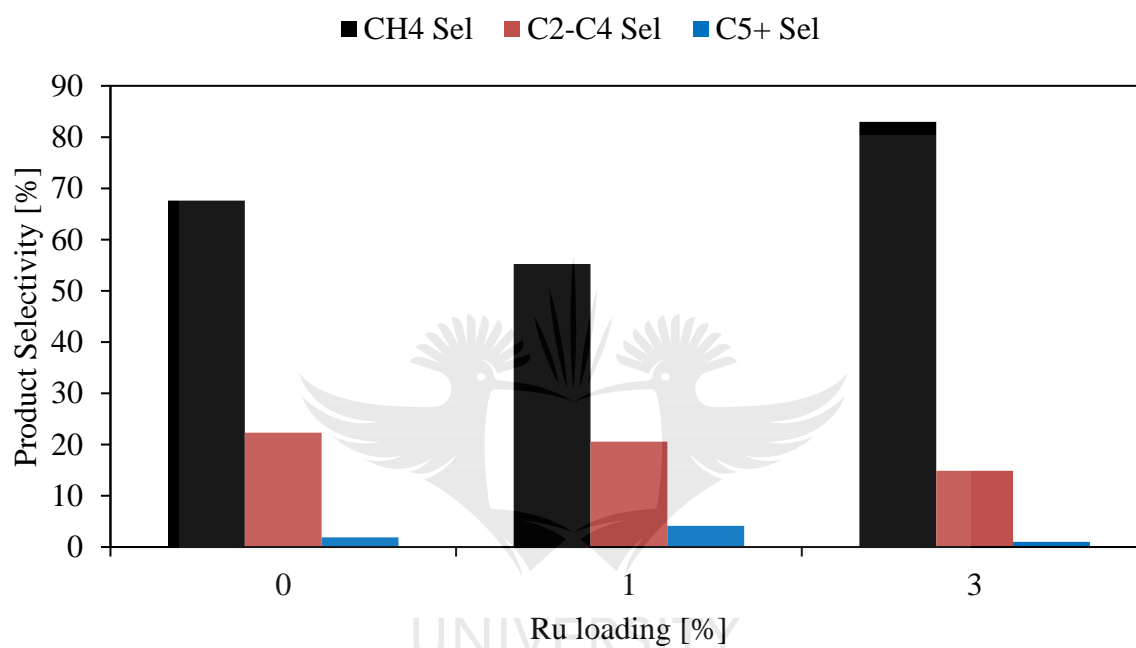
Figure 4. 14: Effect of Ru (1 – 3 wt.%) as a second promoter on product selectivity during CO_2 hydrogenation over 15%Co-6 wt.%K /Al_2O_3 catalysts.
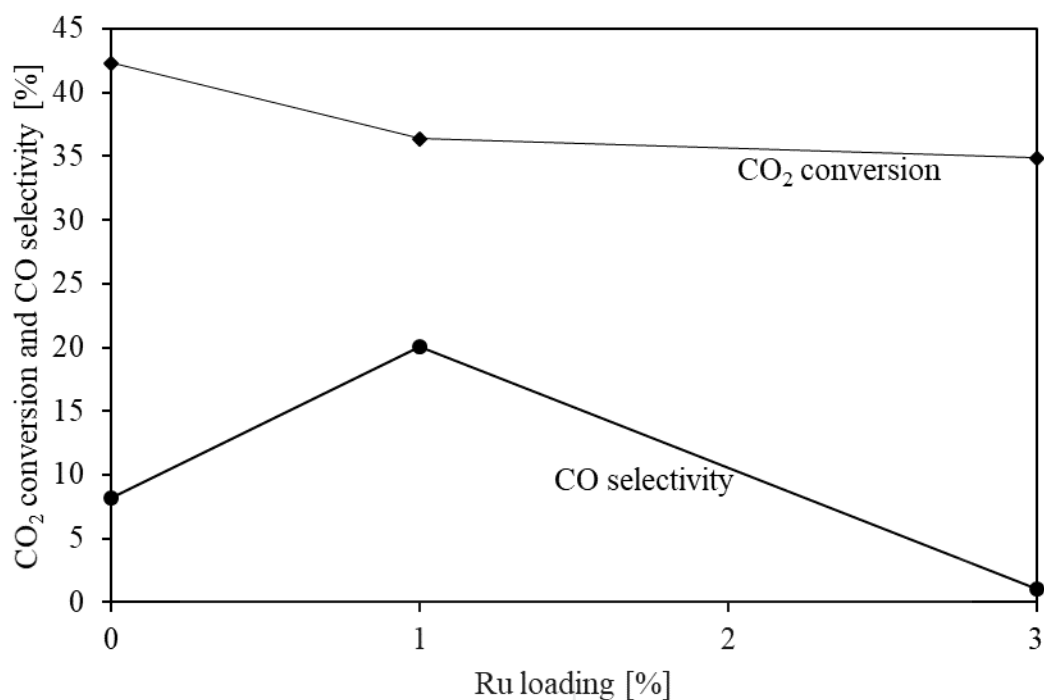
Figure 4. 15: Effect of Ru (1 – 3%) as a second promoter on CO_2 conversion and CO selectivity during CO_2 hydrogenation over 15%Co-6 wt.%K /Al_2O_3 catalysts.

From figures 4.14 and 4.15 above, the product was mainly methane, CO and other hydrocarbons. The ruthenium – free catalyst produced high methane selectivity of 67.6%. The selectivities of $C_2 – C_4$ and C_{5+} hydrocarbons were found to be 22.3 and 1.9% respectively. When 1 wt.% Ru was added to the catalyst, the selectivity of methane was suppressed by 12.4%. The selectivity to $C_2 – C_4$ hydrocarbons also dropped by 1.7%, meanwhile the C_{5+} selectivity was found to be 4.1%. Further ruthenium increase to 3 wt.% resulted in the reaction product shifting towards undesired methane selectivity of 83% and further decrease of $C_2 – C_4$ hydrocarbons and C_{5+} products selectivity to 14.9 and 1.0% respectively. In addition, it was observed from figure 4.15 that the CO_2 conversion over ruthenium-free catalyst was much higher than ruthenium promoted catalysts. We can deduce that the addition of ruthenium to 1 wt.% improves product selectivity as it shifted towards the formation of longer hydrocarbons and produced low methane as compared to ruthenium-free catalyst and catalyst with 3 wt.% ruthenium. During traditional FT synthesis with CO as feed, Ru promoter has been reported to have CO hydrogenation activity [18, 26]. Furthermore, the addition of Ru to Co/Al_2O_3 was found to decrease the selectivity of methane and to increase that of C_{5+} [18]. Hence, it appears that a loading of about 1 wt.% of Ru improves the adsorption and dissociation of CO formed as an intermediate product, leading to lower CH_4 and higher C_{5+} selectivities.

Figure 4.16 shows the effect of ruthenium on the yield of C_{2+} during CO_2 hydrogenation. The highest C_{2+} yield was 10.2% observed for Ru-free catalyst. When 1 and 3 wt.% Ru were added, the C_{2+} yield decreased to 9.0 and 5.6% respectively.
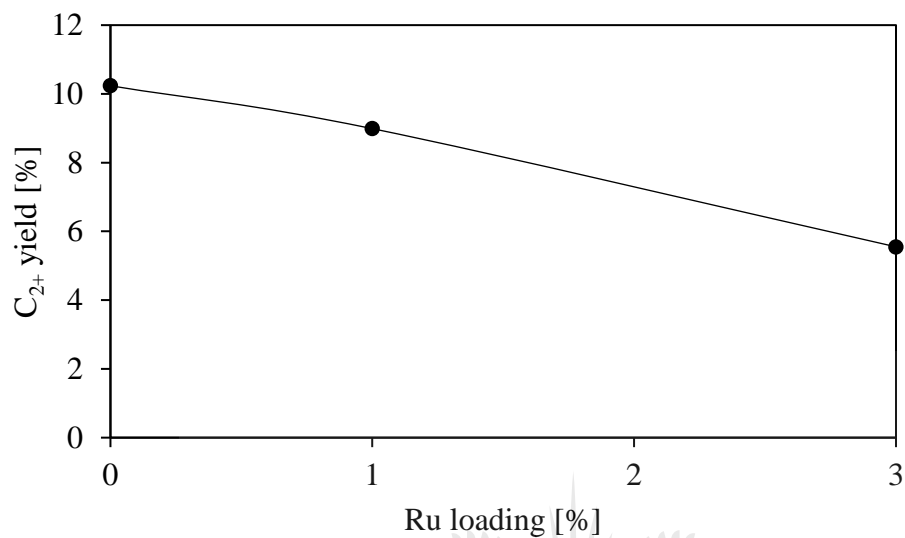
Figure 4. 16: Effect of Ru $(0 - 3$ wt.%) content on C_{2+} yield during CO_2 hydrogenation over 15%Co-6wt.%K/Al_2O_3 catalyst

4.2.3.2 Effect of promotion with Cu

The effect of copper as a second catalyst promoter was also investigated and the results are presented in Figures 4.17 and 4.18.
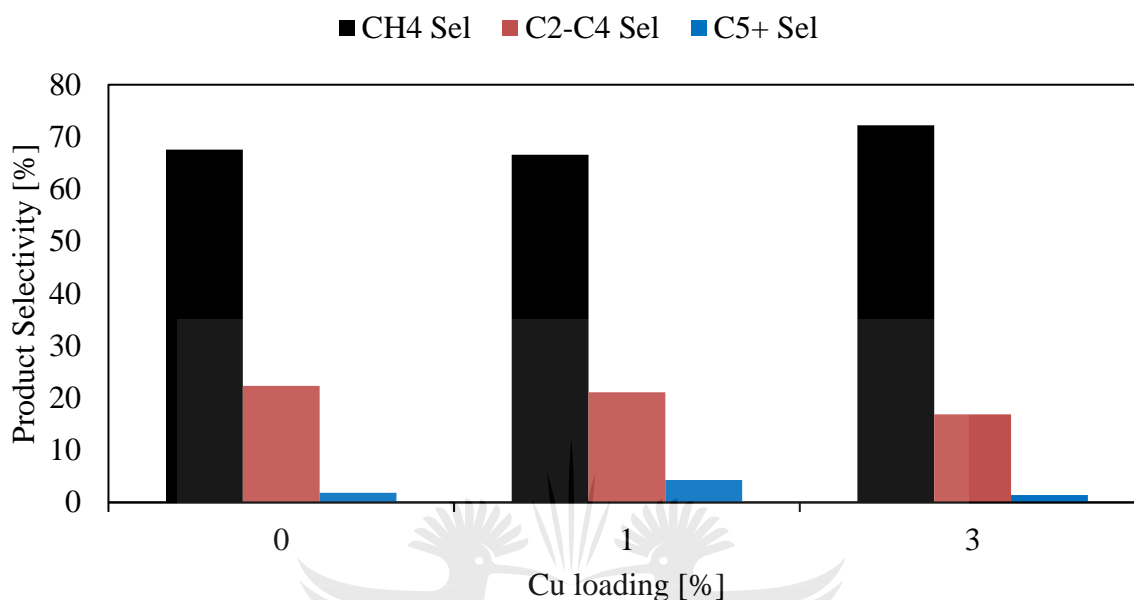
Figure 4. 17: Effect of Cu as a second promoter on product selectivity during CO_2 hydrogenation over 15%Co-6 wt.%K /Al_2O_3 catalysts.

When 1 wt.% copper was added to the catalyst, methane formation was slightly suppressed from 67.6 to 66.6%. The selectivity of $C_2 - C_4$ hydrocarbons decreased from 22.3 to 21.1%. The selectivity of C_{5+} hydrocarbons was found to be 2.4% higher compared to the copper – free catalyst, which produced 1.9% selectivity of C_{5+} hydrocarbons. As the copper loading was increased to 3 wt.%, the selectivity of methane increased to 72.2%. Meanwhile the selectivity of $C_2 - C_4$ and C_{5+} hydrocarbons significantly decreased to 16.9 and 1.4% respectively. It is possible that at higher contents, the Cu aids in H_2 dissociation and spillover and as a result increases slightly the CH_4 selectivity [27].
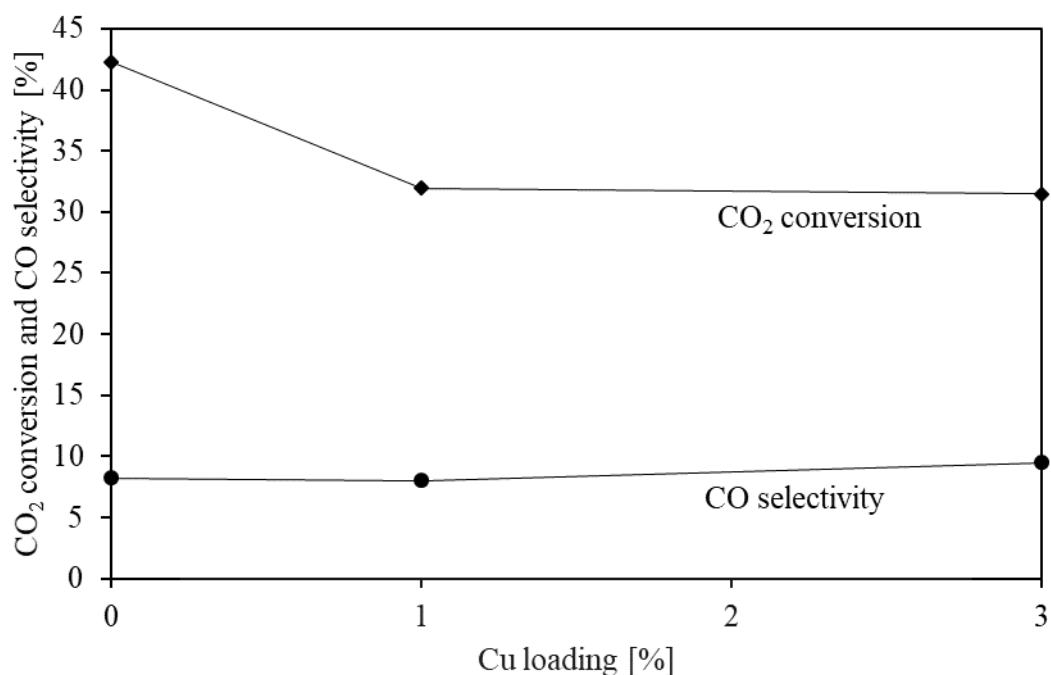
Figure 4. 18: Effect of Cu as a second promoter on CO_2 conversion and CO selectivity during CO_2 hydrogenation over 15%Co-6 wt.%K /Al_2O_3 catalysts.

Moreover, the CO_2 conversion was found to decline remarkably with the addition of copper promoter in the catalyst. The CO_2 conversion decreased from 42.3% in the case of copper – free catalyst to 32.0 and 31.5% for 1 and 3 wt.% copper-promoted catalysts respectively. At the same time, the selectivity to CO slightly increased as the copper loading increased, reaching the highest value of 9.5% at 3 wt.% copper loading.

The effect of Cu on C_{2+} yield during CO_2 hydrogenation over 15%Co-6 wt.%/Al_2O_3 catalyst is shown in figure 4.19. The highest C_{2+} yield was 10.2% observed for Cu-free catalyst. When 1 and 3 wt.% of Cu were introduced in the catalyst, the C_{2+} yield decreased to 8.1 and 5.7% respectively. Cu only slightly increased the RWGS activity of the catalyst.
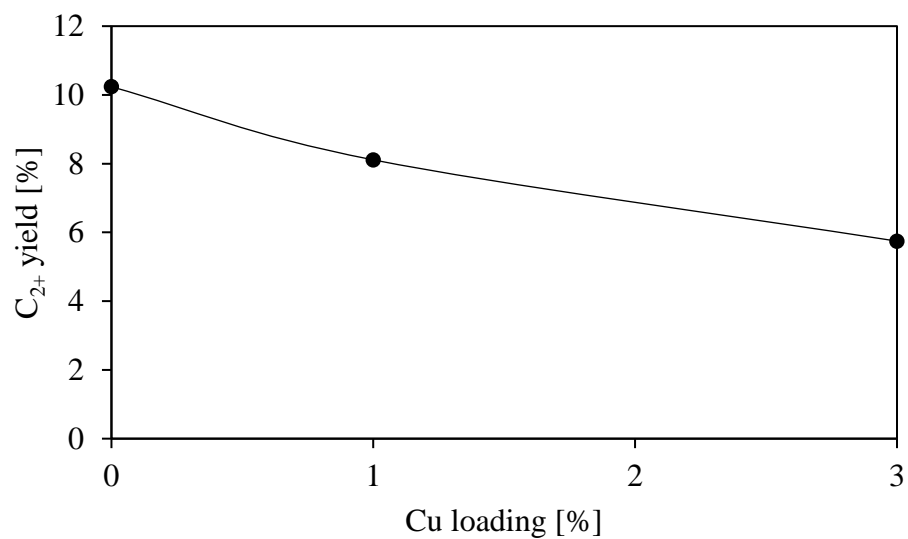
Figure 4. 19: Effect of Cu (0 – 3 wt.%) content on C_{2+} yield during CO_2 hydrogenation over 15%Co-6wt.%K/Al_2O_3 catalyst

4.2.3.3 Effect of promotion with Pd

The effect of palladium as a second catalyst promoter was also investigated and the results are presented in figures 4.20 and 4.21.
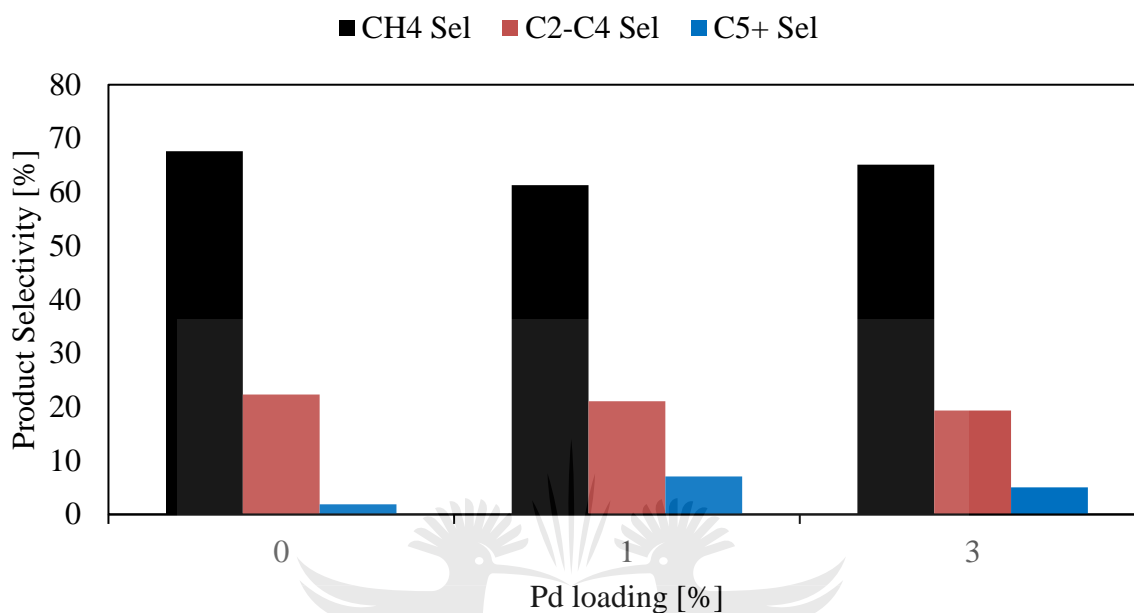
Figure 4. 20: Effect of Pd as a second promoter on product selectivity during CO_2 hydrogenation over 15%Co-6 wt.%K /Al_2O_3 catalysts.

The selectivity of methane slightly decreased from 67.6 to 61.3% when 1 wt.% palladium was added in the catalyst. The $C_2 - C_4$ selectivity decreased to 21.1 from 22.3%. The selectivity of C_{5+} product significantly increased to 7.0% relative to palladium-free catalyst, which produced selectivity of 1.9% towards C_{5+} product. When the content of palladium was increased to 3 wt.%, the production of methane increased to 65.1% and the selectivity of $C_2 - C_4$ and C_{5+} products decreased to 19.4 and 5.0% respectively.
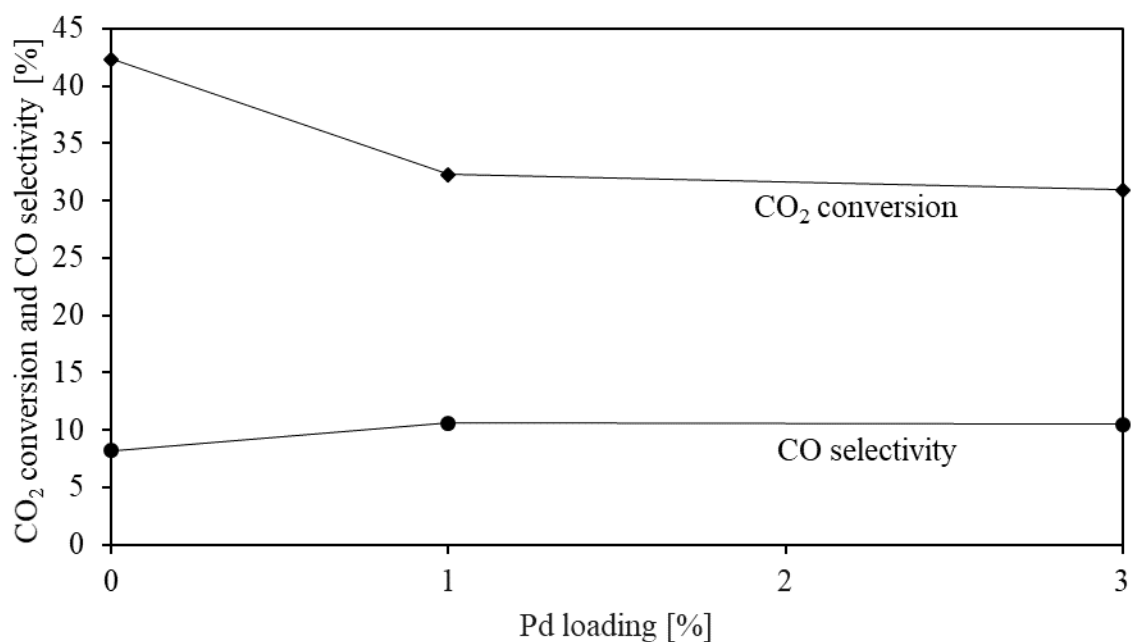
Figure 4. 21: Effect of Pd as a second promoter on CO_2 conversion and CO selectivity

The CO_2 conversion decreased remarkably with the addition of palladium as a second catalyst promoter. The CO_2 conversion decreased from 42.3% to 32.3 and 30.9% when palladium promoter was added to 1 and 3 wt.% respectively. Meanwhile, the selectivity of CO increased with the addition of palladium from 8.2% in the case of palladium – free catalyst to 10.6 and 10.5% respectively when palladium content was increased from 0 wt.% to 1 and 3 wt.% respectively.

The effect of Pd on C_{2+} yield during CO_2 hydrogenation over 15%Co-6 wt.%/Al_2O_3 catalyst is displayed by figure 4.22. The highest C_{2+} yield was 10.2% observed for Pd-free catalyst. When 1 and 3 wt.% of Pd was introduced in the catalyst, the C_{2+} yield decreased to 9.1 and 7.5% respectively.
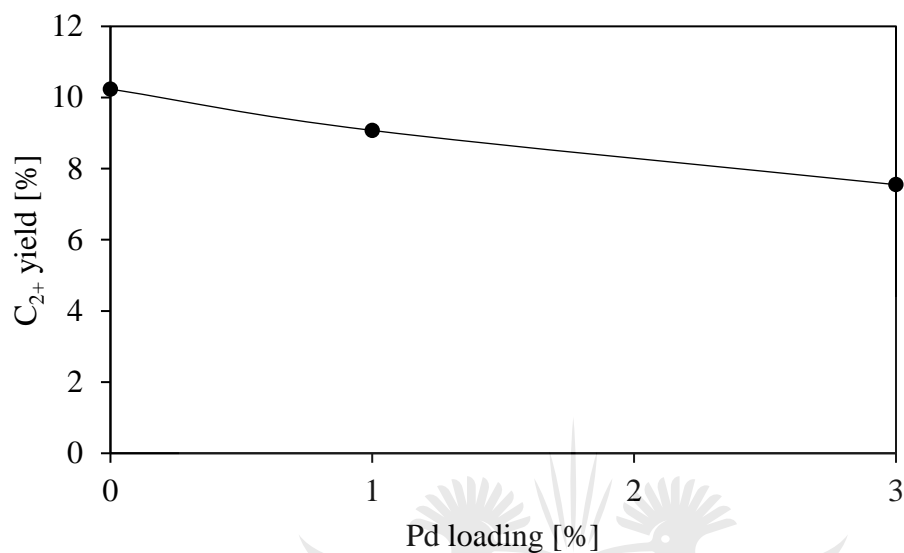
Figure 4. 22: Effect of Pd (0 – 3 wt.%) content on C_{2+} yield during CO_2 hydrogenation over 15%Co-6wt.%K/Al_2O_3 catalyst.

4.2.3.4 Summary of hydrogenation of CO_2 over 15%Co-6%K/Al_2O_3 FT catalysts promoted with Cu, Pd or Ru.

The catalytic performances during CO_2 hydrogenation to hydrocarbons over 15%Co-6%K/Al_2O_3 catalysts promoted with ruthenium, copper and palladium as the second promoter with different loading were evaluated at 300 ^{o}C, 5 bar and 10 ml/min to determine the effect of the second promoter and the results are presented in Table 4.6 below:

Table 4. 6: Catalytic performance of 15%Co-6%K/Al_2O_3 during CO_2 hydrogenation

Catalyst	CO_2 conv. [%]	CH_4 sel [%]	C_2-C_4 sel [%]	C_{5+} sel [%]	CO select. [%]	CH_4 yield [%]	C_{2+} select. [%]	C_{2+} yield [%]	C_{5+} yield [%]	Alpha
15%Co-6%K/Al_2O_3	42.3	67.6	22.3	1.9	8.2	28.6	24.2	10.2	0.8	0.412
15%Co-6%K-1%Ru/Al_2O_3	36.4	55.2	20.6	4.1	20.0	20.1	24.7	9.0	1.5	0.394
15%Co-6%K-3%Ru/Al_2O_3	34.9	83.0	14.9	1.0	1.1	28.9	15.9	5.6	0.4	0.264
15%Co-6%K-1%Cu/Al_2O_3	32.0	66.6	21.1	4.3	8.0	21.3	25.4	8.1	1.4	0.611
15%Co-6%K-3%Cu/Al_2O_3	31.5	72.2	16.9	1.4	9.5	22.8	18.2	5.7	0.4	0.301
15%Co-6%K-1%Pd/Al_2O_3	32.3	61.3	21.1	7.0	10.6	19.8	28.1	9.1	2.3	0.535
15%Co-6%K-3%Pd/Al_2O_3	30.9	65.1	19.4	5.0	10.5	20.1	24.4	7.5	1.6	0.554

As shown earlier, the CO_2 conversion over 15%Co-6%K/Al_2O_3 catalyst was negatively affected by Ru, Cu or Pd at 1 or 3 wt.%, as second catalyst promoter. When either copper or palladium were added as second catalyst promoter, their effect was significant, compared to ruthenium, as they led to lower CO_2 conversion of ca. 32%, when 1 wt.% copper or palladium was added to the catalyst, and ca. 31% in the case of 3 wt.% copper or palladium loaded in the catalyst compared to corresponding CO_2 conversion levels of ca. 36 and 35% in the case of 1 and 3% Ru loading. During traditional FTS, noble metals are known to facilitate the reduction of cobalt oxides [18, 28]. Noble metal promoters are known to improve the extent of catalyst reduction of cobalt and thus increase the conversion on a per gram of catalyst basis. In our case, addition of Ru, Pd and Cu improved catalyst reducibility as shown by TPR data in section 4.2.2.3. In addition, the CO_2 conversion declined with addition of these second catalyst promoters. Jacobs *et al.* [29] reported that not all metals that facilitate cobalt reduction promote activity on a per gram catalyst basis, some, such as Cu, will poison the surface. This is in agreement with the findings from this study.

The product was primarily methane for all the catalysts. Addition of 1 wt.% Ru to the catalyst reduced the methanation ability of the catalyst from 67.6% methane to 55.2%. When Ru content was increased to 3 wt.%, the methane production significantly increased to 83.0%. Addition of 1 wt.% of all second promoters reduced both methane selectivity and yield. The C_{5+} selectivity of 1.9% was observed when the catalyst was only promoted with K, however the addition of Ru, Cu and Pd to 1 wt% resulted in the increased C_{5+} product selectivity with the selectivity of 4.1%, 4.3% and 7.0% respectively. When the content of these promoters was increased to 3 wt%, the selectivity of C_{5+} declined to 1.0%, 1.4% and 5.0% in the case of Ru, Cu and Pd respectively.

The selectivity of CO increases significantly from 8.2 to 20% when 1 wt.% Ru was added to the catalyst and significantly dropped to 1.1% when the Ru content was increased to 3 wt.%. When Cu was added, had negligible effect on CO selectivity when was added to 1 wt.%. When 3 wt.% Cu and Pd (1 and 3 wt.%) were added, the CO selectivity increased. It has since been indicated in section 4.1 that the conversion of CO_2 to longer chain hydrocarbons proceeds via the formation of CO as intermediate product which subsequently undergoes hydrogenation to hydrocarbons.

The addition of Ru resulted in the decrease CH_4 yield from 28.6% in the case of Ru-free catalyst to 20.1% when 1 wt.% Ru was added to the catalyst. The CH_4 yield increased to 28.9% when the Ru content was increased to 3 wt.%. Addition of Cu also led to reduced CH_4 yield to 21.3 and 22.8% when 1 and 3 wt.% Cu were added to the catalyst, respectively. When Pd was added, the same trend was observed as the CH_4 yield decreased to ca.20% when either 1 or 3 wt.% Pd was added to the catalyst.

When 1 wt.% of Ru was introduced to the catalyst, the C_{5+} yield increased from 0.8 to 1.5%. When the Ru content was increased to 3 wt.%, the C_{5+} yield significantly decreased to 0.4%. Similar trend was observed when Cu and Pd were added as the second catalyst promoter. When 1 wt.% of both Cu and Pd were added to the catalyst, the C_{5+} yield increased to 1.4 and 2.3% respectively. When the content of Cu and Pd was increased to 3 wt.%, the C_{5+} yield decreased to 0.4 and 1.6% in a case of Cu and Pd respectively.

However, the C_{2+} selectivity increased with the addition of 1 wt.% of Ru, Cu or Pd from 24.2% to 24.7%, 25.4% and 28.1% respectively. Nonetheless, this selectivity declined to 15.9%, 18.2% and 24.4% when the content of Ru, Cu and Pd was increased to 3 wt.% respectively. The C_{2+} yield on the other hand was negatively influenced by the addition of the second promoter; it decreased with the addition of these second catalyst promoters.

In general, the positive effect of the second promoter to the catalyst is the improved liquid product formation, as shown by the improved C_{5+} selectivity and the chain growth probability, α. The catalyst with only potassium as the promoter had α value of 0.41 and C_{5+} product selectivity of 1.9%. Addition of 1 wt.% Ru to the catalyst resulted in a decreased chain growth probability of 0.39 and 0.26 when the Ru content was increased to 3 wt.%. The value of α increased to 0.61 when 1 wt.% of Cu was added to the catalyst. This value decreased to 0.30 when Cu content was increased to 3 wt.%. In contrast, the value of α was found to increase with the increase in Pd content. The α value increased of 0.535 and 0.554 in the case of 1 and 3 wt.% Pd respectively.

It can be seen (from Table 4.6) that the catalyst promoted by K only has the highest C_{2+} yield. The catalyst promoted by 1% Pd is the best catalyst since it has the second highest C_{2+} yield (very close to that of the catalyst promoted by K only), it has got the highest C_{2+} selectivity, highest C_{5+} selectivity and highest C_{5+} yield (higher C_{5+} yield is the ultimate target since we want liquid fuels formed from this reaction). This finding was compared to results reported in

other studies that used cobalt-based catalysts for CO_2 hydrogenation under various conditions, as summarized in Table 4.7. Our catalyst produced higher methane compared to most catalysts at lower operating conditions.

Table 4. 7: Summary of catalytic performance data for CO_2 hydrogenation over cobalt-based catalysts

Catalyst	Prep. Method	$H_2:CO_2$	T [K]	P [bar]	SV	Conv. [%]	Selectivity [%]				References
							CH_4	CO	C_{2+}	C_{5+}	
100Co/5Cu	Coprecip.	3:1	473		0.2 L/gCat/h						[30]
100Co/5Cu/2K$_2$CO$_3$	Coprecip.	3:1	498		0.16	49				1.12	
100Co/5Cu/2K$_2$CO$_3$	Coprecip.	3:1	498		0.16	56				2.31	
100Co/5Cu/2K$_2$CO$_3$	Coprecip.	3:1	473		0.16	40				1.91	
100Co/5Cu/2K$_2$CO$_3$	Coprecip.	3:1	498		0.16	22				2.81	
100Co/5Cu/2K$_2$CO$_3$	Coprecip.	3:1	473		0.16	10				0.19	
100Co/5Cu/2K$_2$CO$_3$	Coprecip.	3:1	473		0.16	44				1.59	
100Co/5Cu/5CeO$_2$/2K$_2$O$_3$	Coprecip.	3:1	498		0.16	54				1.43	
100Co/5Cu/5CeO$_2$/2K$_2$O$_3$	Coprecip.	2:1	498		0.15	34				2.11	
100Co/5Cu/1CeO$_2$	Coprecip.	2:1	498		0.15	40				0.1	
100Co/5Cu/CeO$_2$/3K$_3$PO$_4$	Coprecip.	3:1	498		0.16	40				1.42	
100Co/5Cu/1CeO$_2$/4,5K$_2$CO$_3$/100MgO	Coprecip.	2:1	513		0.3	21				0.29	
100Co/5Cu/1CeO$_2$/4,5K$_2$CO$_3$/100MgO	Coprecip.	2:1	498		0.15	8				0.51	
100Co/5Cu/1CeO$_2$/6K$_2$CO$_3$/100H.S.C	Coprecip.	2:1	518		0.15	19				2.71	
100Co/5Cu/100CeO$_2$/7K$_2$CO$_3$	Coprecip.	2:1	523		0.15	23				1.61	
100Co/5Cu/1CeO$_2$/4,5K$_2$CO$_3$/100F.C.	Coprecip.	2:1	513		0.075	23				0.24	
100Co/5Cu/1CeO$_2$/3,8K$_2$CO$_3$/50H.S.C.	Coprecip.	2:1	498		0.12	22				1.9	
3%Co/SiO$_2$	Impregnation	4:1, 95%N$_2$	500	1.4	4340/h	9.6	71	25	4.6		[31]
			500		8480	6.5	54	35	11		
			525		8480	12.3	59	33	8.2		

Table 4.7 cont.

Catalyst	Prep. Method	$H_2:CO_2$	T [K]	P [bar]	SV	Conv. [%]	Selectivity [%] CH_4	CO	C_{2+}	C_{5+}	References
			525		16400	9.4	42	49	8.9		
			550		16400	13.7	42	52	5.9		
			550		24600	12	32	52	17		
15%Co/SiO$_2$	Impregnation	4:1, no N$_2$	476	1	2050-3850	10.5	86.9	12.6	0.7	0	
			478	11	450-9620	11.2	89	10.7	0.34	0	
100%Co	Reduction	4:1	493	1	500-3000 h^{-1}	1.9	98	2			[32]
4,5%Co/S1	Impregnation		493			1.8	40	60			
4,6%Co/S3	Impregnation		493			6.3	66	34			
100Co/60MnO/147SiO$_2$/0,15Pt	Precip. and Impregnation	2:1	463	10	30mL/min/g of Co	18	95				[33]
15%Co/Al$_2$O$_3$	Impregnation	2.45:1	493	20	4800 cm^3 (STP)/h/gcat	33	>90				[34]
20%Co/SSP	Impregnation	20:2	493	1	18 L/gcat/h	27	89.5	10.5			[35]
20%Co/MCM-14						28	91.4	8.6			
20%Co/TiSSP						16	92.1	7.9			
Co/TiMCM-14						34	94.9	5.1			
0,5%Pt-25%Co/γ-Al$_2$O$_3$	Impregnation	3:1	493	19.9	5.0 L/gcat/h		93.3		6.66	5.16	[36]
5%Co/Al$_2$O$_3$^{c}	Impregnation	6:1	533	1	13.5 mL/min/(63 to 70 mg of cat)	0.21	35.7				[37]
10%Co/Al$_2$O$_3$^{c}						0.91	74.2				
15%Co/Al$_2$O$_3$^{c}						2.45	87.8				
20%Co/Al$_2$O$_3$^{c}						2.1	85.7				
Co/Al$_2$O$_3$	Solid state reaction of gibbsite and CoNT	10:1	543	1	150 mL/min/gcat	76	82.2	17.8			[38]

Table 4.7 cont.

Catalyst	Prep. Method	H_2:CO_2	T [K]	P [bar]	SV	Conv. [%]	Selectivity [%]				References
							CH_4	CO	C_{2+}	C_{5+}	
Co/Al$_2$O$_3$	Solid state reaction of gibbsite and CoAc					48.7	76.7	23			
Co/Al$_2$O$_3$	Solid state reaction of gibbsite and CoAA					20.3	76.4	23,6			
Co/Al$_2$O$_3$	Solid state reaction of gibbsite and CoCL					6.1	100	0			
Co/Al$_2$O$_3$	Impregnation using CoNT					32.2	86.5	13.5			
20%Co/SiO$_2$		3:1	643	Atmospheric		67.4	95.3	4.2	0.6	0	[39]
20%Co/1%Pd/SiO$_2$						50.7	93.4	6,3	0.3	0	
10%Co/1%Pd/1%K/SiO$_2$						36.4	89.3	8	2.8	0	
20%Co/1%Pd/1%K/SiO$_2$						63.4	80.3	13.9	5.9	0	
10%Co/1%Pd/1%K/SiO$_2$						39.1	82.9	9.5	7.6	0.09	
20%Co/1%Pd/0,5%K/SiO$_2$						62.8	76	15.3	8.8	0	
20%Co/1%Pd/1,5%K/SiO$_2$						59.1	64.7	16.2	19.1	1.26	
20%Co/1%Pd/3%K/SiO$_2$						43.2	53.1	24.3	22.6	2.73	
20%Co/1%K/SiO$_2$						36.1	45.3	16.9	37.8	7.87	
20%Co/1%Pt/1%K/SiO$_2$						36.5	41.5	20.8	37.7	9.58	
20%Co/1%Ru/1%K/SiO$_2$						45.1	52.6	12.6	34.8	5.68	
20%Co/1%Pd/1%Li/SiO$_2$						39.5	56.1	19.2	24.6	1.94	
20%Co/1%Pd/1%Na/SiO$_2$						41.9	48.4	20.3	31.3	7.33	
20%Co/1%Li/SiO$_2$						39.3	58.4	21.4	20.2	0.47	
20%Co/1%Na/SiO$_2$						51.2	42.1	21.7	36.3	5.01	
20%Co/1%K/SiO$_2$						47.6	50.1	17	32.9	3.65	

Table 4.7 cont.

Catalyst	Prep. Method	H_2:CO_2	T [K]	P [bar]	SV	Conv. [%]	Selectivity [%]				References
							CH_4	CO	C_{2+}	C_{5+}	
20%Co/1%Mo/SiO$_2$						64.8	88.7	6.5	4.8	0	
20%Co/1%Cr/SiO$_2$						60.9	75.9	22.8	1.2	0	
20%Co/1%Mn/SiO$_2$						62	91.1	6.9	2	0	
20%Co/1%Na/1%Mn/SiO$_2$						42.7	58.2	19.7	22.2	0,8	
20%Co/1%Na/1%Mo/SiO$_2$						43.9	38.3	15.7	45.9	8.76	
CoCu/TiO$_2$	Deposition-precipitation	73:24	523	50	3000 mL/g/h	23.1	87	1.3	10.2	4.76	[2]
1,5K-CoCu/TiO$_2$						21.2	59.3	4.7	36.5	13.21	
2,0K-CoCu/TiO$_2$						13.8	37.1	19.7	44.6	17.39	
2,5K-CoCu/TiO$_2$						13	22.4	35.1	43.3	23.08	
3,0K-CoCu/TiO$_2$						12.8	21.9	35.9	41.5	19.53	
3,5K-CoCu/TiO$_2$						11.9	18.9	45.9	35.1	16.81	
15%Co-1%K/SiO$_2$	Impregnation	3:1	543	1	0.92 NL/gcat/h	16	37.6	31.9	30.5	7.8	[40]
15%Co-6%K-1%Pd/Al$_2$O$_3$	Impregnation	3:1	573	5	1.2 NL/gcat/h	32.3	61.3	10.6	28.1	7	This study

4.3 Catalyst deactivation rate during CO_2 hydrogenation to hydrocarbons over 6% K-promoted Co/Al_2O_3 catalyst

4.3.1 Introduction

The catalyst stability and activity are essential for hydrocarbon production during CO_2 hydrogenation. Catalyst deactivation is a problem of great and continuing concern in the practice of industrial catalytic processes. Time scales for catalyst deactivation differ considerably; for instance, in the case of cracking catalysts, catalyst mortality may occur within seconds, while in ammonia synthesis the iron catalyst may last for 5–10 years. But it is inevitable that all catalysts will decay [41]. While catalyst deactivation is inevitable for most processes, some of its immediate, drastic consequences may be avoided, postponed, or even reversed. The catalyst stability is very important as it affects the process downtime as a result of catalyst reactivation or replacement, it also affects the operating costs. For that reason, this study focused on establishing the deactivation rates of $15\%Co-6wt.\%K/Al_2O_3$ catalyst. The catalyst deactivation rate was studied over a period of 1033 hours on stream.

4.3.2 Catalyst evaluation for stability during CO₂ hydrogenation

The stability of 15%Co-6%K/Al₂O₃ catalyst during CO₂ hydrogenation was evaluated at 300 °C and 5 bar. The results are presented in figures 4.23 and 4.24.
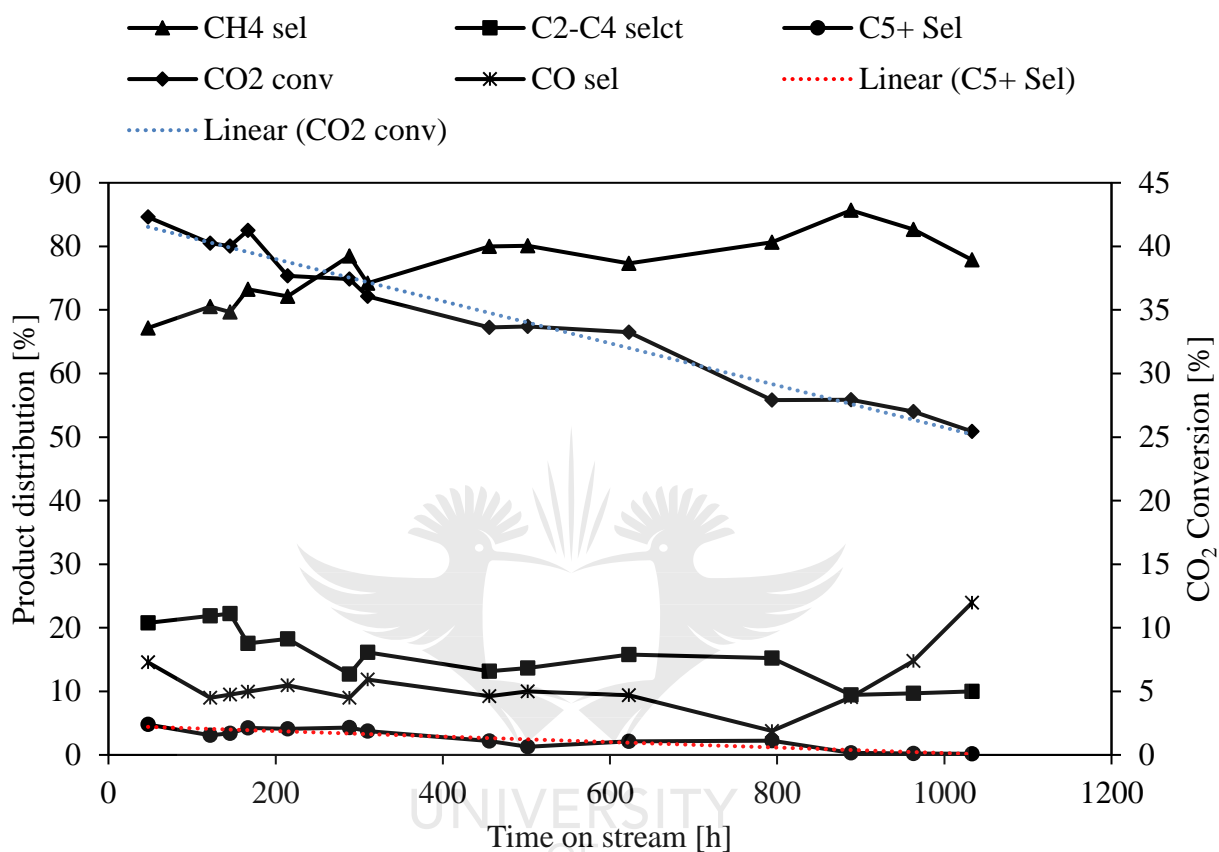

Figure 4. 23: CO₂ conversion and product selectivity as a function of TOS

The CO₂ conversion showed a linear decline with TOS. The C₅₊ selectivity also followed similar trend as it declined linearly until 888 hours on stream, where it switches off. Linear regression was applied to these data (figure 4.24) and the summary of ANOVA and regression statistics are reported in Appendix B.
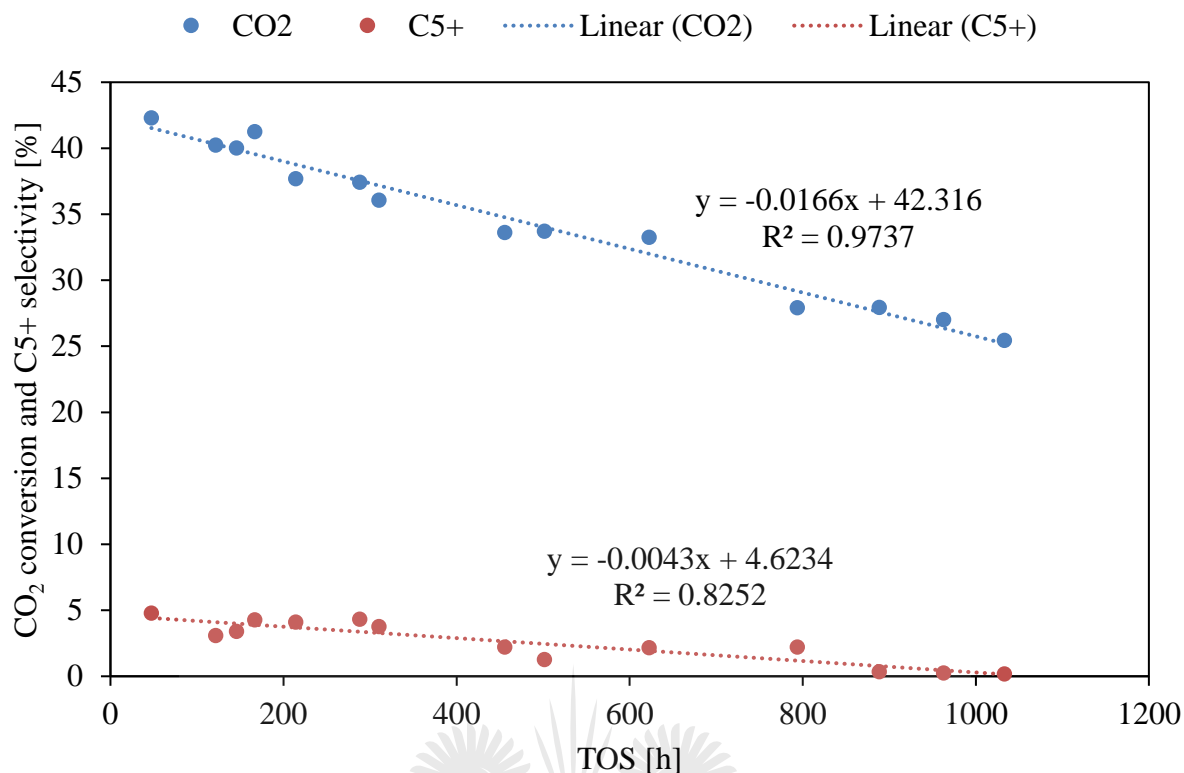
Figure 4. 24: Linear regression of CO_2 conversion and C_{5+} selectivity as a function of TOS

At 95% level of confidence, the confidence interval for the slope related to the change of the CO_2 conversion with time on stream is (-0.018, -0.015). Since the slope of the linear trendline (-0.017) falls in this interval, there is a significant negative relationship between the CO_2 conversion and time on stream. Similarly, the C_{5+} selectivity linearly decreases with an increasing TOS.

The methane selectivity tends to increase with time ranging from 67.2% during the initial 47 h on stream and reached its highest of 85.7% after 888 h and was 77.9% after 1033 h on stream. The $C_2 - C_4$ selectivity was stable during the first 145 h on stream and slightly decreased with time reaching 10.0% after 1033 h on stream. The CO selectivity decreased from 7.3% during the first 47 h on stream to 1.9% after 793 h on stream. Beyond 793 h on stream, the CO selectivity started to increase, reaching 12.0% after 1033 h on stream.
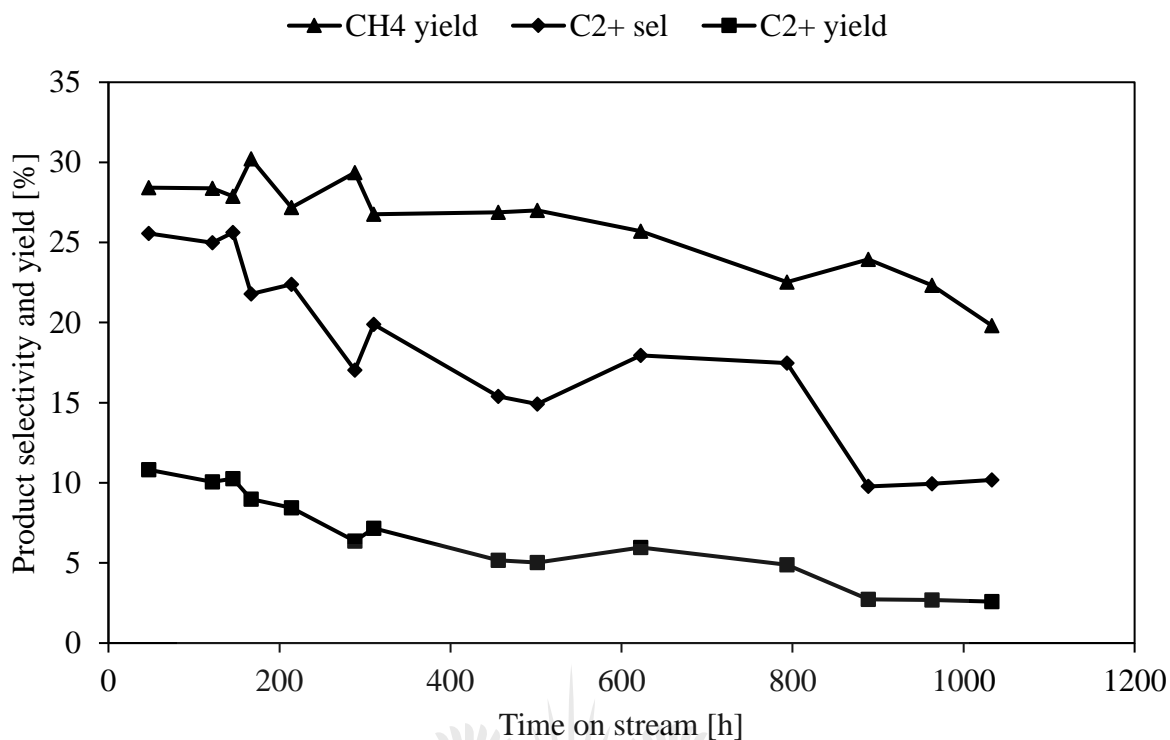
Figure 4. 25: Product selectivity and yield as a function of TOS

The C_{2+} selectivity was stable during the initial 145 h on stream and slightly dropped to 22.4% after 214 h on stream. This selectivity continued to decrease, reaching 10.2% after 1033 h on stream. The CH_4 yield did not significantly change during the first 288 h on stream. However, the yield of CH_4 decreased to 19.8% after 1033 h on stream. The C_{2+} yield was stable during the initial 145 h on stream. However, beyond 145 h on stream, its yield started to decrease and reached 2.6% after 1033 h on stream.

Table 4.8 below summarizes the catalytic performance for 15%Co-6%K/Al$_2$O$_3$ catalyst.

Table 4. 8: Catalytic performance for CO$_2$ hydrogenation as a function of TOS

TOS [h]	CO$_2$ conv. [%]	CH$_4$ sel [%]	C$_2$-C$_4$ sel [%]	C$_{5+}$ sel [%]	CO sel. [%]	CH$_4$ yield [%]	C$_{2+}$ sel. [%]	C$_{2+}$ yield [%]	Alpha
47	42.3	67.2	20.8	4.78	7.3	28.4	25.6	10.8	0.404
122	40.2	70.5	21.9	3.09	4.5	28.4	25.0	10.1	0.405
146	40.0	69.6	22.2	3.40	4.7	27.9	25.6	10.3	0.442
167	41.3	73.2	17.5	4.27	5.0	30.2	21.8	9.0	0.462
214	37.7	72.1	18.3	4.11	5.5	27.2	22.4	8.4	0.450
288	37.4	78.5	12.7	4.32	4.5	29.4	17.0	6.4	0.621
310	36.1	74.2	16.1	3.77	5.9	26.8	19.9	7.2	0.437
456	33.6	80.0	13.2	2.21	4.6	26.9	15.4	5.2	0.431
501	33.7	80.1	13.7	1.26	5.0	27.0	14.9	5.0	0.429
623	33.2	77.3	15.8	2.16	4.7	25.7	18.0	6.0	0.435
794	27.9	80.6	15.3	2.22	1.9	22.5	17.5	4.9	0.437
889	27.9	85.7	9.4	0.34	4.6	23.9	9.8	2.7	0.310
963	27.0	82.7	9.7	0.24	7.4	22.3	9.9	2.7	0.282
1033	25.4	77.9	10.0	0.18	12.0	19.8	10.2	2.6	0.276

A lot of attention has focused on exploring the role of oxidation of metallic cobalt on catalyst deactivation [42–47]. On the other hand, some reports on an industrial Co/Al_2O_3 catalyst using XANES, XRD and magnetic measurements have revealed that oxidation is not a deactivation mechanism during realistic FTS [42, 48]. Saib [49] proposed that deactivation mechanisms include cobalt support compound formation, poisoning, sintering, cobalt reconstruction and the formation of inert carbonaceous phases. The deactivation of cobalt-based catalysts is likely due to a combination of various deactivation mechanisms mentioned above [42, 50]. Various reports suggested that carbonaceous phases that form during FTS will deactivate the catalyst and need to be removed [51–53].

In an earlier study of unpromoted and Re promoted Co/Al_2O_3 catalysts, Schanke *et al.* [54] showed by gravimetric analysis and XPS that reoxidation occurs when water was introduced after reduction of the catalyst. The extent of reoxidation was found to be dependent on the partial pressure of water and the composition of the feed. Even at atmospheric pressure and a low water partial pressure of 2 kPa, without hydrogen in the feed, complete surface reoxidation was found to occur after short exposure times, while only slight indications of reoxidation were seen under hydrogen. On the other hand, at high pressure conditions of 2 MPa, which is comparable to the pressure in an FTS reactor, reoxidation occurred to a greater extent. In their study, the Re promoted catalyst was found to be more vulnerable to reoxidation than the unpromoted catalyst. They concluded that bulk cobalt metal does not reoxidize in H_2O/H_2 mixtures.

As can be seen, the various routes of cobalt-based catalysts discussed above, were relative to FTS operating conditions, which are different from the conditions used in this study where a high temperature on 300 °C and a low pressure were used. To gain more information on the mechanism of catalyst deactivation, XRD analyses of the reduced catalyst before and after reaction were conducted. The data are shown in figure 4.26.
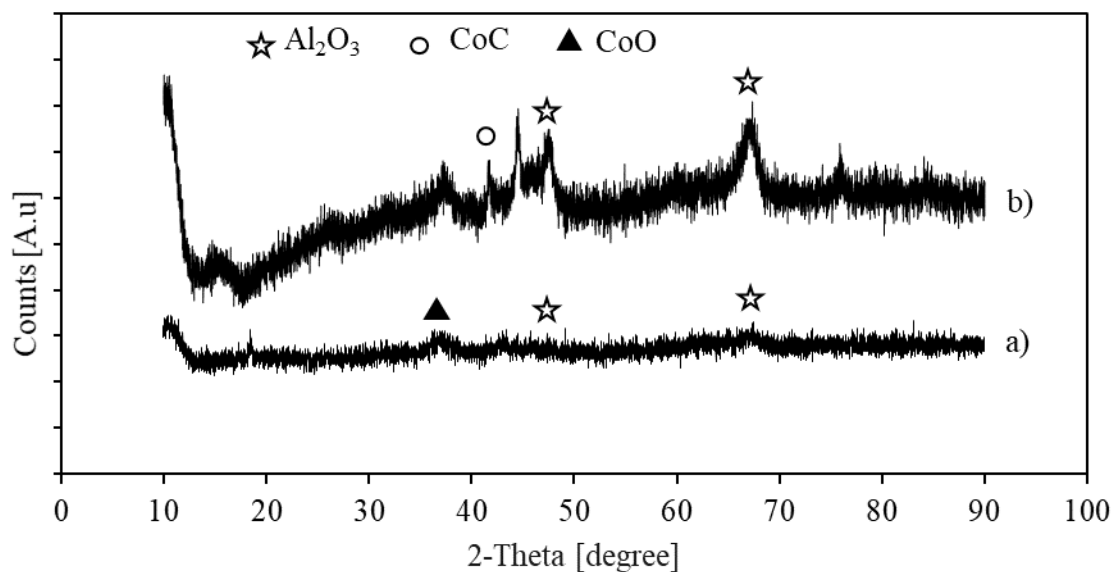
Figure 4. 26: XRD pattern for a) reduced and b) spent catalyst.

CoO was detected in both the fresh and spent catalysts, making it difficult to establish whether some cobalt was oxidized during the CO_2 hydrogenation. However, cobalt carbide was the only observed on the spent catalyst. Formation of carbide-type species was also observed by Johnson *et al.* [55] using XANES spectroscopy of sub-monolayer cobalt deposited on the surface after FT reaction. In-situ XRD results disclosed that [56] the decrease in the FT reaction rate over alumina- and titania-supported cobalt catalysts can be attributed to formation of cobalt carbide. Cobalt carbide itself is inactive in FT. Formation of cobalt carbide was also suggested to be a major reason of catalyst deactivation on carbon-supported catalysts [56 – 57].

The catalyst was promoted with potassium, and it is known that addition of potassium promotes chain growth during traditional CO hydrogenation over Fe – based catalysts. As the TOS was increasing, carbonaceous deposit formed an overlayer on parts of the catalyst. The latter is associated to cobalt rather than potassium as revealed by XRD results of the used catalyst. These deposits tend to lean towards the formation of methane, decrease CO_2 conversion and C_{5+} selectivity as observed in this study [56 – 58]. These findings are in agreement with Rafati *et al.* [59]. Using In-situ XRD experiments, Ducreux *et al.* [56] highlighted that the decrease in the FT reaction rate over alumina- and titania-supported cobalt catalysts was endorsed to the presence of cobalt carbide formation. Formation of cobalt carbide is a major reason for catalyst deactivation on carbon-supported catalysts [56 – 57]. Gruver *et al.* [60] reported the formation of bulk carbide during Fischer–Tropsch synthesis (216 °C and 37 bar), when the catalyst was exposed to pure CO for a period of 8 h. The performance of the catalyst was significantly

132

affected when the synthesis gas with a H_2/CO ratio of 2:1 was reintroduced. They found that the CO conversion had dropped by more than a half, and the methane selectivity had doubled compared to the performance prior to the upset. Moodley [61] reported similar observations. They found that the exposure of a cobalt catalyst to pure CO for even shorter period of 2 h and typical pressures and temperatures of the low temperature Fischer–Tropsch synthesis could result in catalyst deactivation via the formation of bulk cobalt carbide. Bulk cobalt carbide is considered to be a deactivating species in cobalt catalysts [62]. Previous work at the Bureau of Mines indicated that bulk carbide was not an intermediate in the Fischer–Tropsch synthesis nor it was catalytically active [63]. Claeys *et al.* [58] studied the effect of cobalt carbide on FT reaction and reported that carbides exhibited low FTS activity and increased methane formation. Cobalt carbide formation in the spent catalyst in this study can account, at least in part, for the observed catalyst deactivation with the time-on-stream.

REFERENCES

[1] M. Khobragade, S. Majhi, K.K. Pant, "Effect of K and CeO_2 promoters on the activity of Co/SiO_2 catalyst for liquid fuel production from syngas", Applied energy, 94, (2012) 385-394.

[2] Z. Shi, H. Yang, P. Gao, X. Li, L. Zhong, H. Wang, H. Liu, W. Wei, Y. Sun, "Direct conversion of CO_2 to long-chain hydrocarbon fuels over K–promoted $CoCu/TiO_2$ catalysts", Catalysis Today, 311, (2018) 65-73.

[3] J.P. den Breejen, P.B. Radstake, G.L. Bezemer, J.H. Bitter, V. Froseth, A. Holmen, K.P. de Jong, "On the origin of the cobalt particle size effects in Fischer− Tropsch catalysis", Journal of the American Chemical Society, 131, (2009) 7197-7203.

[4] D. Nabaho, J.W. (Hans) Niemantsverdriet, M. Claeys, E. van Steen, "Hydrogen spillover in the Fischer–Tropsch synthesis: An analysis of platinum as a promoter for cobalt–alumina catalysts", Catalysis Today, 261, (2016) 17-27.

[5] M. Jacquemin, M.J. Genet, E.M. Gaigneaux, D.P. Debecker, "Calibration of the X-Ray Photoelectron Spectroscopy Binding Energy Scale for the Characterization of Heterogeneous catalysis: Is everything really under control?", ChemPhysChem, 14 (15), (2013) 3618-3626.

[6] R. Mutschler, E. Moioli, W. Luo, N. Gallandat, A. Züttel, "CO_2 hydrogenation reaction over pristine Fe, Co, Ni, Cu and Al_2O_3 supported Ru: Comparison and determination of the activation energies" Journal of catalysis, 366, (2018) 139-149.

[7] Dry, M.E., "Practical and theoretical aspects of the catalytic Fischer-Tropsch process", Applied Catalysis A: General, 138(2), (1996) 319-344.

[8] M.J. Choi, J.S. Kim, H.K. Kim, S.B. Lee, Y. Kang, K.W. Lee, "Hydrogenation of CO_2 over Fe-K based catalysts in a fixed bed reactors at elevated pressure", Korean Journal of Chemical Engineering, 18(5), (2001) 646-651.

[9] G.P. Van Der Laan, A.A.C.M. Beenackers, "Kinetics and selectivity of the Fischer–Tropsch synthesis: a literature review", Catalysis Reviews, 41(3-4), (1999) 255-318.

[10] R.W. Dorner, D.R. Hardy, F.W. Williams, H.D. Willauer, "Heterogeneous catalytic CO_2 conversion to value-added hydrocarbons", Energy & Environmental Science, 3(7), (2010) 884-890.

[11] R.W. Dorner, D.R. Hardy, F.W. Williams, B.H. Davis, H.D. Willauer, "Influence of Gas Feed Composition and Pressure on the Catalytic Conversion of CO_2 to

Hydrocarbons Using a Traditional Cobalt-Based Fischer−Tropsch Catalyst", Energy & Fuels, 23(8), (2009) 4190-4195.

[12] Y. Zhang, G. Jacobs, D.E. Sparks, M.E. Dry, B.H. Davis, "CO and CO_2 hydrogenation study on supported cobalt Fischer–Tropsch synthesis catalysts", Catalysis today, 71(3-4), (2002) 411-418.

[13] J. Gaube, H.F. Klein, "The promoter effect of alkali in Fischer-Tropsch iron and cobalt catalysts", Applied Catalysis A: General, 350(1), (2008) 126-132.

[14] S.A. Hosseini, A. Taeb, F. Feyzi, F. Yaripour, "Fischer–Tropsch synthesis over Ru promoted Co/γ-Al_2O_3 catalysts in a CSTR", Catalysis Communications, 5, (2004) 137–143.

[15] A. Kogelbauer, J.G. Goodwin, R. Oukaci, "Ruthenium Promotion of Co/Al_2O_3 Fischer–Tropsch Catalysts", Journal of Catalysis, 160, (1996) 125–133.

[16] G. Jacobs, M.C. Ribeiro, W. Ma, Y. Ji, S. Khalid, P.T.A. Sumodjo, B.H. Davis, "Group11 (Cu, Ag, Au) promotion of $15\%Co/Al_2O_3$ Fischer–Tropsch synthesis catalysts", Applied Catalysis A: General, 361 (2009) 137–151.

[17] Z. Shi, H. Yang, P. Gao, X. Li, L. Zhong, H. Wang, H. Liu, W. Wei, Y. Sun, "Direct conversion of CO_2 to long-chain hydrocarbon fuel over K-promoted $CoCu/TiO_2$ catalysts", Catalysis Today, 311, (2018) 65-73.

[18] D. Xu, W. Li, H. Duan, Q. Ge, H. Xu, "Reaction performance and characterization of Co/Al_2O_3 Fischer–Tropsch catalysts promoted with Pt, Pd and Ru", Catalysis Letters, 102, (2005) 229-235.

[19] G. Jacobs, M.C. Ribeiro, W. Ma, Y. Ji, S. Khalid, P.T.A. Sumodjo, B.H. Davis, "Group 11 (Cu, Ag, Au) promotion of $15\%Co/Al_2O_3$ Fischer–Tropsch synthesis catalysts", Applied Catalysis A: General, 361, (2009) 137–151.

[20] S.A. Hosseini, A. Taeb, F. Feyzi, F. Yaripour, "Fischer–Tropsch synthesis over Ru promoted Co/γ-Al_2O_3 catalysts in a CSTR", Catalysis Communications, 5, (2004) 137–143.

[21] A. Kogelbauer, J.G. Goodwin, Jr, R. Oukaci, "Ruthenium Promotion of Co/Al_2O_3 Fischer–Tropsch Catalysts", Journal of Catalysis, 160 (1996) 125-133.

[22] V. Vosoughi, A.K. Dalai, N. Abatzoglou, Y. Hu, "Performances of promoted cobalt catalysts supported on mesoporous alumina for Fischer-Tropsch synthesis", Applied Catalysis A, General, 547, (2017) 155–163.

[23] G. Jacobs, T.K. Das, Y. Zhang, J. Li, G. Racoillet, B.H. Davis, "Fischer–Tropsch synthesis: support, loading, and promoter effects on the reducibility of cobalt catalysts", Applied Catalysis A: General, 233, (2002) 263-281.

[24] G. Jacobs, Y. Ji, B.H. Davis, D.C. Cronauer, A.J. Kropf, C.L. Marshall, Fischer–Tropsch synthesis: Temperature programmed EXAFS/XANES investigation of the influence of support type, cobalt loading, and noble metal promoter addition to the reduction behavior of cobalt oxide particles", Applied Catalysis A: General, 333, (2007) 177–191.

[25] L. Guczi, D. Bazin, I. Kovacs, L. Borko, Z. Schay, J. Lynch, P. Parent, C. Lafon, G. Stefler, Z. Koppany, I. Sajo, "Structure of Pt–Co/Al_2O_3 and Pt–Co/NaY bimetallic catalysts: characterization by in situ EXAFS, TPR, XPS and by activity in Co (carbon monoxide) hydrogenation", Topics in Catalysis, 20, (2002) 129–139.

[26] C.J. Bertole, C.A. Mims, G. Kiss, "Support and rhenium effects on the intrinsic site activity and methane selectivity of cobalt Fischer–Tropsch catalysts", Journal of Catalysis, 221, (2004) 191–203.

[27] W. Ma, G. Jacobs, R.A. Keogh, D. B. Bukur, B. H. Davis, "Fischer–Tropsch synthesis: Effect of Pd, Pt, Re, and Ru noble metal promoters on the activity and selectivity of a 25%Co/Al_2O_3 catalyst", Applied Catalysis A: General, 437–438, (2012) 1–9.

[28] V.M. Belousov, J. Stoch, I.V. Batcherikova, E.V. Rozhkova, L.V. Lyashenko, "Low-temperature hydrogen reduction of pure Co_3O_4 and doped with palladium", Applied Surface Science, 35 (1989) 481–494.

[29] J.B. Hansen, P.E.H. Nielsen, "Methanol synthesis", Handbook of Heterogeneous Catalysis: Online (2008), 2920-2949.

[30] W.W. Russell, G.H. Miller, "Catalytic hydrogenation of carbon dioxide to higher hydrocarbons" Journal of American Chemical Society, 72, (1950) 2446–2454.

[31] G.D. Weatherbee, C.H. Bartholomew, "Hydrogenation of CO_2 on group VIII metals: IV. Specific activities and selectivities of silica-supported Co, Fe, and Ru", Journal of Catalysis, 87, (1984) 352–362.

[32] A. Guerrero-Ruiz, I. Rodriguez-Ramos, "Hydrogenation of CO_2 on carbon-supported nickel and cobalt", Reaction Kinetics Catalysis Letters, 29, (1985) 93–99.

[33] T. Riedel, M. Claeys, H. Schulz, G. Schaub, S.S. Nam, K.W. Jun, M.J. Choi, G. Kishan, K.W. Lee, "Comparative study of Fischer–Tropsch synthesis with H_2/CO and

H_2/CO_2 syngas using Fe- and Co-based catalysts", Applied Catalysis A: General, 186, (1999) 201–213.

[34] C.G. Visconti, L. Lietti, E. Tronconi, P. Forzatti, R. Zennaro, E. Finocchio, "Fischer–Tropsch synthesis on a Co/Al_2O_3 catalyst with CO_2 containing syngas", Applied Catalysis A: General, 355, (2009) 61–68.

[35] J. Janlamool, P. Praserthdam, B. Jongsomjit, "Ti-Si composite oxide-supported cobalt catalysts for CO_2 hydrogenation", Journal of Natatural Gas Chemistry, 20, (2011) 558–564.

[36] M.K. Gnanamani, W.D. Shafer, D.E. Sparks, B.H. Davis, "Fischer–Tropsch synthesis: Effect of CO_2 containing syngas over Pt promoted $Co/-Al_2O_3$ and K-promoted Fe catalysts", Catalysis Communications, 12, (2011) 936–939.

[37] T. Das, G. Deo, "Synthesis, characterization and in situ DRIFTS during the CO_2 hydrogenation reaction over supported cobalt catalysts", Journal of Molecular Catalysis A: Chem, 350, (2011) 75–82.

[38] N. Srisawad, W. Chaitree, O. Mekasuwandumrong, A. Shotipruk, B. Jongsomjit, J. Panpranot, "CO_2 hydrogenation over Co/Al_2O_3 catalysts prepared via a solid-state reaction of fine gibbsite and cobalt precursors", Reaction Kinetics Mechanical Catalysis, 107, (2012) 179–188.

[39] R.E. Owen, J.P. O'Byrne, D. Mattia, P. Plucinski, S.I. Pascu, M.D. Jones, "Cobalt catalysts for the conversion of CO_2 to light hydrocarbons at atmospheric pressure", Chemical Commununications, 49, (2013) 11683–11685.

[40] R.A. Iloy, K. Jalama, "Effect of Operating Temperature, Pressure and Potassium Loading on the Performance of Silica-Supported Cobalt Catalyst in CO_2 Hydrogenation to Hydrocarbon Fuel" Catalysts, 9(10) (2019).

[41] M.D. Argyle, C.H. Bartholomew, "Heterogeneous Catalyst Deactivation and Regeneration: A Review", Catalysts, 5(1) (2015) 145-269.

[42] J. van de Loosdrecht, B. Balzhinimaev, J.-A. Dalmon, J.W. Niemantsverdriet, S.V. Tsybulya, A.M. Saib, P.J. van Berge, J.L. Visagie, "Cobalt Fischer-Tropsch synthesis: Deactivation by oxidation?", Catalysis Today, 123, (2007) 293-302.

[43] P.J. van Berge, J. van de Loosdrecht, S. Barradas, A.M. van der Kraan, "Oxidation of cobalt based Fischer–Tropsch catalysts as a deactivation mechanism", Catalysis Today, 58, (2000) 321-334.

[44] G. Jacobs, T.K. Das, P.M. Patterson, J. Li, L. Sanchez, B.H. Davis, "Fischer–Tropsch synthesis XAFS XAFS studies of the effect of water on a Pt-promoted Co/Al_2O_3 catalyst", Applied Catalysis A: General, 247, (2003) 335-343.

[45] G. Kiss, C.E. Kliewer, G.J. DeMartin, C.C. Culross, J.E. Baumgartner, "Hydrothermal deactivation of silica-supported cobalt catalysts in Fischer–Tropsch synthesis", Journal of Catalysis, 217, (2003) 127-140.

[46] A.M. Hilmen, D. Schanke, K.F. Hanssen, A. Holmen, "Study of the effect of water on alumina supported cobalt Fischer–Tropsch catalysts", Applied Catalysis A: General, 186, (1999) 169–188.

[47] J. Li, X. Zhan, Y. Zhang, G. Jacobs, T. Das, B.H. Davis, "Fischer–Tropsch synthesis: effect of water on the deactivation of Pt promoted Co/Al_2O_3 catalysts", Applied Catalysis A: General, 228, (2002) 203-212.

[48] A.M. Saib, A. Borgna, J. van de Loosdrecht, P.J. van Berge, J.W. Niemantsverdriet, "XANES study of the susceptibility of nano-sized cobalt crystallites to oxidation during realistic Fischer–Tropsch synthesis", Applied Catalysis A: General, 312, (2006) 12-19.

[49] A.M. Saib, "Towards a cobalt FTS catalyst with enhanced stability: a combined approach", Ph.D. Thesis, Eindhoven University of Technology, 2006.

[50] D.J. Moodley, J. van de Loosdrecht, A.M. Saib, M.J. Overett, A.K. Datye, J.W. Niemantsverdriet, "Carbon deposition as a deactivation mechanism of cobalt-based Fischer–Tropsch synthesis catalysts under realistic conditions", Applied Catalysis A: General, 354, (2009) 102–110.

[51] S.L. Soled, E. Iglesia, R. Fiato, G.B. Ansell, United States Patent 5,397,806 (1995), to Exxon.

[52] M.J. van der Burgt, J. Ansorge, Great Britain Patent 2,222,531 (1988), to Shell.

[53] H.A. Wright, United States Patent 6,486,220 B1 (2002), to Conoco.

[54] D. Schanke, A.M. Hilmen, E. Bergene, K. Kinnari, E. Rytter, E. Adnanes, A. Holmen, "Study of the deactivation mechanism of Al_2O_3-supported cobalt Fischer-Tropsch catalysts", Catalysis Letters, 34, (1995) 269-284.

[55] B.G. Johnson, C.H. Bartholomew, D.W. Goodman, "The role of surface structure and dispersion in CO hydrogenation on cobalt", Journal of Catalysis, 128, (1991) 231-247.

[56] O. Ducreux, J. Lynch, B. Rebours, M. Roy, P. Chaumette, "In situ characterisation of cobalt based Fischer-Tropsch catalysts: A new approach to the active phase", Studies in surface science and catalysis, (1998) 125-130

[57] J. Xiong, Y. Ding, T. Wang, L. Yan, W. Chen, H. Zhu, Y. Lu, "The formation of Co_2C species in activated carbon supported cobalt-based catalysts and its impact on Fischer–Tropsch reaction", Catalysis Letters, 102, (2005) 265-269.

[58] M. Claeys, M.E. Dry, E. van Steen, E. du Plessis, P.J. van Berge, A.M. Saib, D.J. Moodley, "In situ magnetometer study on the formation and stability of cobalt carbide in Fischer–Tropsch synthesis", Journal of Catalysis, 318, (2014) 193–202.

[59] M. Rafati, L. Wang, A. Shahbazi, "Effect of silica and alumina promoters on co-precipitated Fe–Cu–K based catalysts for the enhancement of CO_2 utilization during Fischer–Tropsch synthesis", Journal of CO_2 Utilization, 12, (2015) 34–42.

[60] V. Gruver, Z. Xiaodong, J. Engman, H.J. Robota, S.L. Suib, M. Polverejan, "Deactivation of a Fischer-Tropsch catalyst through the formation of cobalt carbide under laboratory slurry reactor conditions", Preprints-American Chemical Society, Division of Petroleum Chemistry, 49, (2004) 192-194.

[61] D.J. Moodley, "On the deactivation of cobalt-based Fischer-Tropsch synthesis catalysts", PhD. Thesis, Eindhoven University of Technology, 2008.

[62] J. Cheng, P. Hu, P. Ellis, S. French, G. Kelly, C.M. Lok, "Density functional theory study of iron and cobalt carbides for Fischer− Tropsch synthesis", The Journal of Physical Chemistry C, 114 (2009) 1085-1093.

[63] United States Bureau of Mines Bulletin 578, Synthetic Liquid Fuels from Hydrogenation of Carbon Monoxide, Washington, US Government Print Office, 1948–1959, p. 19. <http://www.fischer-tropsch.org>.

CHAPTER 5: CONCLUSIONS AND RECOMMENDATIONS

The main objectives of this study were to: (i) evaluate the effect of operating temperature, pressure and potassium loading on $15\%Co/Al_2O_3$ Fischer-Tropsch catalyst during CO_2 hydrogenation to liquid hydrocarbons; (ii) evaluate the effect of noble metals Ru, Pd and Cu as second catalyst promoter on $15\%Co-6\%K/Al_2O_3$ catalyst during CO_2 conversion to liquid hydrocarbons; and (iii) evaluate the $15\%Co-6\%K/Al_2O_3$ catalyst deactivation rate during CO_2 hydrogenation to liquid hydrocarbons at optimum operating conditions. The outcomes of the study are summarized in sections 5.1 to 5.3.

5.1 Effects of operating conditions on CO_2 hydrogenation

TPR data revealed that potassium loading shifted the catalyst reduction to higher temperatures and increased gradually with the increase in potassium loading. This was explained by metal – support interactions, which limit the reducibility of the catalyst. It was also found that potassium improves the surface basicity of the catalyst. XRD revealed that the cobalt particle size increased with potassium loading. A direct relationship between cobalt particle size, CO_2 conversion and product selectivity exist. Methane formation usually increases with the particle size and larger particles has a tendency to lean product towards longer chain hydrocarbons with very small particles favoring the formation of CO. Reaction temperature and pressure were found to be directly proportional to the CO_2 conversion. At higher temperatures, the rate of reaction increases leading to CO formed in the reverse-water-gas-shift reaction being converted to hydrocarbons faster, as a result, the CO selectivity decrease and the selectivity of other hydrocarbons improves. The optimum potassium loading was 6 wt.%. At higher potassium loading, the methane formation was suppressed and the selectivity of C_{2+} hydrocarbons improved. Based on these observations it was concluded that for CO_2 hydrogenation to longer chain hydrocarbons over $15\%Co/Al_2O_3$ catalysts promoted with different potassium loading, CO_2 is first converted to CO via reverse – water – gas – shift reaction, followed by a subsequent hydrogenation of CO to hydrocarbons via modified FT synthesis. Nonetheless, the potassium – free catalyst performed as a methanation catalyst rather than FT catalyst since the selectivity of methane was 97%.

5.2 Effects of Cu, Pd and Ru as second promoter

The addition of a second catalyst promoters improved the catalyst reducibility with palladium shifting the reduction to lowest temperature followed by ruthenium and copper respectively. The catalyst activity decreased with the addition of these metals as a second catalyst promoter as shown by CO_2 conversion. The selectivity of methane slightly decreased with the addition of these promoters and then increased with increasing their content from 1 to 3 wt.%, indicating that the catalyst methanation ability was suppressed and enhanced when a second promoter loading increases. The C_{2+} yield decreased with addition of the second promoter and posed the same trend with promoter loading increase. The CO selectivity increased with addition of the second promoter, with the exception of Ru where the highest CO selectivity was obtained at 1 wt.% loading. These results indicate that the CO produced undergoes secondary reaction to form mostly methane and other hydrocarbons. In general, the positive effect of the second promoter to the catalyst is the improved liquid product formation, as shown by the improved C_{5+} selectivity and the chain growth probability, α.

5.3 Catalyst deactivation

XRD data revealed the presence of cobalt carbide species on the spent catalyst. These species are inactive in FT and has been reported to be the main reason for deactivation on supported cobalt catalysts. CO_2 negatively affected the activity of the catalyst and product distribution as it decreased with TOS. The product formed was predominantly methane. This was explained by the presence of the cobalt carbide. The latter is inactive for FT and lead to the C_{5+} selectivity decrease with a concomitant increase of CH_4 formation. The catalyst was promoted with potassium, and it is known that addition of potassium promotes chain growth during traditional CO hydrogenation over Fe – based catalysts. As the TOS was increasing, it was observed that carbonaceous deposit formed an overlayer on parts of the catalyst leading to formation of methane.
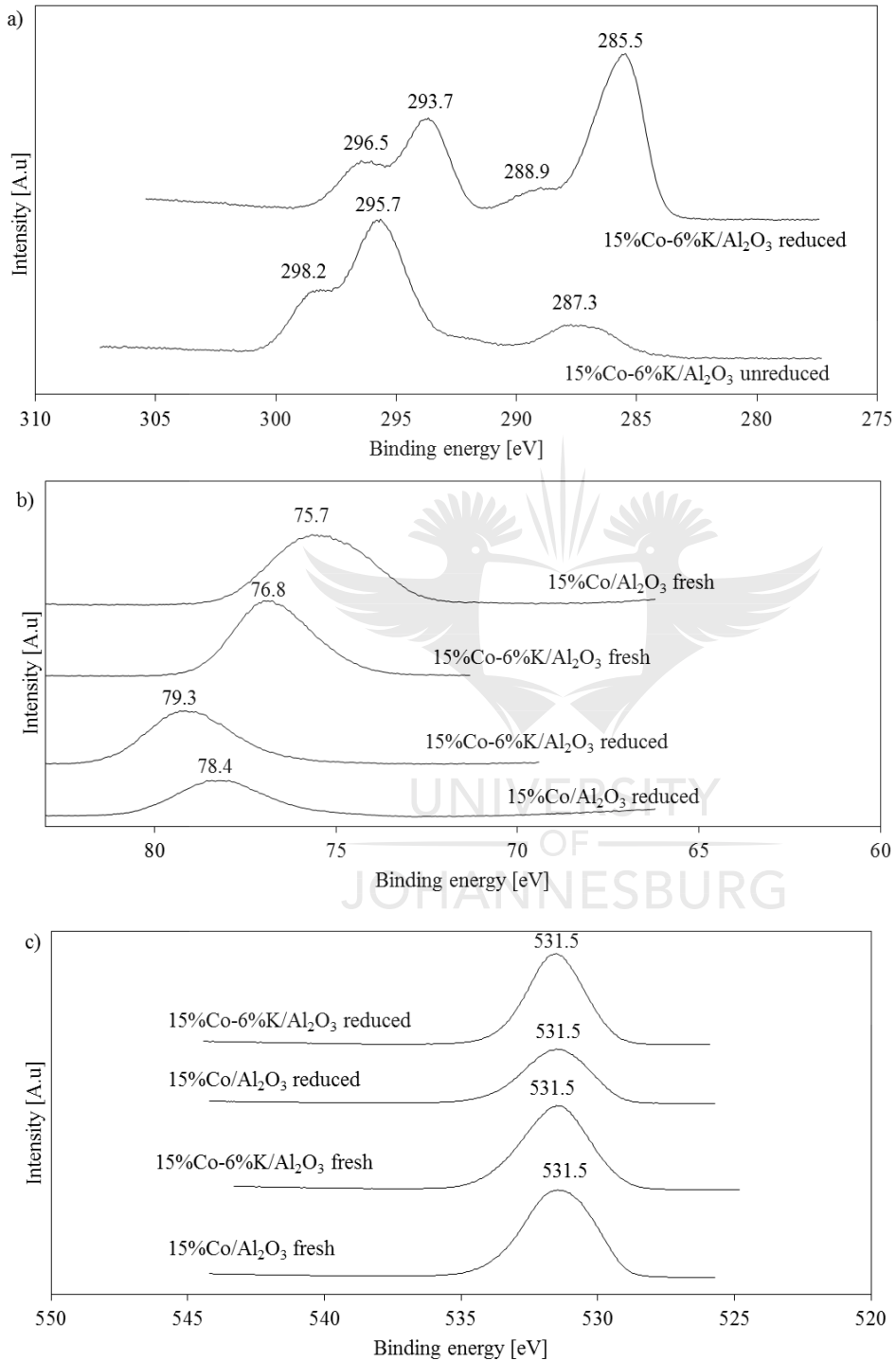
APPENDICES

Appendix A: XPS profiles

Fig. A 1: XPS profiles for unpromoted and K- promoted catalysts for a) K 2P C1s; b) Al 2P and; c) O1s species

Appendix B: Regression statistics and ANOVA outputs

Table A 1: BET surface area as a function of potassium loading

Regression Statistics	
Multiple R	0.977923757
R Square	0.956334875
Adjusted R Square	0.945418594
Standard Error	8.491554314
Observations	6

ANOVA

	df	SS	MS	F	Significance F
Regression	1	6316.982355	6316.982355	87.60628823	0.000725661
Residual	4	288.4259786	72.10649466		
Total	5	6605.408333			

	Coefficients	Standard Error	t Stat	P-value	Lower 95%	Upper 95%	Lower 95.0%	Upper 95.0%
Intercept	126.7032028	5.885737868	21.52715695	2.75412E-05	110.3617748	143.0446309	110.3617748	143.0446309
X Variable 1	-11.613879	1.240822492	-9.359823088	0.000725661	-15.05895454	-8.168803471	-15.05895454	-8.168803471

Table A 2: Pore volume as a function of potassium loading

Regression Statistics	
Multiple R	0.934241052
R Square	0.872806343
Adjusted R Square	0.841007929
Standard Error	0.026775493
Observations	6

ANOVA

	df	SS	MS	F	Significance F
Regression	1	0.019678292	0.019678292	27.44810915	0.00634418
Residual	4	0.002867708	0.000716927		
Total	5	0.022546			

	Coefficients	Standard Error	t Stat	P-value	Lower 95%	Upper 95%	Lower 95.0%	Upper 95.0%
Intercept	0.209576512	0.018558856	11.29253389	0.000350442	0.158048867	0.261104158	0.158048867	0.261104158
X Variable 1	-0.02049822	0.00391255	-5.239094306	0.00634418	-0.031361202	-0.009635239	-0.031361202	-0.009635239

Table A 3: CO_2 conversion as a function of time on stream

Regression Statistics	
Multiple R	0.986777493
R Square	0.973729821
Adjusted R Square	0.97154064
Standard Error	0.957250088
Observations	14

ANOVA

	df	SS	MS	F	Significance F
Regression	1	407.5749831	407.5749831	444.7917149	7.49959E-11
Residual	12	10.99593278	0.916327731		
Total	13	418.5709159			

	Coefficients	Standard Error	t Stat	P-value	Lower 95%	Upper 95%	Lower 95,0%	Upper 95,0%
Intercept	42.31552803	0.447778578	94.50101043	1.31799E-18	41.33990232	43.29115374	41.33990232	43.29115374
X Variable 1	-0.016562315	0.000785313	-21.0900857	7.49959E-11	-0.018273365	-0.014851266	-0.018273365	-0.014851266

Table A 4: C_{5+} selectivity as a function of time on stream

Regression Statistics	
Multiple R	0.90839041
R Square	0.825173138
Adjusted R Square	0.810604232
Standard Error	0.701696957
Observations	14

ANOVA

	df	SS	MS	F	Significance F
Regression	1	27.8879988	27.8879988	56.63933745	6.98741E-06
Residual	12	5.908543437	0.49237862		
Total	13	33.79654223			

	Coefficients	Standard Error	t Stat	P-value	Lower 95%	Upper 95%	Lower 95,0%	Upper 95,0%
Intercept	4.623430387	0.328236967	14.08564804	7.96067E-09	3.908263473	5.338597301	3.908263473	5.338597301
X Variable 1	-0.004332374	0.000575661	-7.525911071	6.98741E-06	-0.005586632	-0.003078116	-0.005586632	-0.003078116

Appendix C: Example of BET machine printout

Serial # 113 Unit 1 Port 2

Sample: Co_6%K_AL2O3
Operator: Khangale
Submitter: Khangale
File: C:\MicroActive for ASAP 2460\d

Started: 2018/04/2 Analysis A N2
Complete 2018/04/2 Analysis B -195.800 °
Report Ti 2018/09/0 Thermal C No
Sample M 0.1960 g Warm Fre 14.5893 c
Free 43.2694 c Equilibrati 10 s
Low Press None Sample D 1.000 g/c
Sample D Automatic No

Summary Report

Surface Area

| BET Surfa 45.8546 m²/g |

t-Plot Exte 46.8397 m²/g

BJH Adso
between 1 56.248 m²/g

| Pore Volume
37,6432 |

Single poi
Increment less than 0.098499 cm³/g

0,00054 t-Plot micr -0.000741 cm³/g
0,00049

BJH Adso
0,00385 between 1 0.100766 cm³/g

BJH Deso
0,00513 between 1 0.101160 cm³/g

Pore Size

Adsorptio 85.9225 Å

BJH Adso 71.658 Å

BJH Deso 50.561 Å

Isotherm Linear Plot

Co_6%K_AL2O3 - A Co_6%K_AL2O3 - D

Relative P	Quantity A	Relative P	Quantity A
0,00553	7,39816	0,995	64,6012
0,01061	8,02914	0,97607	63,3266
0,01702	8,47665	0,95664	62,1618
0,02324	8,77651	0,93169	60,9365
0,02919	9,01265	0,92609	60,6607
0,03507	9,20835	0,90094	59,5816
0,04069	9,37941	0,87649	58,588
0,04605	9,5282	0,85125	57,6156
0,05103	9,66002	0,82629	56,6784
0,05587	9,7838	0,80121	55,7404
0,06103	9,90409	0,75348	53,8832
0,08058	10,326	0,70326	51,604
0,10107	10,7439	0,65486	48,5901
0,12107	11,1367	0,6078	43,959
0,141	11,5214	0,55487	35,1483
0,16098	11,9137	0,50425	26,188
0,18083	12,3059	0,45229	21,1214
0,1909	12,5058	0,38099	17,0146
0,20054	12,6987	0,3312	15,6172
0,21079	12,9098	0,28048	14,3696
0,22074	13,1168	0,25089	13,685
0,23075	13,3264	0,20049	12,6184
0,24068	13,5404	0,1406	11,4403
0,25068	13,7558		
0,29811	14,8558		
0,34953	16,1697		
0,39926	17,5861		
0,44882	19,227		
0,49813	21,2262		
0,54706	23,7877		
0,59569	27,2195		
0,64378	31,872		
0,6942	37,6432		
0,75075	42,2559		
0,79785	44,3511		
0,8372	45,9906		
0,84902	46,5497		
0,87361	47,8583		
0,89777	49,461		
0,92211	51,5553		
0,94607	54,3647		
0,96937	58,2871		
0,97887	60,3904		

BET Report

BET Surfa 45.8546 ± 0.1544 m²/g
Slope: 0.094040 ± 0.000315 g/cm³ ST
Y-Intercep 0.000882 ± 0.000052 g/cm³ ST
C: 107.669691
Qm: 10.5350 cm³/g STP

Correlatio 0.9999269
Molecular 0.1620 nm²

Relative P Quantity A1/[Q(Po/P - 1)]

Relative P	Quantity	1/[Q(Po/P - 1)]
0,05103	9,66002	0,00557
0,05587	9,7838	0,00605
0,06103	9,90409	0,00656
0,08058	10,326	0,00849
0,10107	10,7439	0,01046
0,12107	11,1367	0,01237
0,141	11,5214	0,01425
0,16098	11,9137	0,0161
0,18083	12,3059	0,01794
0,1909	12,5058	0,01887
0,20054	12,6987	0,01975
0,21079	12,9098	0,02069
0,22074	13,1168	0,0216
0,23075	13,3264	0,02251
0,24068	13,5404	0,02341

BET Surface Area Plot

Co_6%K_AL2O3   Not Fitted

Relative P	1/[Q(Po/P	Relative P	1/[Q(Po/P
0,05103	0,00557	0,25068	0,02432
0,05587	0,00605	0,29811	0,02859
0,06103	0,00656		
0,08058	0,00849		
0,10107	0,01046		
0,12107	0,01237		
0,141	0,01425		
0,16098	0,0161		
0,18083	0,01794		
0,1909	0,01887		
0,20054	0,01975		
0,21079	0,02069		
0,22074	0,0216		
0,23075	0,02251		
	0,00039		
0,24068	0,02341		

0,00356

0,00392

---

t-Plot Report

Micropore -0.000741 cm³/g
Micropore *
External S 46.8397 m²/g
Slope: 3.028166 ± 0.056052 cm³/g-Å S
Y-Intercep -0.478735 ± 0.240823 cm³/g ST

Correlatio 0.997951
Surface A 1.000
Density C 0.0015468
Total Surf 45.8546 m²/g
Thickness 3.5000 Å to 5.0000 Å
Thickness Harkins and Jura

Thickness Curve

t = [13.99 / (0.034 - log(P/Po))]

t-Plot Report - Data

Relative P	Statistical	Quantity A	Fitted
0,05103	3,24794	9,66002	
0,05587	3,29724	9,7838	
0,06103	3,34754	9,90409	
0,08058	3,52208	10,326	*
0,10107	3,68654	10,7439	*
0,12107	3,83556	11,1367	*
0,141	3,97643	11,5214	*
0,16098	4,1124	11,9137	*
0,18083	4,24397	12,3059	*
0,1909	4,30977	12,5058	*
0,20054	4,37236	12,6987	*
0,21079	4,4385	12,9098	*
0,22074	4,50241	13,1168	*
0,23075	4,56663	13,3264	*
0,24068	4,6302	13,5404	*
0,25068	4,6942	13,7558	*
0,29811	4,99987	14,8558	*
0,34953	5,34049	16,1697	
0,39926	5,68582	17,5861	
0,44882	6,05229	19,227	
0,49813	6,44633	21,2262	
0,54706	6,87521	23,7877	
0,59569	7,3498	27,2195	
0,64378	7,88073	31,872	
0,6942	8,52471	37,6432	

---

t-Plot
Harkins and Jura

Co_6%K_AL2O3   Not Fitted

Thickness	Quantity A	Thickness	Quantity A
3,52208	10,326	3,24794	9,66002
3,68654	10,7439	3,29724	9,7838
3,83556	11,1367	3,34754	9,90409
3,97643	11,5214	5,34049	16,1697
4,1124	11,9137	5,68582	17,5861
4,24397	12,3059	6,05229	19,227
4,30977	12,5058	6,44633	21,2262
4,37236	12,6987	6,87521	23,7877
4,4385	12,9098	7,3498	27,2195
4,50241	13,1168	7,88073	31,872
4,56663	13,3264	8,52471	
4,6302	13,5404		
4,6942	13,7558		
4,99987	14,8558		

BJH Adsorption Pore Distributio

Faas Correction
Harkins and Jura

t = [13.99 / (0.034 -

Diameter 17.000 Å to 3 000.00
Adsorbate 9.53000 Å
Density C 0.0015468
Fraction o 0.00

Pore Diam Average D

3040.3 - 2	2883,08	
2754.4 - 2	2506,65	
2330.2 - 2	2199,72	
2094.6 - 1	1821,86	0,00105
1653.4 - 9	1097,78	
928.0 - 64	736,623	
646.3 - 37	439,728	0,00693
374.3 - 26	298,52	
262.9 - 20	224,378	
202.5 - 16	179,65	0,00304
165.0 - 13	149,551	0,00251
138.9 - 12	133,626	0,00108
129.1 - 10	113,889	0,00323
104.4 - 84	92,272	0,00438
84.7 - 68.	74,8248	0,01083
68.7 - 58.	62,6366	0,01432
58.4 - 50.	54,0807	0,01142
50.9 - 44.	47,377	0,00793
44.8 - 39.	41,8478	0,00537
39.7 - 35.	37,1854	0,00367
35.3 - 31.	33,1746	0,00256
31.5 - 28.	29,6645	0,00185
28.2 - 25.	26,4814	0,00142
25.2 - 22.	23,6986	0,00087
22.6 - 22.	22,3046	0,00011
22.1 - 21.	21,7882	0,0001
21.5 - 21.	21,2771	7,5E-05
21.0 - 20.	20,7714	6,4E-05
20.5 - 20.	20,2642	5E-05
20.0 - 19.	19,7698	1,4E-05

147

0,98828	62,7249
0,90078	63,3767
0,99172	63,6842
0,99301	64,0202
0,99367	64,2635
0,995	64,6012

* The micropore area is not reported becau

Left column

ort 2

AP 2460\data\...\Co_6%K_AL2O

N2
-195.800 °C
° No
14.5893 cm³ Measured
10 s
1.000 g/cm³
g/cm

Report

log(P/Po))] ^ 0.5

0 Å

Cumulativ	Increment	Cumulativ
0,00039	0,00536	0,00536
0,00092	0,00855	0,01391
0,00141	0,00895	0,02286
0,00246	0,02305	0,04591
0,00631	0,14029	0,1862
0,00987	0,19312	0,37932
0,0168	0,63066	1,00998
0,02194	0,68778	1,69776
0,02585	0,69827	2,39603
0,0289	0,67782	3,07385
0,03141	0,67173	3,74559
0,03249	0,32327	4,06886
0,03572	1,13322	5,20209
0,04009	1,89796	7,10004
0,05092	5,78938	12,8894
0,06525	9,14592	22,0353
0,07666	8,44428	30,4796
0,0846	6,69818	37,1778
0,08997	5,13505	42,3129
0,09364	3,94857	46,2614
0,0962	3,09208	49,3535
0,09806	2,50089	51,8544
0,09948	2,14364	53,998
0,10035	1,47144	55,4695
0,10046	0,1955	55,665
0,10056	0,19236	55,8573
0,10064	0,14089	55,9982
0,1007	0,12356	56,1218
0,10075	0,09826	56,22
0,10077	0,02799	56,248

Column 1

MicroActiv MicroActiv Page 1
Serial # 113 Unit 1 Port 2

Sample: Co_6%K_AL2O3
Operator: Khangale
Submitter: Khangale
File: C:\MicroActive for ASAP 2460\d

Started: 2018/04/2 Analysis A N2
Complete 2018/04/2 Analysis B -195.800 °
Report Ti 2018/09/0 Thermal C No
Sample M 0.1960 g Warm Fre 14.5893 c
Cold Free 43.2694 c Equilibrati 10 s
Low Press None Sample D 1.000 g/c

Automatic No

BJH Adsorption Cumulative Pore Volume (
Harkins and Jura : Faas Correction

Co_6%K_AL2O3

Pore Diam	Pore Volume (cm³/g)
2754,36	0,00039
2330,2	0,00092
2094,65	0,00141
1653,4	0,00246
928,028	0,00631
646,314	0,00987
374,277	0,0168
262,898	0,02194
202,466	0,02585
165,035	0,0289
138,937	0,03141
129,107	0,03249
104,388	0,03572
84,6823	0,04009
68,6788	0,05092
58,4495	0,06525
50,9009	0,07666
44,7568	0,0846
39,6507	0,08997
35,3046	0,09364
31,5394	0,0962
28,2216	0,09806
25,1564	0,09948
22,5727	0,10035
22,0512	0,10046
21,5396	0,10056
21,0293	0,10064
20,528	0,1007
20,0159	0,10075
19,5376	0,10077

Column 2

MicroActiv MicroActiv Page 1
Serial # 113 Unit 1 Port 2

Sample: Co_6%K_AL2O3
Operator: Khangale
Submitter: Khangale
File: C:\MicroActive for ASAP 2460\d

Started: 2018/04/2 Analysis A N2
Complete 2018/04/2 Analysis B -195.800 °
Report Ti 2018/09/0 Thermal C No
Sample M 0.1960 g Warm Fre 14.5893 c
Cold Free 43.2694 c Equilibrati 10 s
Low Press None Sample D 1.000 g/c

Automatic No

BJH Adsorption dV/dD Pore Volume
Harkins and Jura : Faas Correction

Co_6%K_AL2O3

Pore Diam	Pore dV/dD Pore Volume (cm³/g·Å)
2883,08	1,4E-06
2506,65	1,3E-06
2199,72	2,1E-06
1821,86	2,4E-06
1097,78	5,3E-06
736,623	1,3E-05
439,728	2,5E-05
298,52	4,6E-05
224,378	6,5E-05
179,65	8,1E-05
149,551	9,6E-05
133,626	0,00011
113,889	0,00013
92,272	0,00022
74,8248	0,00068
62,6366	0,0014
54,0827	0,00151
47,377	0,00129
41,8478	0,00105
37,1854	0,00084
33,1746	0,00068
29,6645	0,00056
26,4814	0,00046
23,6986	0,00034
22,3046	0,00021
21,7882	0,0002
21,2771	0,00015
20,7714	0,00013
20,2642	9,7E-05
19,7698	2,9E-05

Column 3

MicroActiv MicroActiv Page 1
Serial # 113 Unit 1 Port 2

Sample: Co_6%K_AL2O3
Operator: Khangale
Submitter: Khangale
File: C:\MicroActive for ASAP 2460\d

Started: 2018/04/2 Analysis A N2
Complete 2018/04/2 Analysis B -195.800 °
Report Ti 2018/09/0 Thermal C No
Sample M 0.1960 g Warm Fre 14.5893 c
Cold Free 43.2694 c Equilibrati 10 s
Low Press None Sample D 1.000 g/c

Automatic No

BJH Desorption dV/dD Pore Volume
Harkins and Jura : Faas Correction

Pore Diam	BJH Desorption dV/d dV/dD Por	BJH Desorption Cum Pore Diam Pore Volu
943,351	1,9E-06	818,893 0,00211
541,938	9,4E-06	458,881 0,00411
341,553	2,1E-05	295,22 0,00629
283,486	2,4E-05	273,508 0,00678
229,638	3,7E-05	205,72 0,00877
181,212	5,7E-05	165,778 0,01064
149,178	8E-05	137,99 0,01251
126,466	0,00011	118,211 0,01435
109,587	0,00014	103,161 0,01621
90,4984	0,00024	82,6599 0,02
73,7202	0,00046	67,886 0,02483
61,7609	0,00089	57,489 0,0315
52,9672	0,00224	49,6722 0,04206
45,6158	0,00362	42,6917 0,06357
39,5875	0,00333	37,2708 0,08501
34,6136	0,00157	32,6178 0,09526
29,462	0,00084	27,3027 0,10116

Column 4

MicroActiv MicroActiv Page 1
Serial # 113 Unit 1 Port 2

Sample: Co_6%K_AL2O3
Operator: Khangale
Submitter: Khangale
File: C:\MicroActive for ASAP 2460\d

Started: 2018/04/2 Analysis A N2
Complete 2018/04/2 Analysis B -195.800 °
Report Ti 2018/09/0 Thermal C No
Sample M 0.1960 g Warm Fre 14.5893 c
Cold Free 43.2694 c Equilibrati 10 s
Low Press None Sample D 1.000 g/c

Automatic No

BJH Desorption dV/dlog(D) Pore Volume
Harkins and Jura : Faas Correction

Co_6%K_AL2O3

Pore Diam	dV/dlog(D) Pore Volume (cm³/g
943,351	0,00366
541,938	0,00996
341,553	0,01424
283,486	0,01527
229,638	0,01753
181,212	0,02193
149,178	0,02543
126,466	0,02937
109,587	0,0343
90,4984	0,04607
73,7202	0,07152
61,7609	0,11835
52,9672	0,25643
45,6158	0,35558
39,5875	0,28589
34,6136	0,11814
29,462	0,05308

Column 5

MicroActiv MicroActiv Page 1
Serial # 113 Unit 1 Port 2

Sample: Co_6%K_AL2O3
Operator: Khangale
Submitter: Khangale
File: C:\MicroActive for ASAP 2460\d

Started: 2018/04/2 Analysis A N2
Complete 2018/04/2 Analysis B -195.800 °
Report Ti 2018/09/0 Thermal C No
Sample M 0.1960 g Warm Fre 14.5893 c
Cold Free 43.2694 c Equilibrati 10 s
Low Press None Sample D 1.000 g/c

Automatic No

BJH Desorption dA/dD Pore Area
Harkins and Jura : Faas Correction

Pore Diam	BJH Desorption dA/d dA/dD Por	BJH Desorption Cum Pore Diam Pore Area
943,351	9,4E-05	818,893 0,08955
541,938	0,00085	458,881 0,23683
341,553	0,0028	295,72 0,49192
283,486	0,00363	273,508 0,5622
229,638	0,00727	205,72 0,90842
181,212	0,01402	165,778 1,32195
149,178	0,02352	137,99 1,82309
126,466	0,03683	118,211 2,40265
109,587	0,05706	103,161 3,08284
90,4984	0,11849	82,6599 4,75944
73,7202	0,27379	67,886 7,37674
61,7609	0,63721	57,489 11,6994
52,9672	1,7971	49,6722 19,8227
45,6158	3,50301	42,6917 38,5105
39,5875	3,47253	37,2708 60,1752
34,6136	2,01204	32,6178 72,0176
29,462	1,26614	27,3027 80,03

Column 6

MicroActiv MicroActiv Page 1
Serial # 113 Unit 1 Port 2

Sample: Co_6%K_AL2O3
Operator: Khangale
Submitter: Khangale
File: C:\MicroActive for ASAP 2460\d

Started: 2018/04/2 Analysis A N2
Complete 2018/04/2 Analysis B -195.800
Report Ti 2018/09/0 Thermal C No
Sample M 0.1960 g Warm Fre 14.5893 c
Cold Free 43.2694 c Equilibrati 10 s
Low Press None Sample D 1.000

Automatic No

BJH Desorption dA/dlog(D) Pore Area
Harkins and Jura : Faas Correction

Co_6%K_AL2O3

Pore Diam	dA/dlog(D) Pore Area (m²/g)
943,351	0,17672
541,938	0,89838
341,553	1,90227
283,486	2,28703
229,638	3,4423
181,212	5,35087
149,178	7,47346
126,466	10,0255
109,587	13,5536
90,4984	22,5533
73,7202	42,799
61,7609	84,3517
52,9672	205,571
45,6158	344,349
39,5875	297,865
34,6136	151,111
29,462	79,5982

ata\...\Co_6%K_AL2O3.SMP

C

m³ Measured

3